UNIVERSIDAD DE CHILE
FACULTAD DE CIENCIAS FÍSICAS Y MATEMÁTICAS
DEPARTAMENTO DE INGENIERÍA CIVIL

MECHANICAL STUDY OF SAND-LAPONITE MIXES.

TESIS PARA OPTAR AL GRADO DE MAGÍSTER EN CIENCIAS DE LA INGENIERÍA,
MENCIÓN INGENIERÍA ESTRUCTURAL, SÍSMICA Y GEOTÉCNICA

MEMORIA PARA OPTAR AL TÍTULO DE INGENIERO CIVIL

MARCELO IGNACIO PACHECO DUHALDE

PROFESOR GUÍA:
FELIPE OCHOA CORNEJO

MIEMBROS DE LA COMISIÓN:

DIEGO MORATA CÉSPEDES
FRANCK QUERO

SANTIAGO DE CHILE
2023

TESIS PARA OPTAR AL GRADO DE: MAGÍSTER EN CIENCIAS DE LA INGENIERÍA, MENCIÓN INGENIERÍA ESTRUCTURAL, SÍSMICA Y GEOTÉCNICA
MEMORIA PARA OPTAR AL TÍTULO DE: INGENIERO CIVIL
POR: MARCELO IGNACIO PACHECO DUHALDE
FECHA: 2023
PROFESOR GUÍA: FELIPE OCHOA CORNEJO

ESTUDIO DE LA MECÁNICA DE LAS MEZCLAS ARENA-LAPONITA

Las mezclas arena arcilla nacen principalmente de la necesidad de modificar algunas de las propiedades de los dos suelos involucrados, la arena o la arcilla. Para el caso chileno resulta de principal interés el uso de arcillas súper plásticas en arenas por su potencial efecto mitigador de licuefacción. Actualmente el uso de la laponita, una arcilla artificial supera plástica, como técnica de mejoramiento de suelo y su uso como mitigador de licuefacción presenta una gran oportunidad de estudio.

En el presente trabajo de título se realizó una extensiva revisión bibliográfica del estado del arte de las mezclas arena-arcilla desde una perspectiva geotécnica, con la finalidad de relacionar el comportamiento granular de este tipo de mezclas con el de la laponita con arena de Ottawa. Con esta revisión se determinaron algunos de los principales factores que interfieren en los arreglos granulares de las mezclas, así como algunos parámetros importantes a considerar al momento de la fabricación de estos suelos. Es de principal relevancia el concepto del contenido de finos límite, un valor que se ve afectado tanto como por los tipos de suelos involucrados y por la propiedad analizada.

También se realizó una batería de ensayos geotécnicos en mezclas secas y húmedas de arena de Ottawa con diferentes concentraciones de laponita para determinar los cambios a nivel granular de la mezcla y la variación de las propiedades medidas con el incremento de la concentración de laponita en la mezcla. Se realizaron ensayos de hinchamiento libre, presión de hinchamiento, consolidación y corte simple. De los resultados se obtuvo una relación importante entre la distribución granular de las muestras y su comportamiento frente a los diferentes ensayos. Además, se replanteó la manera en que se supone que las partículas de laponita se distribuyen en los espacios intergranulares de la arena.

De manera general se encontró que los cambios más importantes en cuanto al comportamiento de la mezcla ocurren con un 1% de laponita por masa de arena. A nivel granular la distribución de las partículas de laponita con esta concentración afecta la zona de contactos entre los gruesos, provocando variaciones importantes de las propiedades estudiadas.

Table of Content

Table Index

Figure Index

1 Introduction

1.1 General context

Particulate media encompasses a broad spectrum of domains and disciplines, spanning a diverse array of subjects. Examples of such media include soils, sediments, granular food substances, composites, ceramics, and synthetic materials. Despite soils being composed of discrete particles, they have traditionally been examined and understood as continuous entities. While this approach has facilitated a general comprehension of their behavior, it is crucial not to overlook their particulate nature. The study of phenomena within the framework of continuous assumptions also carries implications at the particle level. Delving into such cases can contribute to a better understanding of certain facets of soil behavior that are often overlooked in conventional analysis (Barber & Ciavarella, 2000).

The constraints inherent in utilizing continuous theories for soil analysis have been acknowledged since the early 20th century (Santamarina, 2003). To enhance the investigation of soil behavior, the field of contact mechanics has played a pivotal role. This discipline within the realm of engineering sciences is devoted to the examination of contact-related issues, which hold significant importance in solid mechanics due to the fact that contacts serve as the primary means of exerting loads on deformable bodies (Barber & Ciavarella, 2000).

Classical contact mechanics is commonly attributed to the pioneering work of Heinrich Hertz. In 1882, Hertz successfully resolved the contact problem involving two elastic bodies possessing curved surfaces. These seminal findings by Hertz serve as the fundamental principles of contact mechanics that persist to the present day (V. Popov, n.d.), giving birth to what is known as Hertzian contact problems. Ideally, the interaction between two soil particles can be examined as a Hertzian contact problem.

Within this field, the distinctive attributes of each particle assume significance, as they exert a profound influence on the overall behavior of the soil. Factors such as shape, size, mineralogy, particle arrangement, porosity, inter-particle forces, and more, all contribute to shaping the general behavior of the soil. Numerous geotechnical phenomena directly stem from the interplay between particles, including soil liquefaction, resistance, and deformability, among others. To comprehensively grasp these phenomena from a discrete perspective, it is imperative to gain knowledge about the various types of forces that manifest within an assembly of particles. Notably, the most pivotal interparticle forces governing soil behavior occur at the boundary level, particle level, and contact level. These encompass skeletal forces, gravitational forces, buoyant

forces, capillary forces, and electrical forces, to name a few. Moreover, understanding the roughness and morphology of particles represents an additional crucial aspect that enhances our comprehension of particulate media and soil behavior.

When addressing soils, it is crucial to acknowledge the diverse range of particle sizes comprising them, spanning from centimeters to nanometers, representing a magnitude difference of 10^7. In the case of the smallest particles, known as clays, the dominant forces governing their interactions differ from those acting upon larger particles, with electrical forces assuming prominence.

Given this complex arrangement, typical of soils, with particles of disparate sizes that generates an interaction between different predominant forces, for example, sand-clay mixtures present a relationship between predominant gravitational forces, of the sands, and electrical forces, of the clays. It is important to understand how these arrangements are related to address some issues and to incorporate this view of soils as particulate media. It is of special attention what happens between sand size particles (2 - 0.075 mm) and clay size (< 0.005 mm).

Considering the intricate arrangement inherent to soils, characterized by the presence of particles of varying sizes, it gives rise to interactions governed by distinct predominant forces. A notable example is observed in sand-clay mixtures, wherein a correlation exists between the prevalent gravitational forces exerted by the sands and the electrical forces exerted by the clays. Understanding the interrelationships within such arrangements becomes vital for addressing certain concerns and incorporating a comprehensive perspective of soils as particulate media. Of particular significance is the examination of interactions occurring between particles of sand size (2 - 0.075 mm) and clay size (< 0.005 mm).

Some phenomena that hold considerable interest for study and contribute to our understanding are dynamic phenomena, typically associated with seismic events or earthquakes. Of particular significance are the dynamic properties of soils, which are influenced by interparticle relationships and granular configurations. While this work does not aim to extensively delve into the intricate connections between the dynamic properties of soils and their reliance on granular arrangements and particle interactions, it is essential to emphasize that both the shear modulus (G) and damping (D) – crucial parameters for characterizing soil response to cyclic stresses – are influenced by the interaction between fine plastic and non-plastic soils with coarse soils, to provide an illustrative example (Verdugo & González, 2015).

Liquefaction, a phenomenon linked to the dynamic response of soils, is characterized by significant deformations or excessive soil movements due to transient excitation. It primarily occurs in non-cohesive saturated soils, specifically sands (C. S. El Mohtar et al., 2013). This phenomenon is often observed during earthquakes of substantial magnitude, wherein undrained cyclic loading induces a progressive buildup of pore pressures. Consequently, effective stresses decrease, ultimately reaching zero and resulting in liquefaction (Ochoa-Cornejo, 2015b). Such liquefaction processes frequently lead to substantial ground movements and large-scale deformations, which, in certain cases, cause catastrophic effects on adjacent structures or severe damage to their structural integrity. The occurrence of liquefaction problems has been frequently documented following notable earthquakes, including the 1964 Nigata, Japan, 1976 Tangshan, China, 1999 Kocaeli, Turkey, 2008 Wenchuan, China, and 2011 Tohoku, Japan earthquakes (Verdugo & González, 2015).

Chile, situated near the Pacific Ring of Fire, an area characterized by numerous active volcanoes and tectonic plate subduction zones, experiences one of the highest levels of seismic activity worldwide. This heightened seismicity is evident from the occurrence of five earthquakes measuring above 7 degrees on the Richter scale within the past decade. Such seismic activity demands careful attention. Although it is acknowledged that ground excitation resulting from an earthquake can trigger liquefaction, the occurrence of this phenomenon necessitates more than just seismic activity.

Prior to the earthquake on February 27, 2010, one of the six largest earthquakes ever recorded (Verdugo & González, 2015), it was believed that soil liquefaction in Chile was improbable or virtually non-existent. However, it was not until the impacts observed in various regions of Concepción and along the Maule coast following this earthquake that the reality of soil liquefaction as a significant risk for the area became apparent. According to Verdugo & González (2015), around 170 sites exhibited evidence of soil liquefaction subsequent to the earthquake on February 27, 2010.

a) b)

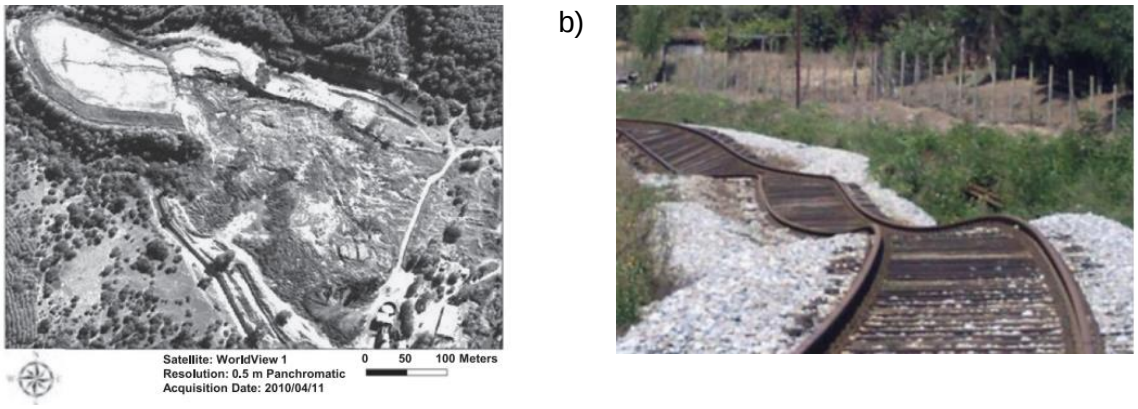

Figure 1-1: (a) Failure in Las Palmas dam and (b) Post liquefaction settlement in the surroundings of Concepción (Verdugo, 2015).

Consequently, it is of paramount importance to investigate one of the most significant and abundant structures in the country, namely, tailings deposits. Tailings, which are waste materials generated by the mining industry, are characterized by Sernageomin as finely ground solids that are discarded during mining operations. It is imperative to store and manage all such waste in designated tailings deposits, which can take various forms and sizes, including tailings reservoirs and dams. Among these, the analysis of tailings dams is particularly crucial. These deposits consist of a wall constructed using the thickest fraction of the tailings, which is separated via a hydrocyclone and subsequently compacted to form the dam wall (SERNAGEOMIN). This is significant because the coarse fraction of tailings primarily comprises sand-sized particles with a certain fine concentration, rendering them non-cohesive soils that may be saturated and hence susceptible to liquefaction.

Presently, Chile is home to approximately 758 active and inactive tailings deposits, with a significant concentration in the Coquimbo region. Considering the associated risks, it becomes necessary to explore means and methods to enhance the resistance to liquefaction of these structures.

1.2 Soil improvement

At present, there exist several approaches to prevent or alleviate the consequences of phenomena like liquefaction. The most commonly employed methods for soil improvement are active techniques, which involve densifying the soil through the application of an impacting source that imparts energy to the granular matrix, thereby reorganizing the particles into a more compact configuration (Ochoa-Cornejo, 2015b). Vibratory compaction, dynamic compaction, and preload are among the widely employed methods within this category. Nevertheless, alternative forms of

soil improvement are being explored, including passive improvement methods that aim to modify the soil behavior without directly altering its matrix. One such method involves the use of colloidal silica and bentonite to enhance the soil's resistance to liquefaction. These passive methods offer potential avenues for improving soil performance without physically modifying the soil structure.

Colloidal silica refers to an aqueous suspension of silica nanoparticles generated through saturated solutions of silica acid. Extensive research highlights the benefits associated with colloidal silica, including its low initial viscosity, effective control over gelation, and sustained mechanical stability. In terms of mitigating liquefaction in sands, even at low concentrations, colloidal silica gel particles demonstrate remarkable efficacy by cementing the grains and stabilizing pore pressure. Furthermore, colloidal silica exhibits non-toxicity, biological and chemical inertness, and possesses a prolonged shelf life (Bao et al., 2019).

Bentonite, an aluminum phyllosilicate and clay primarily composed of montmorillonite, exhibits thixotropic properties when in a solution. This characteristic renders it highly effective in enhancing the performance of loose sands. Similar to colloidal silica, bentonite is environmentally friendly and serves the purpose of improving the behavior of loose sands through gel formation. The high yield stress and viscosity of bentonite dispersion, along with its rapid gelation, have significant implications for the coefficient of permeability of the sand. Therefore, researchers have investigated the use of bentonite in combination with sodium pyrophosphate to enhance its rheological properties and promote better penetration into sands.

Among the innovative soil improvement methods, laponite, an artificial clay, has emerged as a potential alternative to bentonite. Laponite is a disc-shaped clay composed of hectorite, a member of the smectite group. Its idealized dimensions are approximately 25 nm in diameter and 1 nm in height, with a layered structure. Notably, laponite is insoluble in water and exhibits a significant swelling capacity of up to 800% of its original size during free swelling (Pardo Ojeda, 2020). This clay is employed as a rheology modifier and yields highly thixotropic gels. Its unique properties position it as an effective substitute for bentonite, particularly due to its smaller particle size, which facilitates easier application (El Howayek, 2011).

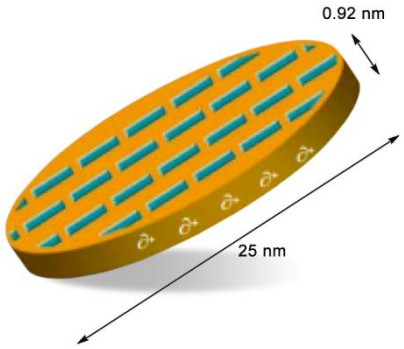

Figure 1-2: Idealize laponite crystal (ByK Instruments, 2014).

Numerous studies have investigated the properties of laponite, including research by Pardo Ojeda, (2020), Shen, (2014) and el Howayek, (2011). These studies have examined the effectiveness of laponite in improving resistance to liquefaction in sands, as highlighted by Ochoa-Cornejo (2015) and Rodriguez (2019). The favorable outcomes reported in these studies underscore the need for further exploration of the interaction between laponite and sand.

Typically, research on liquefaction mitigation has focused on the application of small quantities of laponite, ranging from 1% to 3% in relation to the mass of sand. However, investigations regarding the use of larger quantities of laponite for these purposes are still lacking. Another potential area for the application of laponite lies in the construction of sand and clay barriers. While studies have examined the use of materials like bentonite for such applications (Akgün et al., 2015), it would be worthwhile to evaluate laponite as a potential substitute in these scenarios.

The main objective of this thesis work is to build upon previous studies involving laponite and sand by investigating the incorporation of higher quantities of laponite than previously explored. Additionally, this research aims to address the interaction between coarse and fine particles from the perspective of particle mechanics. By delving into these aspects, this study intends to contribute to a deeper understanding of the behavior and performance of laponite-sand mixtures, thereby expanding the existing knowledge in the field.

1.3 Objetives

1.3.1 General objetive

This study aims to investigate the granular structure formed by sand and laponite in dry conditions at different concentrations, how these mixtures behave when hydrated, and how

the granular structure of the mixes formed in dry conditions influences the granular structure of wet mixtures.

1.3.2 Specific objetives

- Characterize the behavior of Ottawa sand with different concentrations of laponite.
- Assess the performance of Ottawa sand with 1,3 and 5% of laponite in dry conditions.
- Identify the mechanism of interaction between sand and laponite at very low concentrations.

1.4 Methodology

The experimental methodology for this research consist in a wide range of laboratory tests with the purpose of characterize the material. Those tests are:

- Manual granulometry by ASTM sieves.
- Atterberg´s limits.
- Relative density.
- Free swelling and swelling pressure.
- Simple shear.
- Unidimensional compression.
- SEM images.

1.5 Thesis organization

This work is organized in chapters, Chapter 1 describes the motivation, the objectives, and the work distribution. Chapter 2 presents a bibliographic review about sand-fine mixtures with different fine particles. Chapter 3 presents a bibliographic review of nanomaterials and its application in civil engineering and in geotechnical engineering. Chapter 4 describes the methodology followed for the experimental plan and a description of the equipment used. Chapter 5 reports the results of the experimental plan. Chapter 6 presents the discussion and analysis of the obtained results. Chapter 7 presents the main conclusions of this work. Chapter 8 presents the bibliography of this study. Finally, Chapter 9 presents tables and images annex to the study.

2 Bibligraphic review

2.1 Sand-clay mixtures

Sand-fine mixtures are sands with a portion of silt or clay (Ghafarian et al., 2020; Yin et al., 2021). These soil mixtures are used to understand the mechanical behavior of natural soils (Liu et al., 2018; Yin et al., 2021), since different geotechnical properties can be obtained by varying the percentage of fine portions in the mixture. These mixtures are also known as simplified soils (Xenaki et al., 2003).

For mixtures with non-plastic fines, some investigations have focused on the effects of the fines on the liquefaction resistance of sands (Yamamuro et al., 1998), on the small-strain stiffness and shear strength of silty sands (Salgado et al., 2000), and tailings stability (Fan et al., 2022). In general, these studies among others agree that there is a threshold fines content, ranging between 20% and 30%, in which the behavior of the mix changes from a sand-controlled behavior for low fines percentage to a fine controlled behavior for higher fines percentage (Dash et al., 2011; Rahman et al., 2020; Yang et al., 2005). In general, non-plastic fines present some interesting effects on the liquefaction behavior and shear resistance of sands, as well as an impact in the permeability and compressibility of granular soils (Yamamuro et al., 1998; Yang et al., 2005). Conversely, in the case of sand mixed with plastic fines, some studies have reported positive soil erosion prevention (Reddi et al., 1997) and reduction of settlement in embankments through finding the optimum fine content (Kaothon et al., 2022), while others have focused on the compressional behavior of these soils (Martins et al., 2001; M. M. Monkul et al., 2007; Shi et al., 2018). In general, plastic fines in small quantities tend to generate an increase in certain properties of granular soils like shear strength and compressibility while under the fine content threshold, the properties and its improvement can vary depending on the analyzed soil (M. M. Monkul et al., 2007).

Recently, many studies have addressed the behavior of sand with super plastic fines, in which the fines generate a thixotropic structure in the granular void volume, meaning that the fluid formed between the clays and water form a thixotropic fluid that gains shear stress resistance and viscosity with time (El Howayek, 2011; El Mohtar et al., 2013; Santagata et al., 2014; Shen, 2014). Examples of these studies are the ones conducted with natural bentonite to determine its effect on the liquefaction resistance of soils (El Mohtar et al., 2013; Gratchev et al., 2006), or its use to generate environmental barriers for waste disposal (Meier et al., 2017), and to produce

liners for the nuclear industry (Sellin et al., 2014). Other studies have focused on the effects of the sand type in the behavior of sand-bentonite mixes (Vadlamudi et al., 2018; Wang et al., 2021).

Other highly plastic clayey materials are synthesized in the laboratory, like colloidal silica and Laponite (Wallace et al., 2015). Gallagher & Mitchell (2002) studied the effects of colloidal silica in liquefaction mitigation in Monterey sand also, while Gallagher et al. (2007) studied passive site stabilization with colloidal silica grouting. On the other hand, (Ochoa-Cornejo, 2015b; Ochoa-Cornejo et al., 2014, 2016) studied the use of Laponite as a replacement for bentonite in liquefaction mitigation due to its higher thixotropy and smaller particle size. Table 2-1 summarizes some works performed on sands with plastic and super-plastic fines.

Ochoa-Cornejo (2015) used Ottawa sand with laponite in contents of 1, 3 and 5% by dry mass of sand, finding that laponite increase the liquefaction resistance of Ottawa sand. The dynamic properties of this type of mix, such as, maximum shear modulus and damping were also studied (Ochoa-Cornejo et al., 2020).In addition, Pardo Tobar & Orense (2017) performed cyclic simple shear tests on Mercer sand with 1% laponite, finding an increase in the liquefaction resistance of the mixture. Rodriguez (2019) performed monotonic and cyclic triaxial tests on tailing sand with 1 and 3% of laponite by dry mass of sand, finding that laponite increase the liquefaction resistance of tailing sands. Overall, there is an agreement in that small amounts of laponite have beneficial effects on the liquefaction resistance of loose sand, impacting the dynamic properties, the monotonic behavior, representing an effective liquefaction mitigation agent (Getchell et al., 2022). In addition, the observations agree that the handling of Laponite and the ways it interacts with the granular media have a profound effect on the behavior of the granular material (Getchell et al., 2022; Pardo Tobar et al., 2017).

Although many findings report the positive and promising effect of Laponite as a liquefaction mitigation agent, some interesting challenges related to other potential use of this nanomaterial and its effect on the granular fabric can still be explored. Examples of these challenges are related to the granular structure formed by these mixes in dry conditions, how these mixtures behave when hydrated, and how the granular structure of the mixes formed in dry conditions determine the granular structure when the particle arrangement is in contact with water.

Table 2-1: Studies on sand-clay mix.

Author	Sand	Fine	PI	Tests	Objective	Results
Plastic fines						
(Azam, 2007)	Dhahran sand	Al Qatif Clay	95	Swelling pressure.	Understand the behavior of clay–sand mixes on wetting.	Clay–sand mixes with 10% clay through 40% clay captured the transition from a sand-like behavior to a clay-like behavior.
(M. M. Monkul & Ozden, 2007)	Uniform sand.	Kaolinite	19	Oedometer and direct shear	Investigate the compression behavior of clayey soils by defining the transition fines content and granular compression index parameters.	Transition void ratio is not unique. The transition void ratio is defined as when the skeleton void ratio is equal to the maximum global void ratio of the coarse matrix. The shear strength of soil decreases when the limit fine content is reached.
(Mekkiyah & K Huat, 2015)	Karabala city sand	AL-UBAIDI clay	32	Consolidation.	Investigate the compressional behavior of clay soil under the influence of different fine sand content and defining Transition fines content TFSC of clay-fine sand mixture.	The Transition Fine Sand Content (TFSC) in the clay-sand soil mixture occurred at 55 to 70% of fine sand content.
(Dafalla, 2017)	Concrete sand, uniform sand available in Riyadh	Al Qatif Clay	70-80	Compaction, compressibility and swelling	Examine the compression and swell of sand-expansive clay liners to help designers to optimize and select the appropriate mix.	Addition of less expansive soil material to bentonite can reduce the compressibility by 60% to 70% for10% and 15% clay content, respectively.
(Amri et al., 2019)	Dune sand from the northern region of Zaafrane in the province of Djelfa, Algeria.	Clay from a road project site Ksar el Boukhari-Boughenzoul	41	Atterberg limits, Compaction tests, unconfined compression, triaxial tests and free swelling.	Investigate clayey soil treatment effect by using dune sand on geotechnical, structural, and mineralogical properties.	The addition of dune sand on plastic clay leads to a significant improvement in the geotechnical characteristics: reduction of liquid limit and the limit of plasticity with the decrease of the plasticity index due to the replacement of cohesive clay particles by dune sand.
(Phanikumar et al., 2021)	Fine sand	Amalapuram clay	70	Swell potential and swelling pressure.	Investigate the effect of fly ash and sand on the swelling of clay.	The increase in sand or fly ash content decreases the swelling potential of clays.

Super plastic fines						
(Mollins et al., 1996)	Knapton quarry sand.	Wyoming bentonite	359	Swelling and hydraulic conductivity tests	Investigate the swelling behavior and hydraulic conductivity of Na-bentonite powder and sand/bentonite mixes.	The swelling behavior of the mixtures can be characterized by a threshold stress that is a function of clay content. A very low bentonite content can lead to an uneven bentonite distribution within the mixture.
(Cui et al., 2012)	Quartz sand from Yongdeng in Gansu province in China	GMZ bentonite	195	Swelling pressure and swelling deformation.	Verify the influence of the sand content ratio and the initial dry density on the swelling characteristics of GMZ bentonite–sand mixtures.	With the increase of initial dry density, the maximum swelling pressure increase exponentially and the maximum swelling strain increase.
(Vadlamudi & Mishra, 2018)	Local available sand	Bentonite	313-568	Oedometer	Understand the influence of sand particle size on the consolidation characteristics of sand–bentonite mixtures.	The particle size of the sand has a definite influence on the coefficient of consolidation, the coefficient of volume change, the time needed to reach 90% consolidation, and the compression index.
(Wang et al., 2021)	Natural quartz sand	GMZ bentonite	239	Swelling test.	Identify the effect of sand grain size on the micro structural behavior and macroscopic swelling of bentonite–sand mixtures with varying boundary conditions.	The swelling process is affected by the boundary conditions of the test's apparatus. An increase in particle size causes a decrease in swelling pressure and strain.

2.1.1 Experimental studies on sand-clay mixtures

Some studies of sand-clay mixes are presented to contextualize the mechanical behavior of sands with plastic fines, focusing on the void ratio characterization, shear strength properties, and consolidation behavior.

Vallejo & Mawby (2000) investigated the behavior of the void ratio of dry Ottawa sand with varying contents of dry kaolinite (PI = 30%), revealing that the maximum and minimum void ratio exhibited a decreasing to a threshold fines content, beyond which they increased, as shown in Figure 2-1a). The observations suggest that, as the fines portion increases the particles tend to accommodate in the pore space of the granular structure of sand particles. However, as the fines content reaches the threshold, the void ratio starts to increase as the fines enter sand particles contact, similar to the case of sands with non-plastic fines. In the same study, direct shear tests on Ottawa sand and dry kaolinite with a plasticity index showed that the residual strength is uniform, regardless of the fines content, as shown in Figure 2-1 b). On the other hand, Monkul & Ozden (2007) conducted simple shear tests on sand mixed with kaolinite, showing that the peak shear strength diminishes progressively with an increase in fines content (Figure 2-1 c)).

Regarding consolidation behavior of these types of materials, Monkul et al. (2005) studied the unidimensional compression of a wet mixture of sand with different concentrations of kaolinite (IP 19%) to address the influence of the intergranular void ratio on the one-dimensional compression of the soil, reporting there is a fines content threshold -approximately 23% of fines- below which the behavior of the soil is controlled by the granular matrix, while beyond the threshold the behavior is controlled by the fine portion of the material. The study also reported that this threshold is not constant, but depends on factors such as the effective stress, void ratio, and maximum void ratio of the granular matrix. To analyze the state of the coarse particles granular arrangement, the parameter “granular compression coefficient” Cc-s is defined, based on the decrease in the skeleton void ratio with the increase in compression stress (M. Monkul et al., 2005).

$$C_{c-s} = \frac{\Delta e_{sk}}{\Delta \log(\sigma)} \qquad 1$$

The granular compression coefficient represents the slope of the skeleton void ratio versus the compression stress, reflecting the behavior of coarse particles under compression. Small values of Cc-s implies small compression, while higher values of Cc-s suggest higher compression. The granular compression coefficient, under the same compression stress and different fine content, distinguishes the effect of the fine content on the behavior of the samples. Generally, an increase in the fine content results in an increase in the Cc-s, indicating greater compressibility. Figure 2-1

d) shows the variation in the granular compression coefficient from M. Monkul et al. (2005). There is a non-linear relationship between Cc-s and the content of fines, FC. The intersection of the tangent of these curves represents the limit fines content, in this case around 23-25%. Similar works have been performed by Shi & Yin (2017) and Vijaya Kumar (1996) on mixtures of sands and plastic soils. Therefore, the behavior of sand-clay mixtures is heavily reliant on the properties of each clay and sand components, with practical applications vary depending on the proportions used, as well as the thresholds delimiting when the mixture exhibit clay-like characteristics.

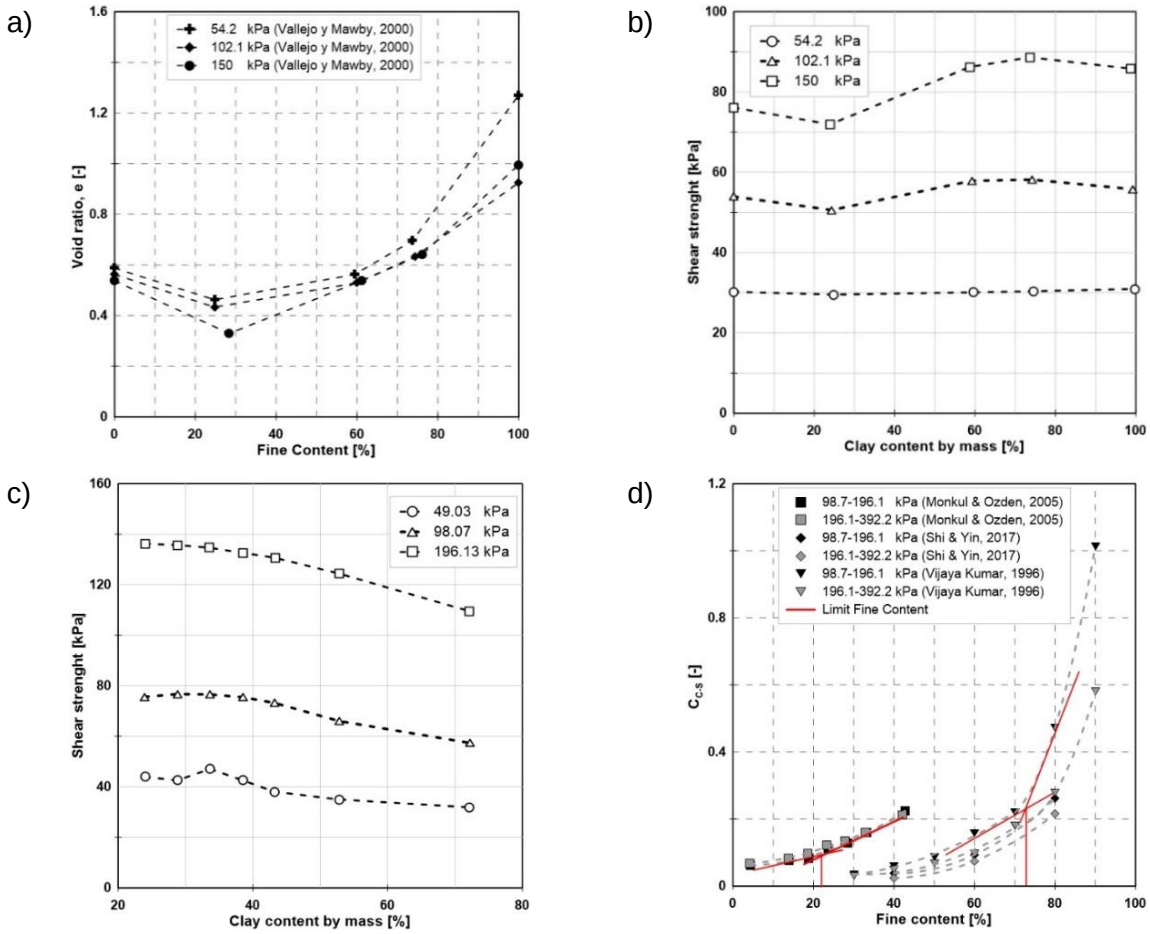

Figure 2-1: a) Void ratio of dry Ottawa sand with kaolinite at different compression strength (Vallejo & Mawby, 2000), b) Peak shear strength of sand-clay mix vs fine content (Vallejo & Mawby, 2000), c) Peak shear strength vs fine content in direct shear (M. Monkul & Ozden, 2007) and d) Variation of the granular compression ratio with the content of fines.

2.2 Factors that influence the mechanical response of the mixtures

2.2.1 Void ratio

2.2.1.1 Global void ratio

The global void ratio or void ratio (e) is defined as the relation between the void volume and the solid volume of a soil, it has been extensively used in soil mechanics as a density parameter to characterize the behavior of a soil (J. Yang et al., 2015). For example, the density-dependent stress-strain behavior of sands has been characterized in the framework of critical state soil mechanics, which defines a single critical state line in the space of void ratio and effective stress (J. Yang et al., 2015).

$$e_{global} = \frac{V_{void}}{V_{solid}} \quad 2\text{-}2$$

2.2.1.2 Skeleton void ratio

When clays or silts are mixed with sands, their behavior is modified; it is for these cases where the global void ratio may not be effective to characterize the behavior of the soil. Based on the hypothesis that the fines can be located in the interparticle spaces of the sand, the skeleton void ratio is defined as the ratio between the volume of voids plus the volume of fines and the volume of coarse solids (J. Yang et al., 2015). In this way, it is considered that the fines do not contribute to the transfer of stresses between particles.

$$e_{skeleton} = \frac{V_{void} + V_{fines}}{V_{coarse}} \quad 2\text{-}3$$

$$= \frac{V_v}{V_c} + \frac{V_f}{V_c} \quad 2\text{-}4$$

$$= \frac{V_v}{V_c}\left(\frac{V_c + V_f}{V_c + V_f}\right) + \frac{V_f}{V_c} \quad 2\text{-}5$$

$$= \frac{V_v}{V_c + V_f}\left(\frac{V_c + V_f}{V_c}\right) + \frac{V_f}{V_c} \quad 2\text{-}6$$

$$= e\left(\frac{1}{1 - FC}\right) + \frac{V_f}{V_c} \quad 2\text{-}7$$

$$= \frac{e}{1 - FC} + \frac{V_f}{V_c}\left(\frac{V_c + V_f}{V_c + V_f}\right) \quad 2\text{-}8$$

$$= \frac{e}{1 - FC} + \frac{FC}{1 - FC} \quad \text{2-9}$$

$$= \frac{e + FC}{1 - FC} \quad \text{2-10}$$

However, it should be mentioned that this definition does not differentiate between the specific gravity of fines and coarses particles, in addition the content of fines FC is expressed as a function of the total mass of soil.

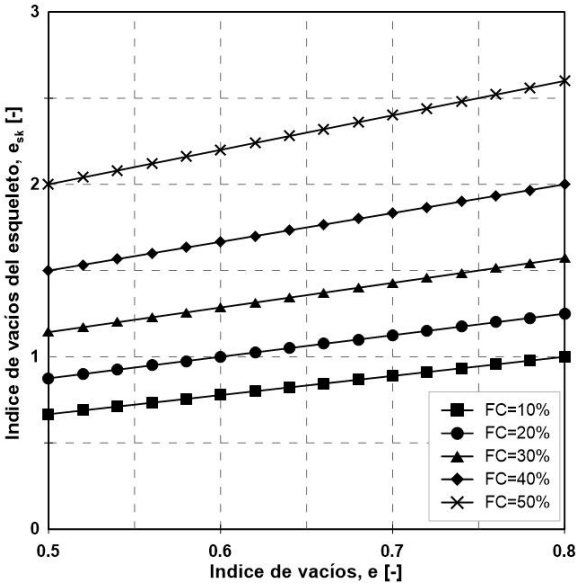

Figure 2-2: Skeleton void ratio sensitivity analysis.

As can be seen in Figure 2-2, the skeleton void ratio varies linearly with the increase in the global void ratio, and it also presents an important variation according to the fines content. For the same global void ratio, the skeleton void ratio can be more than two times its original value with a 50% change in fines content.

2.2.1.3 Equivalent skeleton void ratio

Considering that the above situation is ideal and unrealistic since it assumes that no particles are located in the contacts of the coarse particles, another definition of void ratio has been developed. This time with a portion of the fine particles located in the intergranular spaces and another located in the contact zone between particles, so that a percentage of these contributes to the transmission of stress and the other does not. Therefore, a parameter b is defined that represents the portion of particles found in the intergranular spaces.

$$e_{eqsk} = \frac{e + (1-b)FC}{1-(1-b)FC} \qquad 2\text{-}11$$

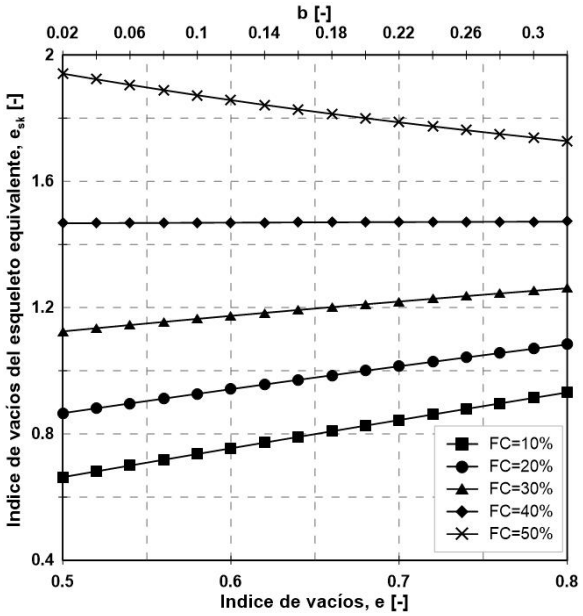

Figure 2-3: Equivalent skeleton void ratio sensitivity analysis.

As observed in Figure 2-3 and from Equation 2-11 for the case where b=0 the results correspond to the skeleton void ratio. With the increase in the fines content, the equivalent skeleton void ratio increases, therefore it is sensitive to the variation of fines; however, with the increase of the parameter b, the equivalent skeleton void ratio decreases, tending to converge in a point, from the equation it can be seen that if b=1 the global void index is equal to that of the equivalent skeleton. The equation is sensitive to both the parameter b and the content of fines.

2.2.1.4 Void ratio summary

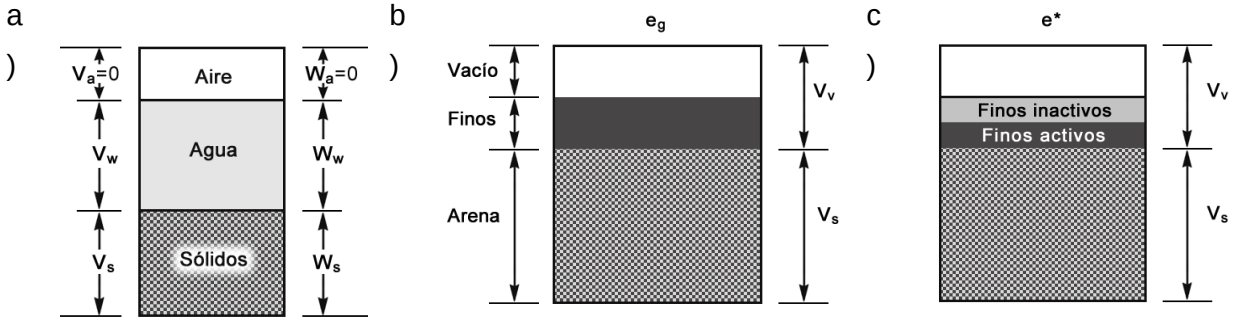

Figure 2-4: Phase diagram a) global void ratio, b) skelton void ratio and c) equivalent skeleton void ratio.

- Global void ratio

$$\boldsymbol{e = \frac{V_V}{V_S + V_f}} \quad \text{2-12}$$

- Skeleton void ratio

$$\boldsymbol{e_{sk} = \frac{V_V + V_f}{V_S}} \quad \text{2-13}$$

- Equivalent skeleton void ratio

$$\boldsymbol{e_{ske} = \frac{V_V + V_{fna}}{V_S + V_{fa}}} \quad \text{2-14}$$

2.2.1.5 Void ratio relation

It is possible to find a relationship between the void ratios assuming different specific gravities and expressing the fines content as a function of sand mass.

$$e_{skeleton} = \frac{V_v + V_f}{V_c} \quad \text{2-15}$$

$$= \frac{V_v}{V_c} + \frac{V_f}{V_c} \quad \text{2-16}$$

$$= \frac{V_v}{V_c}\left(\frac{V_c + V_f}{V_c + V_f}\right) + \frac{V_f}{V_c} \quad \text{2-17}$$

$$= \frac{V_v}{V_c + V_f}\left(\frac{V_c + V_f}{V_c}\right) + \frac{V_f}{V_c} \quad \text{2-18}$$

$$= e\left(\frac{V_c + V_f}{V_c}\right) + \frac{V_f}{V_c} \quad (2\text{-}19)$$

$$= e\left(\frac{V_c}{V_c} + \frac{V_f}{V_c}\right) + \frac{V_f}{V_c} \quad (2\text{-}20)$$

$$= e\left(1 + \frac{V_f}{V_c}\right) + \frac{V_f}{V_c} \quad (2\text{-}21)$$

$$= e + e\frac{V_f}{V_c} + \frac{V_f}{V_c} \quad (2\text{-}22)$$

$$= e + \frac{V_f}{V_c}(e + 1) \quad (2\text{-}23)$$

$$= e + \frac{W_f G_{sg}}{W_g G_{sf}}(e + 1) \quad (2\text{-}24)$$

$$= e + FC\frac{G_{sg}}{G_{sf}}(e + 1) \quad (2\text{-}25)$$

As can be seen in Figure 2-5, the skeleton void ratio is almost insensitive to the change in specific gravity between fines and coarse particles.

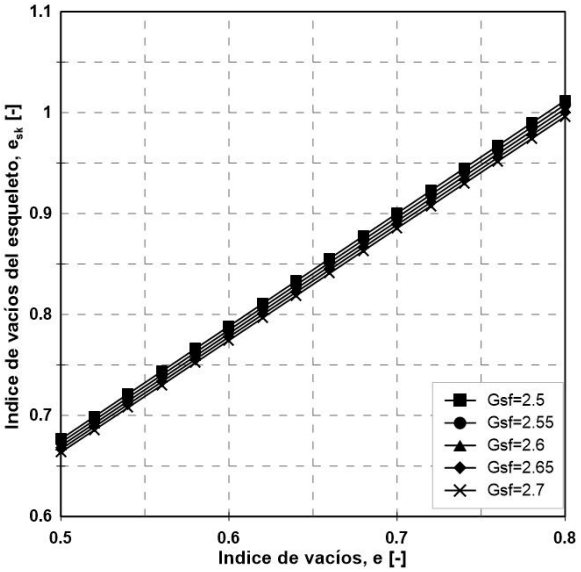

Figure 2-5: Void ratio relation sensitivity analysis.

2.2.2 Fines in asperities

2.2.2.1 Asperity definition

The surface of soil particles is not smooth, especially when examined on a small scale (H. Yang et al., 2016). The roughness of the surface has effects on the packing, the shear modulus, the behavior against compression and shear strength of the soil.

2.2.2.2 Asperities size and shape

The roughness of a particle can have different sizes and shapes depending on the type of fine or coarse particle and the soil being tested.

The theoretical exercise of determining the influence of roughness can be carried out, for example, in the amount of fine particles that could be located in the spaces between them. For this, perfectly round particles with triangular asperities and as semicircles are assumed.

2.2.2.3 Fine particles in asperities calculations

An interesting exercise that sheds light on how important it is to consider roughness when modeling a particle is to determine in a theoretical and simplified way the amount of fine particles that could be located only on the roughness of a sand particle.

To do this, a flat particle of 0.216 mm in diameter and semicircular asperities with a radius of 0.0008 mm will be assumed, the average radius of asperities in sands (Alshibli et al., 2004). Then a circle is drawn that surrounds all the asperities and the available area in the enclosed space is determined, this is repeated for triangular shaped asperities. With this it:

Table 2-2: Type and size of roughness.

Asperities	Available area [mm^2]
Circular	11.875*10^-5
Triangular	26.927*10^-5

If this is transformed into a mass of fines, it is equivalent to 0.3% of the sand mass for circular asperities and 0.7% for triangular asperities.

2.2.3 Particle diameter

Digital image analysis provides the ability to rapidly analyze the characteristics of a particle (Kuo et al., 1996). There are multiple ways to measure the size of an irregular particle profile in the microscope, these are chosen according to their theoretical significance or ease of measurement (Walton, 1948).

The size can be defined by the diameter of the circle with the same perimeter as the projection of the particle, the dimensions of the particle in various directions, the opening of the finest sieve that the particle can pass through or the average diameter of the particle (Santamarina et al., 2001) (Walton, 1948). Within these we can define three in particular:

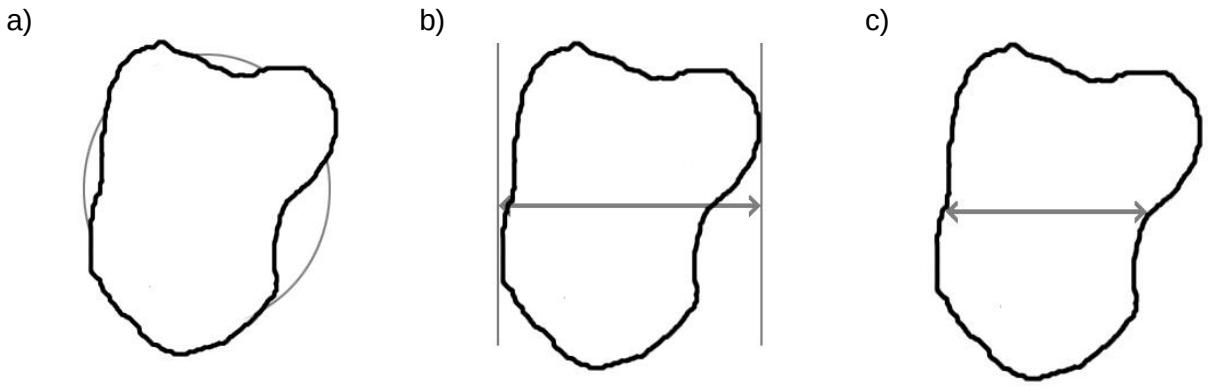

Figure 2-6: a) Equivalent diameter, b) Feret`s diameter y c) Martin`s diameter (Santamarina et al., 2001).

- Equivalent diameter: Diameter of the circle of equal area to the projection of the particle.

- Feret`s diameter: Distance between two parallel lines tangent to opposite sides of the particle projection (Walton, 1948)**.**

- Martin`s diameter: Length of the bisector of the area of the projection of the particle (Walton, 1948).

2.2.4 Interparticle forces

Interparticle forces can be classified according to the location of their generating mechanism. (Santamarina, 2003).

2.2.4.1 Granular skeleton forces

Forces transmitted along granular chains formed by the soil skeleton (Santamarina, 2003).

To determine the behavior of the contacts between soil particles it is necessary to know the Hertzian contact theory, which deals with the way to resolve the contact between two bodies.

2.2.4.2 Hertzian contact theory

The contact of any axially symmetric body can be resolved by the multifactorial dimensionality reduction algorithm or MDR. This algorithm represents three-dimensional contacts as contacts of a one-dimensional array of independent springs (Wrinkler foundation).

The resolution of a contact problem by MDR requires:

- Replace the three-dimensional elastic or viscoelastic body with a Winkler foundation.

In the case of elastic bodies, the foundation consists of linear-elastic springs with normal stiffness.

$$\Delta k_z = E^* \Delta x \qquad 2\text{-}26$$

Where E^* is given

- Second the three-dimensional profile z=f(r) is transformed to a planar profile g(x) (Figure 2-7)

$$g(x) = |x| \int_0^{|x|} \frac{f`(r)}{\sqrt{x^2 - r^2}} dr \qquad 2\text{-}27$$

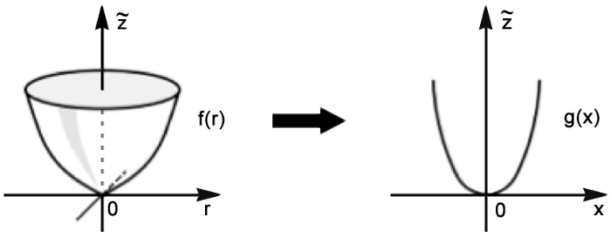

Figure 2-7: Three-dimensional profile to plane profile (V. L. Popov et al., n.d.).

Now the plane g(x) is pressed into the elastic foundation with a normal force F_N.

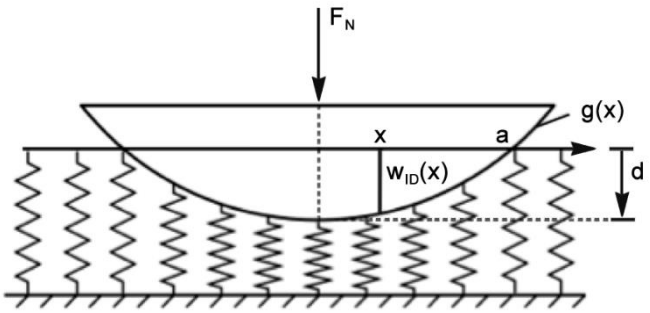

Figure 2-8: Plane pressed against elastic foundation (V. L. Popov et al., n.d.).

The displacement of the normal surface at a position x in the contact area is equal to the difference between the indentation depth and the profile shape g:

$$w_{1D}(x) = d - g(x) \tag{2-28}$$

At the edges of the contact, x=+-a, the displacement of the surface must be zero

$$w_{1D}(\pm a) = 0 \rightarrow d = g(a) \tag{2-29}$$

This equation determines the relationship between the indentation depth and the contact radius a. This relationship is independent of the elastic properties of the medium.

The force of a spring at a position x is proportional to the displacement at this position.

$$\Delta F_N(x) = \Delta k_z w_{1D}(x) = E^* w_{1D}(x) \Delta x \tag{2-30}$$

The sum of all the spring forces must equal the external normal force. In the limiting case of very small spring spacing, the sum becomes an integral:

$$F_N = E^* \int_{-a}^{a} w_{1D}(x)dx = 2E^* \int_{0}^{a} [d - g(x)]dx \tag{2-31}$$

This equation provides the normal force as a function of the contact radius considering the depth of indentation. Now, defining the linear force density:

$$q_z(x) = \frac{\Delta F_N(x)}{\Delta x} = E^* w_{1D}(x) = E^* \begin{cases} d - g(x), |x| < a \\ 0, |x| > a \end{cases} \tag{2-32}$$

The stress distribution in the original three-dimensional system can be determined from the one-dimensional linear force density by the integral:

$$\sigma_{zz}(r) = -p(r) = \frac{1}{\pi}\int_{r}^{\infty} \frac{q`_z(x)}{\sqrt{x^2 - r^2}}dx \qquad 2\text{-}33$$

The normal displacement of the surface w(r) is given by the transform (V. Popov, n.d.):

$$w(r) = \frac{2}{\pi}\int_{0}^{r} \frac{w_{1D}(x)}{\sqrt{r^2 - x^2}}dx \qquad 2\text{-}34$$

2.2.4.3 The sphere problem

The profile of a sphere of radius R can be defined as:

$$f(r) = R - \sqrt{R^2 - r^2} \qquad 2\text{-}35$$

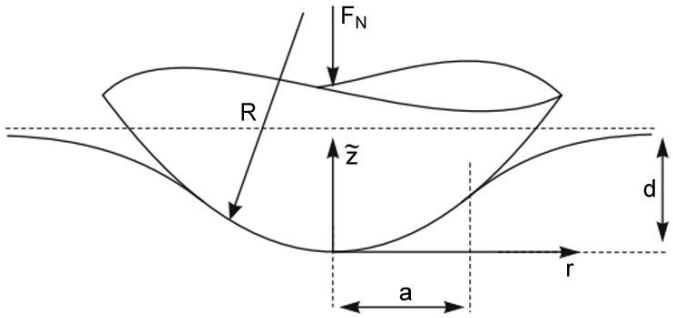

Figure 2-9: Sphere problem (V. L. Popov et al., n.d.).

For the case where r<<R this function can be approximated as:

$$f(r) \approx \frac{r^2}{2R} \qquad 2\text{-}36$$

Which agrees with Hertz's classical work of a normal indentation with a parabolic shape, assuming a contact radius a much smaller than the sphere radius R. The solution is given by:

$$g(x) = \frac{|x|}{R}\int_{0}^{|x|} \frac{rdr}{\sqrt{x^2 - r^2}} = \frac{x^2}{R} \qquad 2\text{-}37$$

$$d(a) = \frac{a^2}{R} \tag{2-38}$$

$$F_N(a) = \frac{2E^*}{R}\int_0^a (a^2 - x^2)dx = \frac{4}{3}\frac{E^* a^3}{R} \tag{2-39}$$

And by:

$$\sigma_{zz}(r;a) = -\frac{2E^*}{\pi R}\int_r^a \frac{x}{\sqrt{x^2 - r^2}}dx = -\frac{2E^*}{\pi R}\sqrt{a^2 - r^2}, \qquad r \le a, \tag{2-40}$$

$$w(r;a) = \frac{2}{\pi R}\int_0^a \frac{(a^2 - x^2)}{\sqrt{r^2 - x^2}}dx = \frac{a^2}{\pi R}\left[\left(2 - \frac{r^2}{a^2}\right)\arcsin\left(\frac{a}{r}\right) + \frac{\sqrt{r^2 - a^2}}{a}\right], \qquad r > a \tag{2-41}$$

The average pressure at the contact is equal to:

$$p_0 = \frac{4E^* a}{3\pi R} \tag{2-42}$$

Despite this, if the solution is considered without the approximation, the following equations are obtanined:

$$g(x) = |x|\int_0^{|x|} \frac{rdr}{\sqrt{R^2 - r^2}\sqrt{x^2 - r^2}} = |x| artanh\left(\frac{|x|}{R}\right) \tag{2-43}$$

$$d(a) = a\ artanh\left(\frac{a}{R}\right) \tag{2-44}$$

$$\begin{aligned} F_N(a) &= 2E^*\int_0^a \left[a\ artanh\left(\frac{a}{R}\right) - x\ artanh\left(\frac{x}{R}\right)\right]dx \\ &= E^* R^2\left[\left(1 + \frac{a^2}{R^2}\right) artanh\left(\frac{a}{R}\right) - \frac{a}{R}\right] \end{aligned} \tag{2-45}$$

The average pressure at the contact is:

$$p_0 = \frac{E^* R^2}{\pi a^2}\left[\left(1 + \frac{a^2}{R^2}\right) artanh\left(\frac{a}{R}\right) - \frac{a}{R}\right] \tag{2-46}$$

Stresses and displacements can only be partially expressed by elementary functions (V. L. Popov et al., n.d.):

$$\sigma_{zz}(r;a) = -\frac{E^*}{\pi}\int_r^a \left[\frac{xR}{R^2-x^2} + artanh\left(\frac{x}{R}\right)\right]\frac{dx}{\sqrt{x^2-r^2}} = -\frac{2E^*}{\pi R}\sqrt{a^2-r^2}, \qquad 2\text{-}47$$

$$= -\frac{E^*}{\pi}\left[\frac{R}{\sqrt{R^2-r^2}}artanh\left(\frac{\sqrt{a^2-r^2}}{\sqrt{R^2-r^2}}\right) + \int_r^a artanh\left(\frac{x}{R}\right)\frac{dx}{\sqrt{x^2-r^2}}\right], \quad r \le a, \qquad 2\text{-}48$$

$$w(r;a) = \frac{2}{\pi}\left[a\ artanh\left(\frac{a}{R}\right)arcsin\left(\frac{a}{r}\right) - \int_0^a x\ artanh\left(\frac{x}{R}\right)\frac{dx}{\sqrt{r^2-x^2}}\right], \qquad 2\text{-}49$$

$$= \frac{2}{\pi}\left\{\begin{array}{c} artanh\left(\frac{a}{R}\right)\left[a\ arcsin\left(\frac{a}{r}\right) + \sqrt{r^2-a^2}\right] - R\ arcsin\left(\frac{a}{r}\right) \\ +\sqrt{R^2-r^2}arctan\left(\frac{a\sqrt{R^2-r^2}}{R\sqrt{r^2-a^2}}\right) \end{array}\right\}, r > a \qquad 2\text{-}50$$

If the sensitivity of the equations, both the approximate one and the one without approximation, is analyzed, it is found that for r<<R both solutions are practically the same, so the approximation is a valid solution for a relationship between a and R less than 0.2. In turn, the solution is very sensitive to the variation of the radius of the spherical particle that rests on the elastic surface.

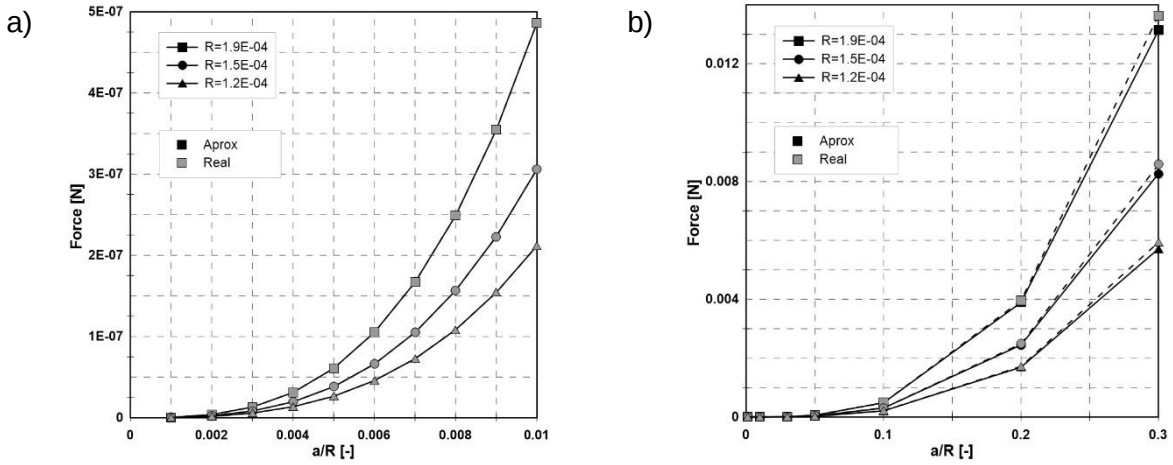

Figure 2-10: Sphere problem sensitivity analysis.

2.2.4.4 Santamarina`s definition of the granular skeleton forces

Santamarina (2003) defines the normal forces N and tangential forces T that develop in the particles contacts when an effective effort is applied at the edges. The normal force n on the contacts is related to the applied effective stress and the particle diameter d. The first order approximation $N=d^2\sigma$ is correct for a simple cubic packing of spheres of equal size. For a random

packing of spheres, the average normal contact force N is related to the void ratio e through empirical or semi-empirical correction functions, representing functions like the following.

$$N = \sigma` d^2 \left[\frac{\pi(1+e)^2}{12}\right] \quad \text{2-51}$$

2.2.4.5 Gravitational forces

Forces associated with the weight of the particles, considering that they are spherical, can be defined as:

$$W = \frac{1}{6}\pi G_s \gamma_w d^3 \quad \text{2-52}$$

2.2.4.6 Electrical forces

The van der Waals attraction between two spherical particles of equal diameter is:

$$Att = \frac{A_h}{24t^2} d \quad \text{2-53}$$

Where t is the separation between the particles, A_h is Hamaker's constant, which for the case of silica-water-silica is 0.64*10-20 [J] (Santamarina, 2003).

Israelachvili (2011) defines the electrical attraction between two flat particles per unit area as:

$$F = \frac{-A_h}{6\pi D^3} \quad \text{2-54}$$

With D the distance between the particles and F in J/m^3.

2.2.4.7 Capillary forces

A molecule in a fluid experiences attractive Van der Waals forces to the surrounding molecules. These forces act in all directions, so they tend to cancel out, however, this is not the case for the water molecules on the surface of the fluid, they feel an effective attractive force normal to the surface of the fluid. Observing this on a macro scale creates a surface tension T_s that characterizes the interface (T_s =0.0727 N/m for water-air interaction at room temperature). As this generated membrane tends to shrink, the fluid inside has a positive tension. This stress is calculated using Laplace's equation (Santamarina, 2003).

$$u = T_s\left(\frac{1}{r_1} + \frac{1}{r_2}\right) \quad \text{2-55}$$

With r1 and r2 the radius of the air-water interface. As already mentioned, the surface tension T_s will depend on the fluids involved, a summary of the surface tension of some fluids interacting with air is presented below.

Table 2-3: Surface tensión of different fluids.

Substance	T_s(mN/m)
Water	71.9
Toluene	27.9
Benzene	28.2
Glycerin	59.4
Petroleum	26

2.2.4.7.1 Spherical particles

Considering two spherical particles of radius R in contact. The water meniscus between them is confined by the two particles and an imaginary toroid, the radius of the toroid is r1, and the distance from the center to the inner wall of the toroid is r2, as shown in Figure 2-11, for the case of the toroid this radius is negative.

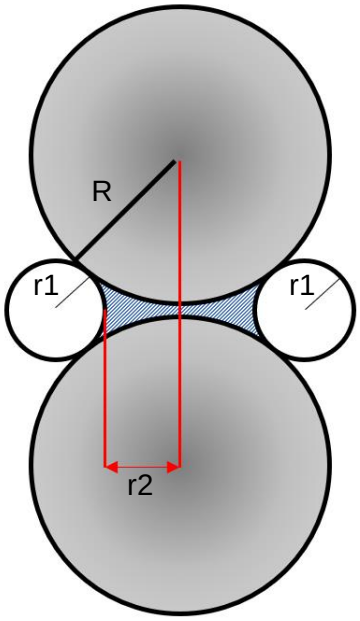

Figure 2-11: Water meniscus between two spherical particles.

The contact force that the meniscus imposes on the particles is the resultant between the fluid pressure acting on the cross-sectional area of the meniscus and the surface tension acting around the perimeter.

$$F = u(\pi r_2^2) + T_s(2\pi r_2) \quad \text{2-56}$$

This analysis assumes that the contact between the particles is punctual. For the geometry of the toroid assumed for the meniscus:

$$(R + r_1)^2 = R^2 + (r_1 + r_2)^2 \quad \text{2-57}$$

$$r_1 = \frac{r_2^2}{(2R - 2r_2)} \quad \text{2-58}$$

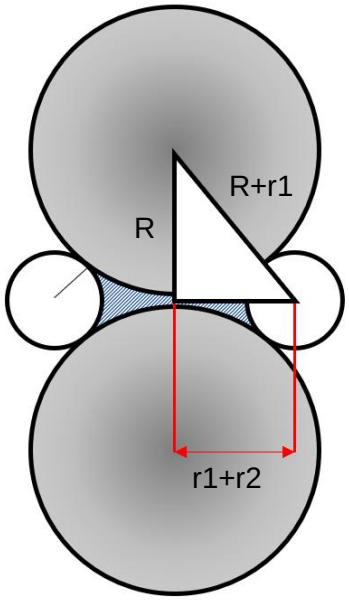

Figure 2-12: Geometry of the toroid.

The choice of the geometry of the toroid implies several assumptions, first that the contact angle between the surface of the water and the particles is zero and that these do not have asperities. Second, that the effect of gravity on the geometry of the meniscus is negligible.

If an alpha variable is considered:

$$\alpha = \frac{r_2}{R} \quad \text{2-59}$$

And if the equations 2-58 and 2-56 are replaced, it remains that:

$$u = T_s\left(\frac{2(R-r_2)}{r_2^2} - \frac{1}{r_2}\right) = \frac{T}{R\alpha}\left(\frac{2}{\alpha} - 3\right) \quad \text{2-60}$$

Then the force is:

$$F = T_s \pi R(2-\alpha) \quad \text{2-61}$$

The effective stresses can be estimated for a given arrangement of particles, for a simple cubic arrangement, the force is distributed over the effective area used by a particle, $4R^2$.

$$SC\ \sigma`_{eq} = \frac{F}{4R^2} = \frac{\pi T_s}{4R}(2-\alpha) \quad \text{2-62}$$

If the geometry of the meniscus between two particles is considered, the volume of the meniscus can be calculated in terms of the diameter of the particle and the radius of the meniscus. Furthermore, the calculated volume can be related to the moisture content w. For a single cubic packing the water content is**:**

$$SC\ w = \frac{9}{8G_s}\left(\frac{\alpha^4}{1-\alpha^2}\right)\left[1 - \frac{\alpha(2-\alpha)}{2(1-\alpha)} arcsin\left(\frac{2(1-\alpha)}{\alpha^2 + 2(1-\alpha)}\right)\right] \quad \text{2-63}$$

Where Gs is the specific gravity, for small values of alpha the first-order Taylor expansion is:

$$w = \frac{9}{8G_s}\left(\frac{r_2}{R}\right)^4 \quad \text{2-64}$$

The equations allow to determine the capillary force in the contact between two equal spherical particles in terms of their size (Santamarina et al., 2001).

$$F = T_s R\pi\left[2 - \left(\frac{8}{9} w G_s\right)^{\frac{1}{4}}\right] \quad \text{2-65}$$

$$SC\ \sigma`_{eq} = \frac{\pi T_s}{4R}\left[2 - \left(\frac{8}{9} w G_s\right)^{\frac{1}{4}}\right] \quad \text{2-66}$$

2.2.4.7.2 Flat particles

For the case of two flat particles, the radius r2 is much greater than r1, so the term 1/r2 can be ignored in Laplace's equation, so that the suction remains only in terms of r1. Also, the separation between the particles is twice r1, so the water content for equispaced disks is:

$$w = \frac{W_w}{W_s} = \frac{A2r_1\gamma_w}{W_s} = \frac{2A}{W_s/g} r_1 \frac{\gamma_w}{g} = S_a r_1 \frac{\gamma_w}{g} \qquad 2\text{-}67$$

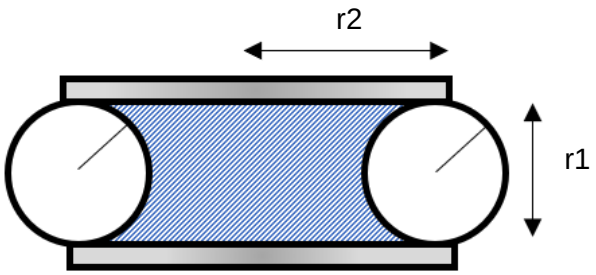

Figure 2-13: Meniscus between two flat particles.

Where A is the surface area of a particle, γw is the unit weight of water, S_a is the specific surface area, and g is gravity. Solving the equation for r1 and substituting into Laplace's equation, the suction becomes:

$$u = T_s \frac{1}{r_1} = T_s \left(\frac{S_a \gamma_w}{wg}\right) \qquad 2\text{-}68$$

Finally, the interparticle force due to capillary forces is:

$$F = \frac{T_s S_a \gamma_w}{wg} \pi r_2^2 \qquad 2\text{-}69$$

2.2.4.8 Capillary forces with Hertzian contact

If the deformation of the particles when they come into contact together with the effects of capillary forces is taken into account, the equation 2-40 must be replaced in equation 2-39, and an expression for the stress distribution is obtained in the parabolic contact.

$$\sigma_{zz} = \frac{3F_N}{2\pi a^3}\sqrt{a^2 - r^2} \quad \text{2-70}$$

$$= \frac{3F_N}{2\pi a^2}\sqrt{1 - \left(\frac{r}{a}\right)^2} \quad \text{2-71}$$

With r the distance from the center of the contact and a the radius of the contact. From equation 2-71:

$$a^3 = \frac{RF_N}{E}\frac{3}{4} \quad \text{2-72}$$

$$\frac{a}{R} = \sqrt[3]{\frac{3F_N}{4R^2E}} \quad \text{2-73}$$

The force F_N distributed across the contacts can be expressed in terms of the average normal stress for an equivalent continuous medium σ. For SC simple cubic packing the area contribution for a sphere is $4R^2$, so $F_N=4\sigma R^2$. The radius of contact in terms of the applied stress

$$\frac{a}{R} = \sqrt[3]{\frac{3\sigma}{E}} \quad \text{2-74}$$

The area affected by the meniscus between two spherical particles in the unsaturated condition is reduced by the contact area, which depends not only on the skeletal strength, but also on the contribution of the meniscus to the local force. Combining Hertz's theory with the capillary force calculated in equation 2-66 the corrected area is (Santamarina et al., 2001):

$$\frac{a}{R} = \sqrt[3]{\frac{3}{E}\left\{\sigma + \frac{\pi T_s}{4R}\left[2 - \left(\frac{8}{9}wG_s\right)^{\frac{1}{4}}\right]\right\}} \quad \text{2-75}$$

2.2.4.9 Particle size and predominant forces

To determine the relationship that exists between the interparticle forces, their dependence on the diameter of a particle was graphed, in Figure 2-14 it is shown that the predominant forces for

coarse particles according to the USCS are Weight and capillarity, on the other hand for fine particles are the electric forces of Van der Waals.

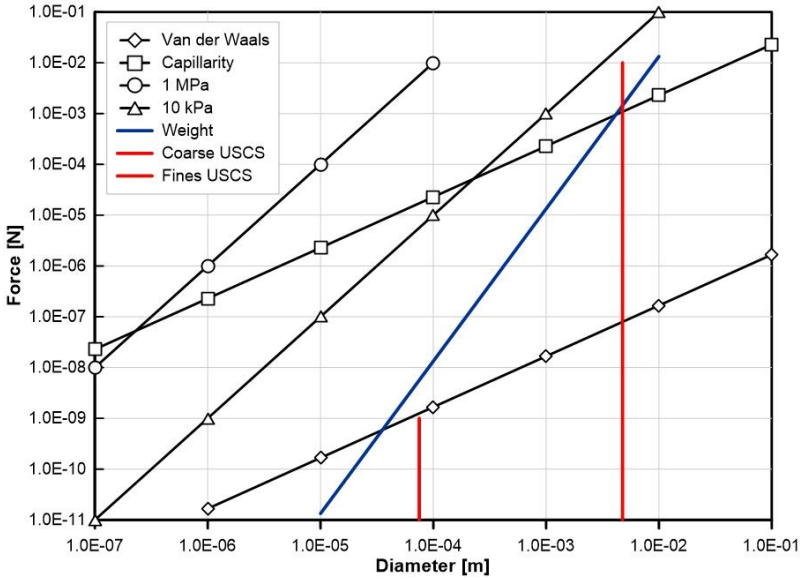

Figure 2-14: Force versus particle size (Santamarina 2003).

3 Laponite

The term “nanomaterial” was first introduced by Richard Feynman, in his 1960 talk, he described them as a valuable tool for numerous fields of research. Since then, significant contributions have been made in the realm of nanomaterials. Notably, in 1981, Heinrich Rohrer and Gerd Binning created the Scanning Tunneling Microscope (STM), which allows for imaging surfaces on an atomic level. In 1985, Harold Kroto discovered the backminsterfullerene, recognized as the first nanomaterial. In 1991, Sumio Iijima discovered multiwall carbon nanotubes, and in 2004, Andre Geim and Konstantin Novoselov discovered graphene. From a technical perspective, the International Organization for Standardization (ISO) defines the term "nano" as referring to dimensions between 1 and 100 nm (ISO, 2008).

Presently, research on nanomaterials enjoys widespread popularity and is making significant contributions to several fields of vital importance, including science, technology, engineering, medicine, and others (Dolez, 2015). From an industrial viewpoint, the global nanomaterial market was valued at a range between USD 4.1 and 14.7 billion in 2015, and it was predicted to increase to between USD 11.3 and 55 billion by 2020 and 2022 (Inshakova & Inshakov, 2017).

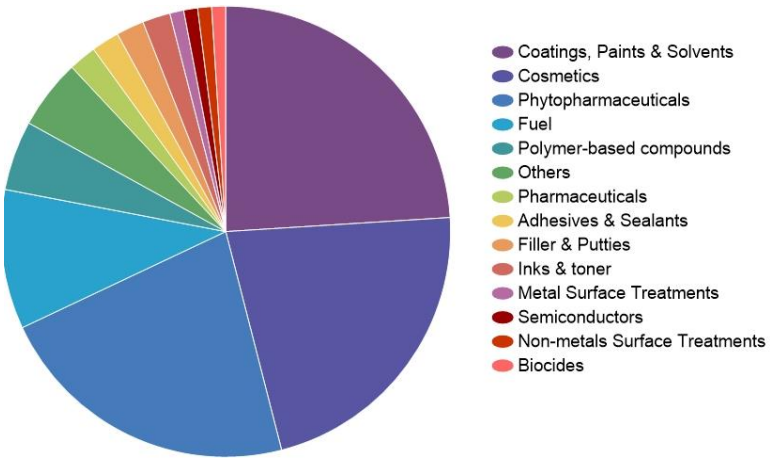

Figure 3-1: Distribution of nano-enabled products on the 2014 compilation of the mandatory declaration of produced and imported manufactured nanomaterials in France (Dolez, 2015).

There are several classifications of nanomaterials based on different criteria, including origin, preferential dimensions, and chemistry (Das & Ansari, 2009). The origin classification refers to whether the material is natural or artificially synthesized. Preferential dimensions classify nanomaterials based on their size and shape, such as uni, bi, or three-dimensional nanomaterials. The chemistry classification considers the composition of the nanomaterial and the elements and

compounds forming its structure, such as metal alloys, metal oxides, semiconductors, silicates, and more. Each of these classifications helps to determine the suitability of a nanomaterial for specific industrial applications (Das & Ansari, 2009). Table 3-1 provides further details on these classifications.

Table 3-1: Nanomaterial classification (Das & Ansari, 2009).

Dimensions		Origin						
		Anthropogenic						Natural
		Polymers	**Nano objects based on carbon**	**Silicates, carbonates y nitrites**	**Semiconductors**	**Metal oxides**	**Metal and metal alloys**	
0D	Quantum dots Hollow spheres Full spheres	Thermoplastics Thermosets Elastomers	Fullerenes			Anatase titanium dioxide		
1D	Nanofibers Nanotubes Nanorods	Thermosets Elastomers	Graphenes	Boron nitride Halloysite	Nano silicone		Platinum, Copper and Tungsten	Halloysite
2D	Nanoplates Nanocoating Nanofilms			Clay	Nano silicone	Zinc oxide Anatase titanium dioxide		Smetic clay
3D	Nano composites Nano-structured materials							Bones

Nanomaterials find applications in several industries, including pharmaceuticals, cosmetics, clothing, glass, automotive, aerospace, and antibacterial agents (Charitidis et al., 2014). Additionally, they have numerous scientific and technological applications, such as in catalysis, photochemistry, sensors, tagging, optical electronics, and magnetic devices (Das & Ansari, 2009).

Engineering is no exception to the fields in which nanomaterials are applied, in civil engineering are used to generate stronger structural composites, lighter structures, enhanced properties of cementitious materials, and improved heat and sound insulation, among others (Daniyal et al., 2018).

In the construction industry, nanomaterials are commonly used to enhance the properties of concrete. For instance, carbon nanotubes are used to increase the mechanical and thermal properties of concrete. Additionally, titanium dioxide nanoparticles are used to impart self-cleaning and antibacterial properties to concrete surfaces (Olar, 2011).

In Geotechnical engineering, nanomaterials are primarily used to mitigate the effects of highly harmful phenomena in soils, such as liquefaction and slope failures. Liquefaction is a large-strain phenomenon that occurs in saturated loose sand deposits during earthquakes (Ochoa-Cornejo, 2015b). For loose sands, liquefaction can be defined as a state of softening when the pore pressure reaches the value of the confining pressure of the soil (Ishihara, 1993). On the other hand, slope failures can be triggered by various factors, including changes in topography, seismic activity, groundwater flows, loss of strength, stress changes, and weathering (Lee W. et al., n.d.).

To prevent these phenomena, it is necessary to improve the soil response. For this purpose, there are several methods of soil stabilization or improvement, which can be broadly classified as chemical and mechanical stabilization. Chemical stabilization involves changes in the chemical composition of the soil matrix. This can be achieved by applying heat, using polymers or resins in the soil, adding enzymes, adding cement to the soil, or altering the ionic or charge makeup of the soil. On the other hand, mechanical stabilization can be achieved by adding different fibers in fine soils or by compaction in coarse soils (Majeed & Raihan Taha, 2013).

Other classification of soil strengthening methods of liquefiable soils is passive and active methods. Active methods aim to densify the soil by using an impact source like dynamic compaction. Passive methods aim to have an impact on the behavior of the soil without rearranging the particles. One of the most common passive methods is the permeation grouting, these methods can be time consuming and expensive, in search of new alternatives has emerged the permeation with highly plastic nanoparticle (Ochoa-Cornejo, 2015b).

The use of highly plastic nanoparticles in permeation grouting has shown promising results in preventing liquefaction and improving the soil response. These nanoparticles can be injected into the soil in a liquid form and will then solidify upon contact with the soil particles, forming a solid matrix that increases the soil's strength and stiffness. This technique has been tested in laboratory experiments and has shown improvements in soil shear strength and stiffness, as well as reductions in settlement and liquefaction potential (Ochoa-Cornejo, 2015b).

In recent years, considerable attention has been given to the study of laponite, a highly plastic artificial clay classified as a nanomaterial. Laponite is renowned for its thixotropic properties and is widely utilized in various industries as a rheology modifier, including the cosmetic industry. Moreover, there have been several investigations on the potential applications of laponite in civil engineering, particularly in addressing challenges such as liquefaction resistance and cement response. This paper aims to discuss the relevant studies on the utilization of laponite in civil engineering and its potential for enhancing the properties of cementitious materials and mitigating liquefaction risks in soils.

3.1 Global nanomaterial scenario

3.1.1 Uses and fields of application

Nanotechnologies have a wide range of applications in engineering, serving to enhance the performance of products in diverse fields such as pharmaceuticals, biomedicine, chemistry, polymers, electronics, transportation, construction, and the aerospace industry, among others.

In contemporary times, the cosmetic industry has become one of the most prominent fields where nanomaterials are extensively utilized. This industry is highly active in terms of nano-related patents (Dolez, 2015). Nanomaterials offer significant advantages to cosmetics, as they can enhance characteristics such as skin penetration, UV protection, transparency, and durability of effects.

In contemporary engineering, the automobile industry is a crucial sector that has actively incorporated nanomaterials in its products. Toyota, in 1986, initiated the development of a hybrid nanocomposite material composed of clay and nylon. This material was utilized in 1990 to manufacture timing belt covers, which substantially enhanced their performance. In addition, modern automotive tires incorporate nanomaterials as a filler for rubber compounds. Nanoparticles are also added to automobile paints to increase their scratch resistance. These developments reflect the growing importance of nanotechnology in the automobile industry (Dolez, 2015).

In recent years, the construction industry has also witnessed the benefits of nanomaterials. Primarily, there are three main products in the industry where nanomaterials are employed: concretes, paints and coatings, and insulation. Nanomaterials are used in concretes to enhance their regularity and porosity, leading to better performance. In paints, nanomaterials provide UV protection, increased durability, and antibacterial properties. In addition, for insulation purposes, nanomaterials help generate nanopores that improve thermal and acoustic insulation, thus producing better outcomes than traditional insulators (Dolez, 2015).

3.2 Nanomaterials in Civil Engineering

The incorporation of nanotechnology in the construction industry has experienced a notable surge, with particular attention given to the integration of nanomaterials into cement composites. The addition of nanoparticles to cement has been a subject of extensive research, with the aim of enhancing the properties of the cement. Table 3-2 showcases the diverse range of nanomaterials utilized, the application areas, and the properties being targeted for improvement.

Table 3-2: Nanomaterials used in civil engineering (Daniyal et al., 2018).

Nanomaterials	Base materials	Possible benefits
Carbon nanotube (CNT)	Cement and concrete	Improvement in mechanical strength
	Ceramics	Enhancement in thermal mechanical properties
	Nanoelectrical mechanical systems	Real-time health assessment of structures
	Solar cell	Efficient electron mediation
Silicon dioxide	Cement and concrete	Enhancement in mechanical Strengths and durability
	Glass	Antireflective and heat isolation
Titanium dioxide	Solar cell	Non-utility power production
	Glass	Antifogging, hydrophilicity, fouling resistance
	Cement and concrete	Self-cleaning, rapid hydration and improvement in mechanical strengths
Ferric oxide	Cement and concrete	Improvement in mechanical strengths and durability
Copper oxide	Cement and concrete/steel	Improved mechanical strength and durability, enhanced weldability, and corrosion resistance of steel
Aluminum oxide	Cement and concrete	Enhancement in mechanical strengths
Zirconium oxide	Cement and concrete	Improvement in mechanical strengths
Zinc oxide	Cement and concrete	Improvement in mechanical strengths
Calcium carbonate	Cement and concrete	Enhancement in mechanical strengths

Nanomaterials	Base materials	Possible benefits
Chromium oxide	Cement and concrete	Improvement in mechanical strengths
Silver	Cement and concrete	Antimicrobial properties
Laponite	Soil, cement, and drilling fluids	Liquefaction mitigation, carbonation resistance and heat resistance

In civil engineering, nanomaterials have also found applications in soil mechanics. For instance, colloidal silica, which is an aqueous suspension of microscopic silica particles produced from saturated solutions of silicic acid (Gallagher & Mitchell, 2002), has been employed as a permeability reducer in coarse soils. Gallagher and Mitchell (2002) reported that the addition of colloidal silica to sands resulted in an increase in liquefaction resistance compared to clean sands. Other studies have investigated the effects of nano clays in collapsible soils, and the use of carbon nanotubes to enhance the stiffness and reduce the ductility of fine soils.

Ghasabkolaei (2017) studied the addition of nano silica to clayey soils, finding that nano silica does not produce changes in the soils but the reaction with the silt present in the clays does, this produced an increase in the compression resistance of soils as shown in Figure 3-2. This figure compares the compressive strength of a soil with different percentage of nanosilica, obtaining a peak compressive strength with 1.5% of added nanosilica.

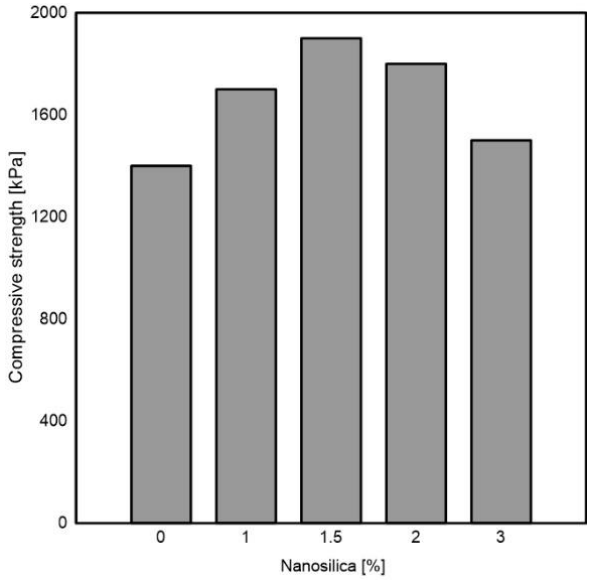

Figure 3-2: Percentage of nanosilica added to clayed soils and its compressive resistance (Ghasabkolaei et al., 2017).

In recent years, another nanoparticle has been increasing its appearance in studies and evaluation of its applications, laponite an artificial clay that has made its way as a possible substitute for other nanoparticles like bentonite.

3.2.1 Laponite

Laponite is a 2:1 layered artificial smectite clay mineral, first discovered by Dr Barbara S. Neumann in 1964 (Shafran et al., 2020), that consists of one octahedral sheet sandwiched between two tetrahedral sheets and its formula is $Na^{+}_{0.7}[(Si_8Mg_{5.5}Li_{0.3})O_{20}(OH)_4]^{-0.7}$ (Getchell et al., 2022; Ochoa-Cornejo et al., 2016; Shen, 2014). Laponite has chemical composition analogous to that of naturally occurring smectite clay minerals (e.g., Na-montmorillonite) (El Howayek, 2011). Its idealized dimension are 25 nm of diameter and 1 nm of height as shown in Figure 3-3 a).

Typically, the tetrahedral sheet consists of SiO_4 tetrahedra arranged such that three basal oxygen ions are shared with the three neighboring tetrahedral, whereas the fourth O^{2-} ion (apical oxygen) is free to bond to the octahedral sheet (Amonette, 2002; El Howayek, 2011). The octahedral sheet consists of one central cation filling the sites between two planes of apical oxygen and hydroxyl. There are two types of octahedral sheets: trioctahedral and dioctahedral. If the central cations are divalent cations (e.g., Mg2+), they will occupy all the three possible octahedral sites and create a trioctahedral sheet. If the central cations are trivalent cations (e.g. Al3+), they will occupy two of every three possible octahedral sites and produce a dioctahedral sheet (Shen, 2014).

Isomorphic substitution is the substitution of some atoms in the tetrahedral or octahedral sheets for other atoms such as Si^{4+} by Al^{3+} in the octahedral sheet; Al^{3+} replaced by Mg^{2+} and Mg^{2+} replaced by Li^{+} in the tetrahedral sheet. The effect of such phenomenon results in a negative charge imbalance on the material, which then can attract cations to its surface. The attracted cations are held in a diffuse region on both sides of the laponite crystal. These regions are known as the double layer. Laponite RD is a special case of smectite where cation substitution occurs only in the octahedral sheet. In particular, some of the divalent magnesium cations (Mg^{2+}) in the central layer are replaced by monovalent lithium cations (Li^{+}) leading to the formation of negative charges, which are balanced by the sodium ions (Na^{+}) located at the surface (Figure 3-3 b)). The sodium ions tightly hold the two 2:1 crystal layers together. Due to a protonation process of the OH^{-} groups, a positive charge is formed at the edge of the crystal structure (El Howayek, 2011; Ochoa-Cornejo, 2015b; Shen, 2014)

a)

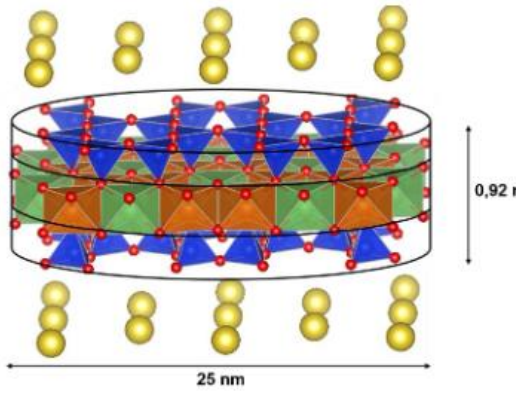

b)

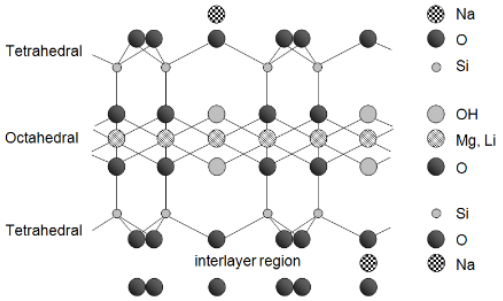

Figure 3-3: a) Shape, dimensions, and structure of a laponite particle (VESTA software)(Pardo Ojeda, 2020) b) Idealized structural formula of Laponite RD (El Howayek, 2011).

When laponite is dispersed in water, it rapidly delaminates into a clear colloidal dispersion of charged disk-like, fairly uniform crystals. The sodium cations adsorbed to the layer surface may be easily dissolved resulting in strongly negatively charged faces and weak positively (ph dependent) edge to edge to edge charge. These cations are called “exchangeable cations” and they are quantified by the cation exchange capacity, CEC (El Howayek, 2011; Shen, 2014).

Laponite particles are transparent, the powder in dry form appears to be white due to the refraction of light (Siddique et al., 2023; Wallace & Rutherford, 2015). When dispersed in water, laponite hydrates, swells up to 800% of its size in free swelling (Pardo Ojeda, 2020), and forms a colorless transparent monodisperse suspension. Due to the milling portion of the manufacturing process of the synthetic clay, the particle size is relatively uniform, which differs from natural clays that typically show larger variation (Siddique et al., 2023; Wallace & Rutherford, 2015).

3.2.1.1 Production

The modern process to produce laponite retains similarities to the synthesis process originally proposed by Dr Neumann (Shafran et al., 2020), and are as it follows:

Figure 3-4: Involved process in the production of laponite (Pardo Ojeda, 2020).

Laponite is artificially produced by the dissolutions of lithium fluoride, magnesium chloride, sodium silicate and calcium carbonate in distilled water, the mix then is boiled for at least 20 hrs, then a

hydrothermal treatment is applied to the solution for 10 to 20 hrs or until the mass of the solution stays constant. After the hydrothermal treatment, the solid product obtained is washed to eliminate the salts excess, after that is oven dried and grinded, the details of the production can be found in the technical information of laponite RD by ByK Instruments.

1.1.1. Laponite grades

There are multiple types of Laponite grades depending on its properties and uses, the most common and used in geotechnical engineering is Laponite RD. Generally, laponite products can be divided into two basic grades: gel forming grades and sol forming grades. When dispersed in water, gel forming grades of laponite form clear, colorless, high viscosity colloidal dispersions. Sol forming grades of laponite follow the same dispersion characteristics, except that low viscosity sols are formed. Laponite can be used for many applications, which fall into two key areas: rheology modifier and film former (Shen, 2014).

Table 3-3: Laponite grades (BYK Instruments, 2014).

Laponite Grade	Gel type	Features
RD	Gel forming	General purpose grade
RDS	Temporary solution forming	General purpose solution grade
S482	Permanent solution forming	Very high solution stability grade
SL25	Permanent solution forming	A long term stable aqueous dispersion of Laponite
EP	Gel forming	Organic modification for extra performance in “difficult” system
JS	Temporary solution forming	High solution stability grade
XLG	Gel forming	High purity, certified low heavy metal and low microbiological content
XLS	Temporary solution forming	High purity, certified low heavy metal and low microbiological content
XL21	Gel forming	High purity, certified low heavy metal and low microbiological content
D	Gel forming	Optimized for rapid dispersion in sorbitol solution

3.3 Experimental evaluation of laponite´s properties

Multiple authors have developed experimental programs with laponite, these programs seek to evaluate the physical, chemical, and geotechnical properties of laponite for various applications. However, it is important to first discuss the double layer theory, as it is related to some of the phenomena observed in laponite solutions and mixtures.

3.3.1 Double Layer Theory

The double layer theory explains some of the interaction that laponite and water have and it works under three assumptions, the first one is that the particles are parallels, the second is that there is no contact between them and the third is that the particles are equispaced.

Smectites, on which laponite is based, absorb water between the tetrahedral- octahedral-tetrahedral (TOT) layers, this phenomenon produces the swelling in clays, some of the parameters that control this, are the charge density in the surface of the clay, the ions between the TOT layers, the concentration and type of electrolytes in water.

With this, it can be introduced two types of swelling, the internal crystal swelling that consists in the hydration of the interchangeable cations between the TOT layers, these hydrated cations reorder between the layer producing a swelling. The second type of swelling is the osmotic, this swelling is based on the repulsion between the electric layers given a considerable concentration of ions near the clay particle, this swelling act in larger distance than the internal crystal but with minor pressure.

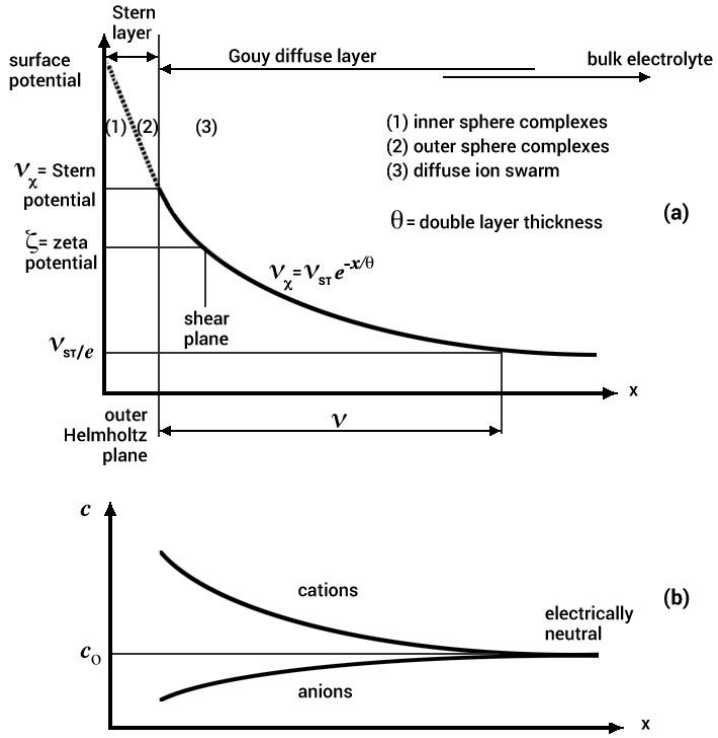

Figure 3-5: (a) Surface potential versus distance (Santamarina, 2001); (b) Concentration of cation and anions versus distance (Santamarina, 2001)

Figure 3-5 (b) present that the concentration of cations near the clay particles is extremely high and as the distance increase the concentration diminish exponentially, the opposite is for the anions. The surface of the clay is charged negatively and with the cloud of ions form, what is called, the diffuse electrical double layer (Figure 3-5 (a)), when the two negatively charged potential field overlap, they repel each other until equilibrium of ions concentrations is reached.

Analyzing the sensitivity of the equations proposed by (Komine & Ogata, 1996, 1999) against the interparticle distance, which in this case is defined as part of the void ratio and the concentration of ions in the medium where they are found, an inversely proportional relationship is obtained to the concentration of ions at which it is quite sensitive and a relationship, also inversely proportional to the void ratio, but with less sensitivity.

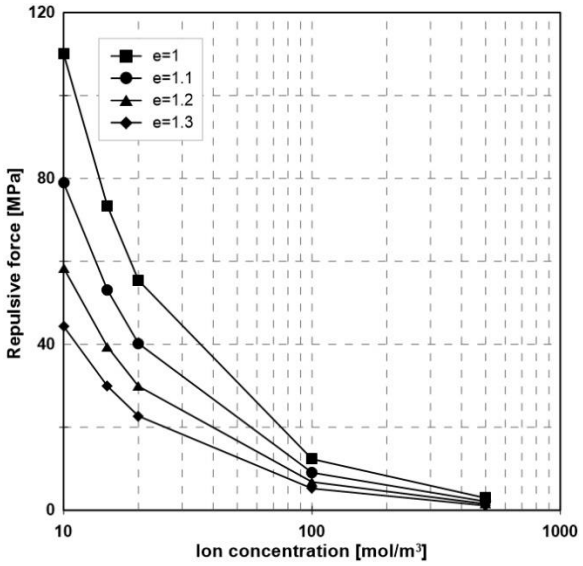

Figure 3-6: Sensitivity of the double layer versus ion concentration and void ratio.

The next sections show the main characteristics of laponite measured by diverse authors.

3.3.2 Physicochemical properties

3.3.2.1 Dry laponite

3.3.2.1.1 Fourier-Transform Infrared Spectroscopy (FTIR)

The Fourier-transform Infrared Spectroscopy is a method used to identify unknow materials and consists in radiating the material with infrared light, the signal received is decodified with Fourier-Transform. As shown in Figure 3-7 the existent studies show similar results, the small differences between them can be explained by the condition in which the tests was made, wet or dry (Pardo Ojeda, 2020).

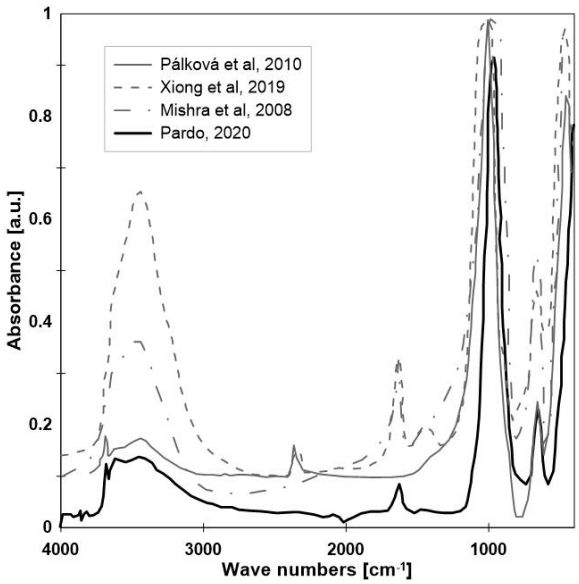

Figure 3-7: Infrared spectrum obtained by diverse authors (Mishra et al., 2008; Pàlkovà et al., 2010; Pardo Ojeda, 2020; Xiong et al., 2019).

The first absorption peak, observed between the wave numbers of 417-433 cm^{-1}, is associated with the Si-O-Mg or Si-O-Si bonds. The second peak, located between 652 and 654 cm^{-1}, corresponds to the vibrational movements of the Mg-O bonds or Li-O. The third peak corresponds to the vibrational movements of the Si-O bond, which is the most intense, in agreement with the more abundant elements in this type of mineral. The fourth peak is located between 1620 to 1640 cm^{-1}. Other peaks observed in this range are discarded as they corresponded to water. The similarities between the studies indicates that the commercially available laponite is homogeneous (Pardo Ojeda, 2020).

3.3.2.1.2 X ray difraction (XRD)

It's used to determine the crystalline structure of a substance; the x ray diffraction consists in radiating the material with x rays and measure the diffraction angle and the light intensity. In Figure 3-8 is shown that roughly the studies coincide, the differences are related to the different emission anodes used in each study.

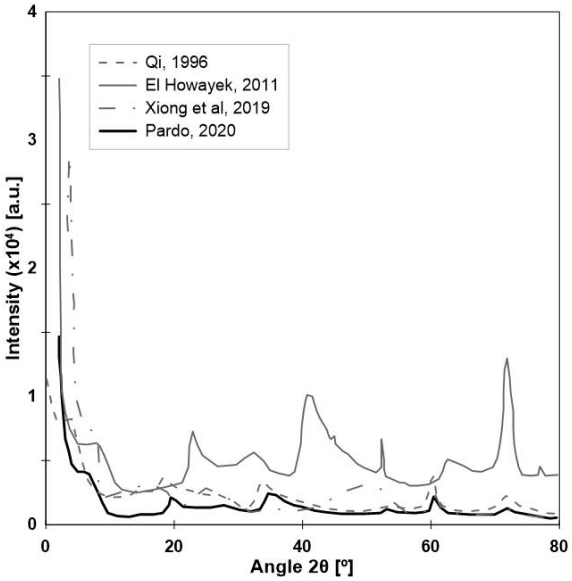

Figure 3-8: X ray diffraction of laponite obtained by diverse authors (El Howayek, 2011; Pardo Ojeda, 2020; Qi et al., 1996; Xiong et al., 2019).

The results correspond to a common reflection of a silicate mineral in 2:1 layers, in particular for an smectite like laponite (Pardo Ojeda, 2020).

3.3.2.1.3 Thermogravimetric analysis (TGA)

Is used to characterize the hydration state of some materials and its thermic stability. Thermogravimetric analysis consists in the continuous registration of the specimen mass in a controlled atmosphere. Figure 3-9 shows the studies of three authors with different temperature increment ratios, the differences observed can be explained by the different increment ratios.

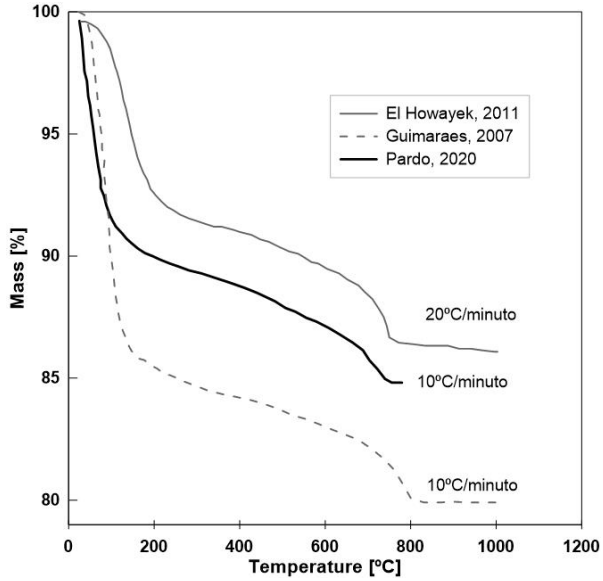

Figure 3-9: Thermogravimetric analysis obtained by diverse authors (De et al., 2007; El Howayek, 2011; Pardo Ojeda, 2020).

The results show that the dehydration process of laponite occurs in three steps, primary dehydration on the external surface of the particles, secondary dehydration between the layers and the dihydroxylation.

3.3.2.1.4 Specific surface

Different authors report values for the specific surface of laponite, these authors used the Brunauer – Emmett – Teller (BET) method, the results and the fluid used to make the test are presented in Table 3-4, the temperature and gas pressure varies with each test.

Table 3-4: Specific surface of laponite measured by different authors (El Howayek, 2011; Herrera et al., 2004; Pardo Ojeda, 2020; Qi et al., 1996).

Autor	SSA [m^2/g]	Adsorption
Pardo, (2020)	322	Gaseous N_2
BYK additives & Instruments, (2013)	370	Gaseous N_2
Herrera, (2003)	370	Gaseous N_2
Qi et al, (1996)	372	Gaseous N_2
El Howayek, (2011)	473	Water steam

It is possible to theoretically calculate the specific surface of laponite, Pardo Ojeda (2020) calculated its surface by unitary cell getting a specific surface of 759.66 [m^2/g] and by particle shape, getting a value of 859.25 - 845.88 [m^2/g]. The methods explained previously considered an isolated laponite particle while the BET method depends on the void spaces between the

particles, this explains the differences in the specific surface measured and calculated, the fact that the spaces between particles differ is related to the double layer theory explained previously, the conditions of ions concentrations and water content directly affects the available space between the clay particles.

3.3.2.2 Laponite suspensions

3.3.2.2.1 Colloidal suspension state

Laponite suspensions are a non-ergodic colloidal suspension, these can be found in two states, glass or gel, these states are hard to differentiate, but in Table 3-5 are presented the principal characteristic of each state.

Table 3-5: State of laponite solutions (Pardo Ojeda, 2020; Tanaka et al., 2004).

Glass	Gel
• Homogenous structure • Elasticity is a product of the caging of the particles. • The kinetic of solidification is called aging. • The longitude scale between the particles is of the order of the colloids size.	• No homogenous structure, possess a hierarchical structural organization. • The elasticity es a product of a mechanical percolated net and is lower than glass. • The kinetic of solidification is called gelification. • The length of the fundamental unit of the net is bigger than the colloids size.

A phase diagram has been proposed for laponite suspensions Figure 3-10, this diagram shows the ergodic (suspension and liquid) and the non-ergodic (glass and gel) states, the differences between the phases are due to the disposition of the particles shown in Figure 3-11.

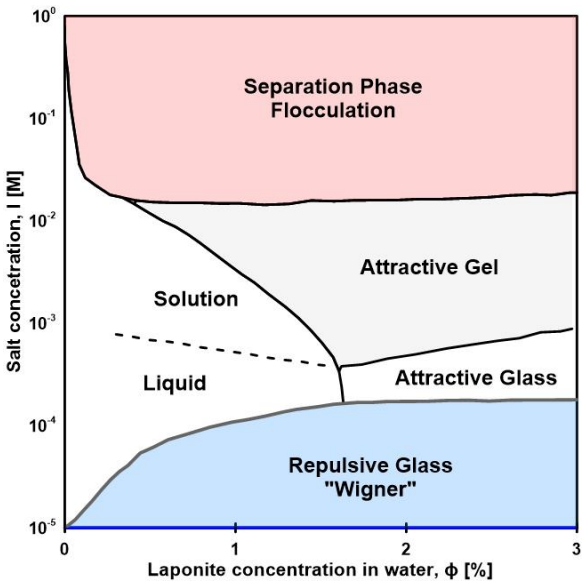

Figure 3-10: Laponite phase diagram (Tanaka et al., 2004).

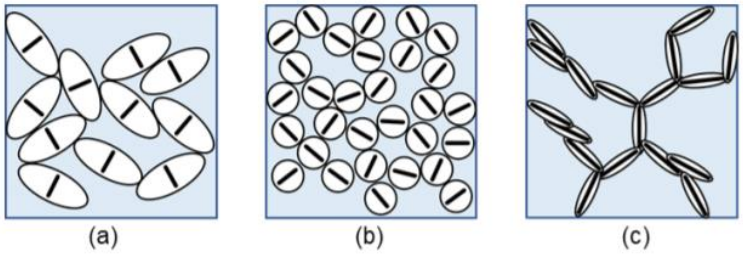

Figure 3-11: Particle disposition in laponite (a) Repulsive glass “Wigner” (b) Attractive glass (c) Attractive gel “house of cards” (Tanaka et al., 2004).

These diagrams are closely related to the double layer theory, as already discussed, the interparticle attraction and repulsion depends on ion concentration in water, as shown in Figure 3-10 the phase of the laponite will depend on the concentration of salt and the laponite concentration, the repulsion between laponite particles decrease with the increase in the concentration of salts, this can be seen in Figure 3-11 as the particles are far from each other in the repulsive glass phase and are nearly touching in the attractive gel.

3.3.2.2.2 Rheological properties

Some authors have characterized the viscosity of laponite with amplitude sweep tests, these tests show an increment in the viscosity with the aging, the concentration of laponite and with the salt

concentration, with the increase of temperature the tests show a decrease in viscosity, as shown in Figure 3-12.

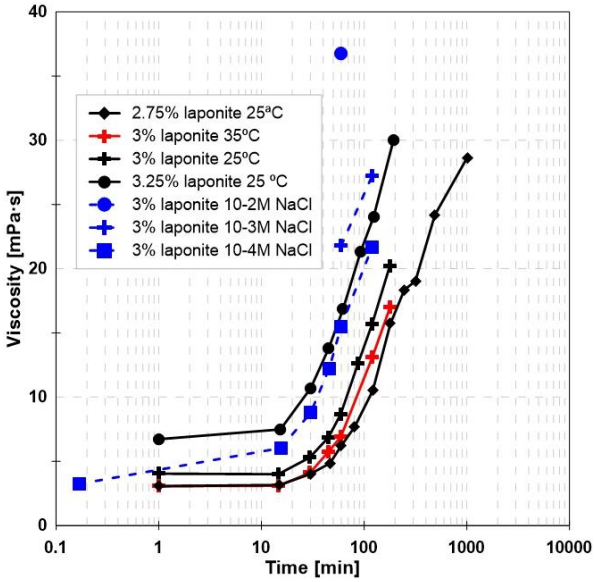

Figure 3-12: Viscosity versus aging time at different temperatures, concentration, and salt concentration (El Howayek, 2011).

3.3.3 Geotechnical properties

3.3.3.1 Consolidation and swelling of laponite

The clays behavior depends on its tensional state during the proves of saturation and desaturation, in the case of laponite, its behavior also depends on the aging, the index of compression and recompression of laponite increase in 1% and 35% with an aging of 12 hrs as shown in Figure 3-13.

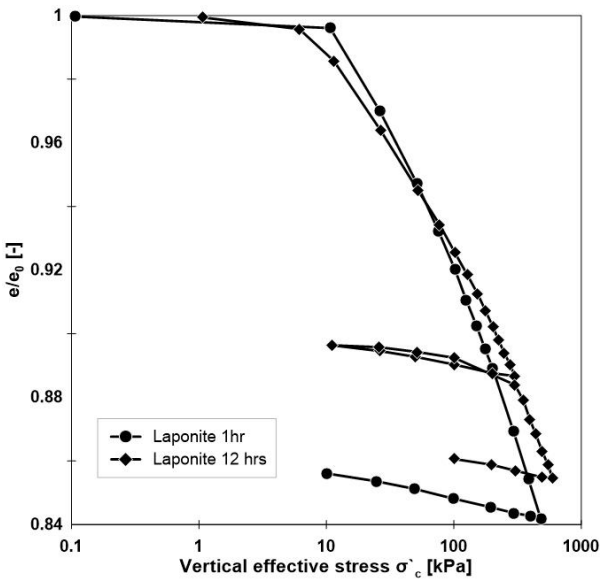

Figure 3-13: Consolidation of laponite with different aging (Pardo Ojeda, 2020).

The swelling of laponite is consequence of its water adsorption capacity and can be measured by an oedometer or visually, the results shown in Figure 3-14 compare studies on laponite and bentonite in samples made at density of 1.2Mg/m^3 and a water content between 20 and 30%. Bentonite reaches its second swelling at approximately 400 hrs. and the deformation don't exceed the 300% so laponite swelling is 2.5 times greater than bentonite.

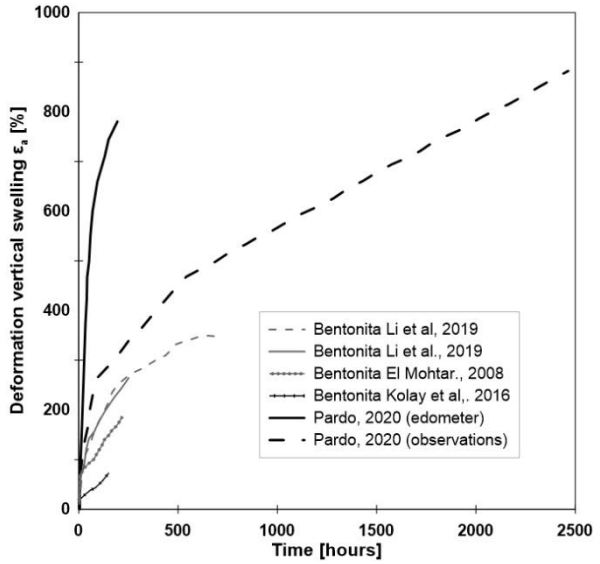

Figure 3-14: Laponite swelling obtained by diverse authors (Kolay & Ramesh, 2016; E. Mohtar et al., n.d.; Pardo Ojeda, 2020).

As mentioned before the swelling of laponite its directly related to the double layer theory, but also is the consolidation, both properties depend on the ion concentration in water and acts according to the previously discussed about the double layer theory. The pressure generated by the swelling of laponite was also measured and is shown in Figure 3-15.

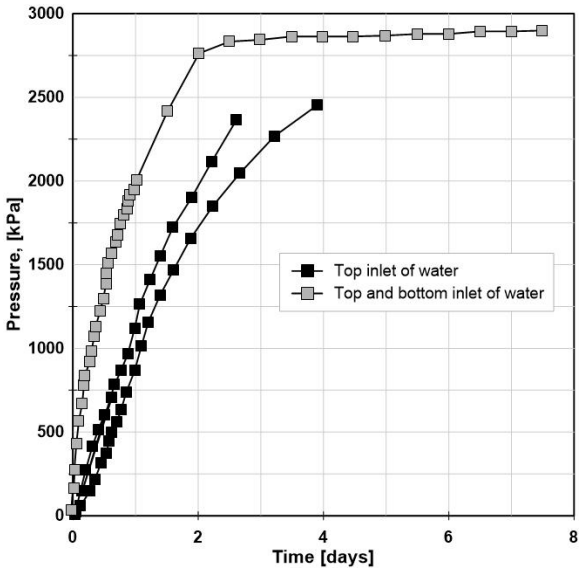

Figure 3-15: Swelling pressure of laponite.

3.3.3.2 Atterberg`s limits

The tests were made according to ASTM standard of Atterberg`s limits and shows the extremely high IP of laponite, it's important to note that laponite change is properties with aging and the results presented were determined at zero aging time.

Table 3-6: Atterberg limit of laponite obtained by different authors (Al-Mukhtar et al., 2000; El Howayek, 2011; Pardo Ojeda, 2020; Wallace & Rutherford, 2015),

Autor	Liquid limit [%]	Plastic limit [%]	Plasticity index [%]
Wallace & Rutherford, (2015)	1150	240	910
Al.Mukhtar et al., (2000)	1050	250	800
El Howayek, (2011)	1280	180	1100
Pardo, (2020)	1017	187	829

3.3.3.3 Shear resistance

Wallace & Rutherford (2015) made vane shear tests on samples of slurry mixtures that were left self-weight consolidate for 6-336 h, to measure the undrained shear resistance of laponite, the

results shown in Table 3-7 evidence an increase in the average peak shear resistance with the concentration and the aging of laponite.

Table 3-7: Undrained maximum shear resistance at 7 and 14 days of laponite (Wallace & Rutherford, 2015).

Concentration [%]	$S_{u,peak,MV}$ (7 days) [kPa]	$S_{u,peak,MV}$ (14 days) [kPa]
4	0.3	0.36
4.25	0.34	0.4
4.5	0.4	0.42

The change in peak undrained shear strength with depth was also measured, finding no significant changes with the increase in depth. The constant measured undrained shear strength with depth is likely due to the thixotropy of the sample being a result of both the formation of the transparent soft clay surrogate gel after hydration and a consolidation process comparable to natural clays. For the set time the gel formation process is dominating since the low buoyant unit weight of the samples range from 10.0 to 10.1 kN/m^3, and therefore the change in effective stress with depth is significantly less than with natural clays (Wallace & Rutherford, 2015).

3.3.4 Civil engineering applications

Next, some of the results of different studies that have used laponite are presented. These studies are related to the different branches of civil engineering.

3.3.4.1 Drilling fluids

Huang (2019) evaluated the influence of laponite in the thermal stability of a drilling fluid, based on water, to overcome the problem of polymer degradation. They studied the changes in the fluid viscosity with the temperature, for this the drilling fluid was mixed with laponite and a thermo polymer, then the rheological parameters were measured with a TGA test. It was found that the addition of laponite to the thermopolymer improved the fluid viscosity at all temperatures as shown in Figure 3-16. The properties of the drilling fluid improved at all temperatures of aging especially between 150 and 180 Celsius.

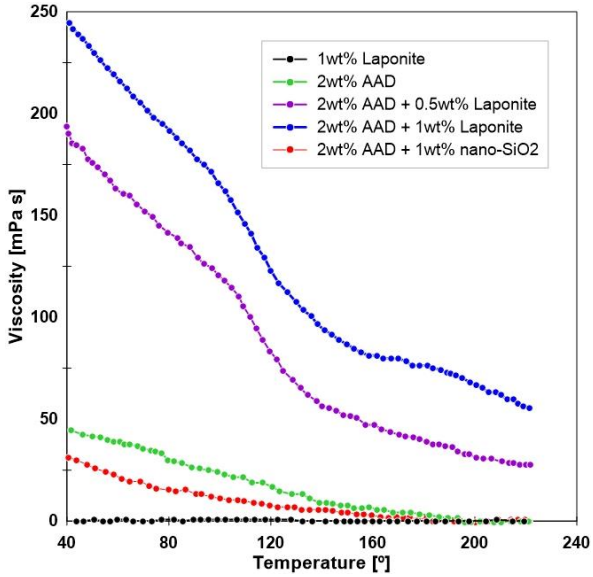

Figure 3-16: Influence of laponite in the viscosity of drilling fluids (X. Huang et al., 2019).

3.3.4.2 Improved cement response

Elkatatny (2019) conducted a study to investigate the effect of incorporating laponite into slurry cements used in oil wells to reduce cement segregation. The study involved preparing seven samples of slurry cements with varying concentrations of laponite, followed by measuring the density variation, slurry rheology, unconfined compression resistance, and permeability of each sample. The results indicated that the addition of laponite yielded better outcomes than the commercial dispersant used for comparison. The laponite effectively decreased the density variation, increased the plastic limit, and reduced the permeability, all while maintaining cost-effectiveness. Figure 3-17 depicts the density variation of the sample with the optimal amount of laponite compared to the control sample.

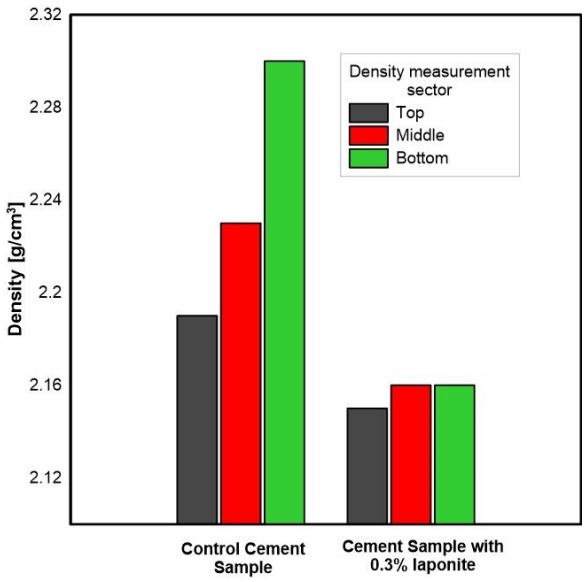

Figure 3-17: Comparison of density variation vertically along the length of samples with (SMP3) and without (ComD) Laponite (Elkatatny, 2019).

In continuation of the previous research work on laponite and slurry cements, Elkatany (2021) conducted a study to investigate the impact of laponite addition on the carbonation resistance of slurry cements. The experimental program comprised four samples of slurry cement, each with varying laponite concentrations. The samples were subjected to high-pressure and high-temperature conditions in a chamber and then saturated with CO2 for 10 days. The resultant samples were evaluated for stress resistance, permeability, and microstructure. The findings revealed that the incorporation of laponite significantly improved the carbonation resistance, compression resistance, and stress resistance of the samples in comparison to the samples without laponite, as illustrated in Figure 3-18.

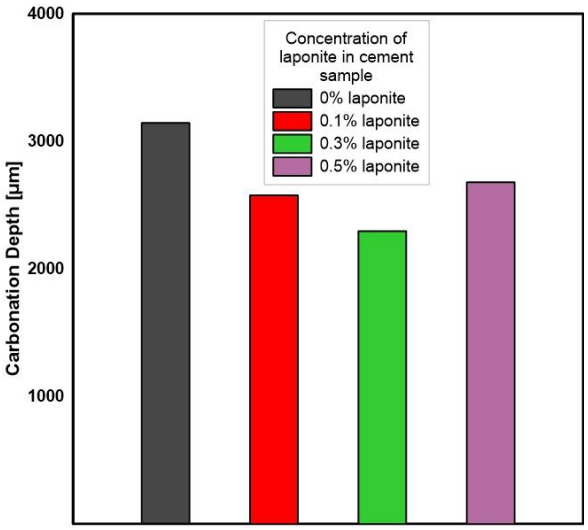

Figure 3-18: Carbonation depth in cement samples with different concentration of laponite(Elkatatny, 2021).

The samples showed a decrease in the carbonation depth with the increase in laponite concentration until a maximum of 0.3% of laponite, above that value the carbonation depth increased again.

3.3.4.3 Scale models

The potential of laponite as a transparent soil to observe deformation in geotechnical models has been extensively studied. Zhang (2020) evaluated the properties of laponite as a transparent soil, while Iskander (2015) proposed its use to visualize the saturation of granular soils due to its color change from white to transparent depending on the degree of saturation. Yang (2018) used laponite to visualize the effects of dissociation of hydrate gas in clayed soils. These studies demonstrate the versatility of laponite as a geotechnical material and its potential for various applications in the field.

3.3.4.4 Improvement of adobe bricks performance

It has been studied the use of laponite as a stabilizer for earthen bricks, also known as adobe bricks. In their research, Scalisi and Sposito (2017) investigated the incorporation of laponite in the soil-water mixture used to produce adobe bricks. These bricks were then subjected to a series of tests including compression and flexural strength, abrasion resistance, capillary water absorption, and impact resistance. The results indicated that the addition of laponite significantly

increased the average compression resistance of adobe bricks, and the performance in terms of flexural strength, abrasion and impact resistance was satisfactory.

3.3.5 Geotechnical applications

3.3.5.1 Increase in liquefaction resistance

Ochoa (2015; 2016), Pardo & Orense (2017), Y.Huang & Wang, (2016) and Rodriguez (2019) investigated the effects of laponite in sands, specifically the influence of laponite in the liquefaction of sands, both Ochoa and Rodriguez performed triaxial tests in specimens of sand with laponite, meanwhile Pardo & Orense did cyclic simple shear tests in sands with laponite. These studies were seeking to determine if laponite has an effect in the liquefaction resistance of sands.

The studies followed different methodologies, Ochoa (2015; 2016) made cyclic triaxial tests in specimens of clean Ottawa sand and sand with laponite. The samples were prepared by dry pluviation with laponite concentrations of 1 to 5 % per dry mass of sand, these samples were tested with different aging periods and different relative densities.

Pardo & Orense (2017) made cyclic simple shear test in Mercer sand with laponite, the samples were prepared with different densities and tested at the same CSR.

Y.Huang & Wang, (2016) made undrained cyclic triaxial tests in Shanghai silty sands, the samples were dry mixed and after that, water was added. The concentration of laponite used were 2, 2.5, 3 and 3.5 %.

Rodriguez (2019) made monotonous triaxial tests and cyclic triaxial tests on tailing sands with laponite, the samples were prepared with laponite concentration of 0 and 1 % by the wet tamping method, these were tested in different confinement pressures.

The four studies concluded that adding laponite to sands increased the liquefaction resistance, represented by an increase in the number of cycles to liquefaction as shown in Figure 3-19.

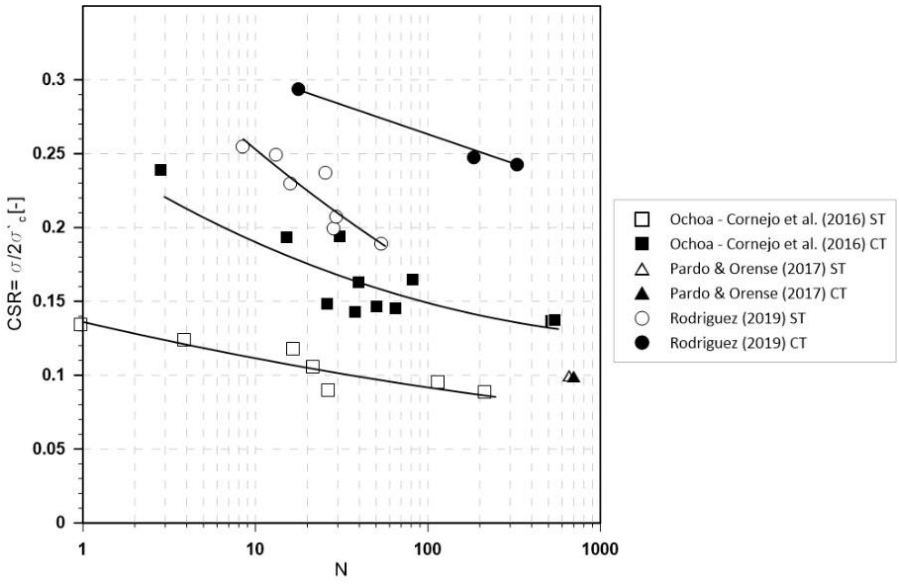

Figure 3-19: Cyclic resistance of sand (ST) and sand with laponite (CT) (Pardo Ojeda, 2020).

3.3.5.2 Increase in the initial small strain shear modulus of sands

Ochoa-Cornejo, (2015b, 2017) and Ochoa-Cornejo et al. (2020) investigated the effects of laponite in the small strain stiffness of Ottawa sand in undrained Resonant Column tests, to do this samples of clean Ottawa sand and dry mixes of 1 and 3% laponite were prepared and consolidated at 25, 100 and 300 kPa. The results showed that the initial shear modulus (G_0) is dependent on the amount of laponite present and the consolidation stress. With 1% laponite a significant increase in G_0 relative to clean sand was observed at all confining stresses as shown in Figure 3-20.

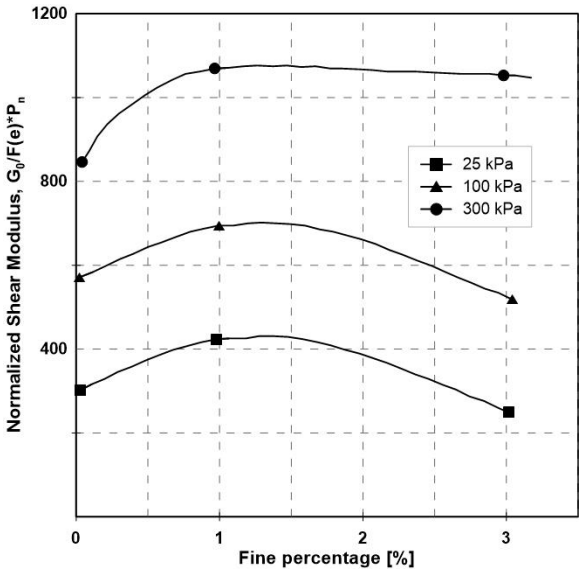

Figure 3-20:Effect of laponite percentage on the normalized initial shear modulus at 25, 100 and 300 kPa(Ochoa-Cornejo, 2015b).

Table 3-8: Laponite studies summary.

Title	Authors	Sample preparation	Laponite type	Laponite concentration	Sand type	Gs	RD	Tests	Objective
Liquefaction mitigation with nanoparticles	Ochoa-Cornejo, 2015	Dry pluviation	Laponite RD	1-3-5% by dry mass of sand	Ottawa	2.65	20%	Cyclic triaxial test	Liquefaction mitigation
Geotechnical Properties of laponite RD	Wallace & Rutherford, 2015	Hydration	Laponite RD	4-4.25-4.5% by mass of water	-	-	-	Vane shear test. Hydraulic conductivity	Laponite characterization
Cyclic behavior and pore pressure generation in sands with laponite, a super-plastic nanoparticle	Ochoa-Cornejo et al., 2016	Dry pluviation	Laponite RD	1-3-5% by dry mass of sand	Ottawa	2.65	20%	Cyclic triaxial test. Resonant Column Test	Liquefaction mitigation
Laboratory investigation of liquefaction mitigation in silty sand using nanoparticles	Y. Huang & Wang, 2016	Dry mix Wet tamping	-	2-2.5-3-3.5% by dry mass of sand	Shanghai	2.69	-	Cyclic triaxial test	Liquefaction mitigation
Experimental study on the self-healing effect of laponite on the liquefaction resistance of sand	Pardo Tobar & Orense, 2017	Slurry deposition	Laponite RD	1% by dry mass	Mercer	-	-	Cyclic simple shear test	Liquefaction mitigation
Discussion on: Laboratory investigation of liquefaction mitigation in silty sand using nanoparticles	Ochoa-Cornejo et al., 2017	Dry pluviation	Laponite RD	1% by dry mass	Ottawa	2.65	25%	Resonant column Cyclic triaxial test	Liquefaction mitigation
Experimental study of the injectability and effectiveness of laponite	(Mele et al., n.d.)	Wet pluviation	Laponite RD	1% by dry mass	Leighton Buzzard	-	40%	Viscosity test Permeability tests	Verify injectability of laponite and

mixtures as liquefaction mitigation technique								Cyclcic triaxial test	liquefaction resistance
Quantification of the transparency of the transparent soil in geotechnical modeling	Yi et al., 2018	-	-	-	-	-	-	Light detection	Quantification of transparency in transparent soils
Cyclic response of tailing sands with nanoparticles	Rodriguez, 2019	Wet tamping	Laponite RD	1% by dry mass of sand	Tailings	2.75	40%	Cyclic triaxial test	Liquefaction mitigation
Centrifuge testing of liquefaction mitigation effectiveness on sand foundations treated with nanoparticles	Y. Huang et al., 2019	Slurry deposition	-	3% by mass of water	From Fujian Province, China	2.65	45%	Dynamic centrifuge model test	Non disruptive liquefaction mitigation
Soil improvement by Re-orienting magnetic particles using a magnetic field	Jiang & Rutherford, n.d.	Hydration	Laponite RD	4.5-7-10-12% by mass of water	-	-	-	Shear strength	Effect of magnetic particles in shear resistance in transparent soils.

3.3.6 Scope for future research

The applications of laponite in civil engineering to solve specific problems like liquefaction mitigation, degradation of polymer fluids, improvement in cement response and its uses to model the behavior of soils have developed the research about this artificial clay. But there are certain directions in which research is not conducted which could possibly be the following:

- Extended analysis of the durability of the improvement in the liquefaction resistance in soils when laponite is added, a long-term study of the effects of weather conditions in the performance of laponite.
- The cost of adding laponite to big extension of soils is not being considered. So, cost analysis studies of great scale application of laponite in sand structures to improve liquefaction resistance, for example in tailing dams.
- The characterization of sands with laponite has been focused on small percentages of laponite. So is required an increase in the percentage of laponite in the sands specimens to obtain a complete characterization of sand laponite interaction.
- The use of laponite in regular construction is not studied yet, research about application and efficiency of laponite in construction concrete to decrease segregation is required.
- Extend the studies of carbonation resistance to regular concrete for application in structures exposed to environments with a tendency to produce carbonation.
- A precise analysis of the optimum amount of laponite for the applications mentioned before.
- Analysis of optimal temperature in laponite applications.
- Studies of optimal methods for the application of laponite to different materials.
- The use of laponite in copper mining as a replacement of bentonite used in the process of flotation, this change could allow saving water and the use of sea water.

4 Experimental Methods

The present study encompasses an experimental program that involves a series of characterization tests including granulometries, maximum and minimum density, and Atterberg limits, to determine the differences in parameters of the mixtures with varying percentages of fines. Furthermore, shear resistance tests will be conducted to verify the variation in resistance due to the addition of fines, consolidation tests will be carried out to determine the properties of wet mixes, and free swelling tests will be performed to study the behavior of the distribution of fines in intergranular spaces.

This chapter presents the materials and equipment utilized during the study, along with a description of the methodologies adopted for conducting the main tests.

4.1 Material Description

4.1.1 Ottawa sand

This study works with graded Ottawa sand, a uniform (Cu=1.7) and clean fine-to-medium sand (D_{50}=0.35mm) with less than 5% of fines, a specific gravity Gs=2.65, and maximum and minimum void ratios emax=0.783 and emin=0.48 (Ochoa-Cornejo, 2015a). Figure 4-1 a) shows the grain size distribution of Ottawa sand, characterized by its round shape and regularity in (Figure 4-1 b), Figure 4-1 c) shows a close up of a single sand particle and its asperities.

a)

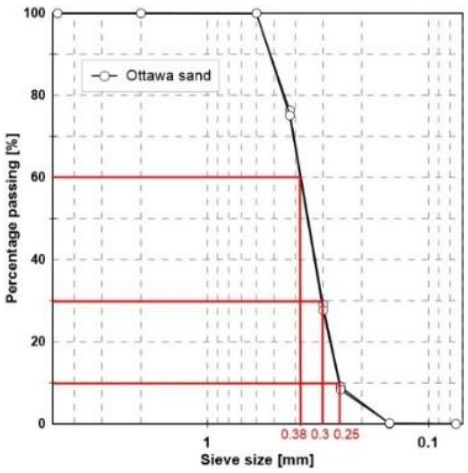

b)

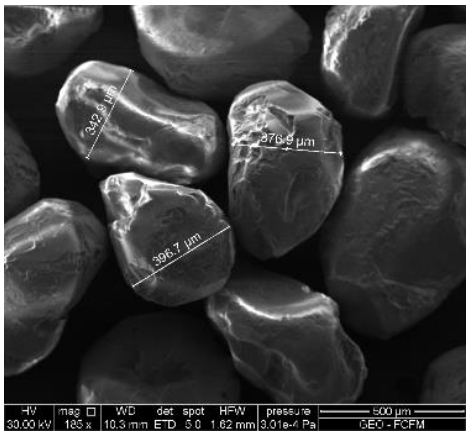

c)

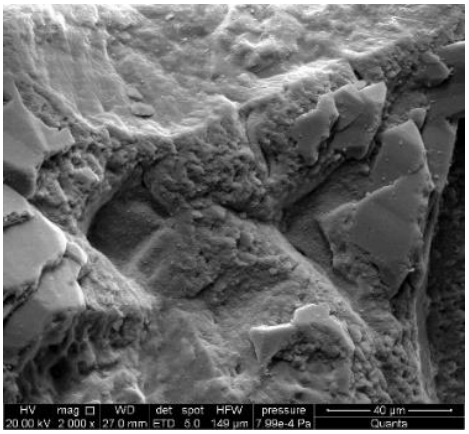

Figure 4-1: Ottawa sand a) granulometry b) SEM image from sieve 40 (0.425mm) and c) SEM image of asperities.

4.1.2 Laponite

Laponite, the RD type used in this research, is artificially produced by the dissolutions of lithium fluoride, magnesium chloride, sodium silicate and calcium carbonate in distilled water. The mix then is boiled for 20 hrs, with a hydrothermal treatment applied to the solution for 10 to 20 hrs. After hydrothermal treatment, the solid product obtained is washed to eliminate the salts, and oven dried and grinded (Pardo Ojeda, 2020). Laponite is a disc shaped artificial clay with layered structure, with similar chemistry to hectorite, and idealized dimensions of 25 nm in diameter and 1 nm in height. It is soluble in water, with huge swelling potential (Pardo Ojeda, 2020). Figure 4-2 a) shows the granulometry of laponite used in this study, characterized by the irregular shape of its aggregates as observed in Figure 4-2 b), while Figure 4-2 c) shows its idealized crystal structure.

a)

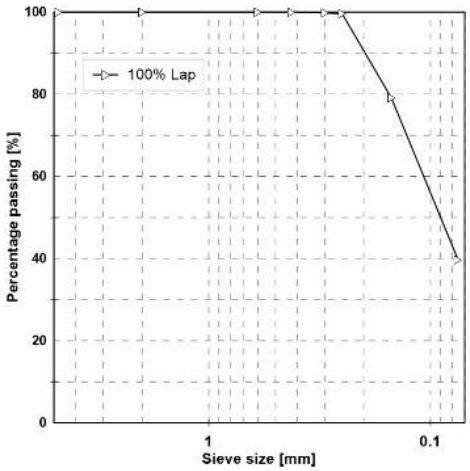

b)

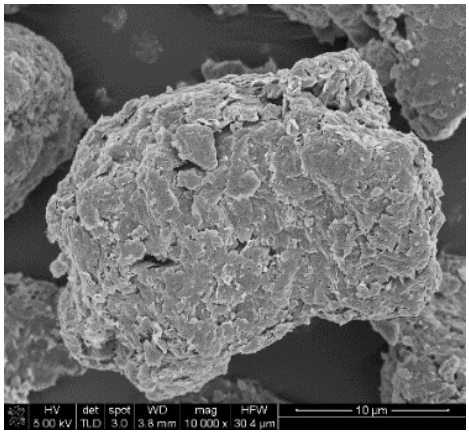

c)

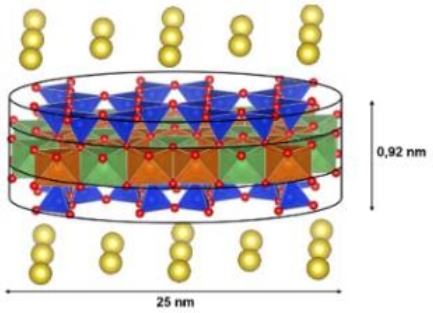

Figure 4-2: a) Laponite RD granulometry, b) Laponite powder aggregate SEM image and c) Idealized laponite structure (Pardo Ojeda, 2020).

Table 4-1: Laponite characterisitics.

Characteristic	Description
Appearance	White powder
Density	1000 kg/m^3
Surface area (BET)	370 m^2/g
Ph (2% suspension)	9.8
Chemical composition (dry base) SiO_2	59.5%
Chemical composition (dry base) MgO	27.5%
Chemical composition (dry base) Li_2O	0.8%
Chemical composition (dry base) Na_2O	2.8%
Chemical composition (dry base) Lost by ignition	8.2%
Resistencia del gel	22g min
Sieve analysis	2% Max>250 microns
Free moisture	10% Max

4.2 Equipment

For the development of the experimental program, various equipment present in the Laboratory of Solids and Particulate Media (Mecesup) was used. These equipments are described below.

4.2.1 Granulometry

For the granulometric analysis of the Ottawa sand with laponite, ASTM sieves present in the Solids Laboratory were used.

Figure 4-3: ASTM sieves.

4.2.2 Atterberg´s limits

To carry out the Atterberg Limit tests, the equipment indicated in the ASTM D4318 standard was used, a Casagrande ladle, metal containers and a non-absorbent surface.

4.2.3 Relative density

To carry out this test, a metal mold, a funnel and a hammer were used.

4.2.4 Free swelling

To carry out this test, an oedometer with a capacity for a test tube of 5 centimeters in diameter and 0.5 cm high was used. The equipment consists of a consolidometer load cell that is left outside the load frame and flooded to allow swelling.

4.2.5 Oedometric consolidation

To carry out the test, an oedometer with a capacity for a test tube 5 centimeters in diameter and 2 cm high was used. This equipment consists of a frame where the loading chamber is placed, to later be loaded using metal weights, the height variation is measured by a dial. The equipment allows the test tube to be completely submerged in addition to allowing double or simple drainage.

4.2.6 Simple shear

It is an electromechanical loading system, composed of a compressed air system that allows applying a vertical tension on the test tube, and a mechanical system that applies a displacement at the base of the test tube through a shear cell. The vertical and horizontal deformation of the specimen is measured by a system of dials, the vertical load and the applied shear force is measured through an electronic load cell with a voltage reading system.

The equipment allows testing cylindrical specimens with a diameter of 7 cm and a height of 2 cm and has a maximum applied vertical stress capacity of 7 kg/cm^2. This equipment allows the test to be carried out under controlled deformation, that is, regulating the speed of movement of the equipment (Conejera, 2016).

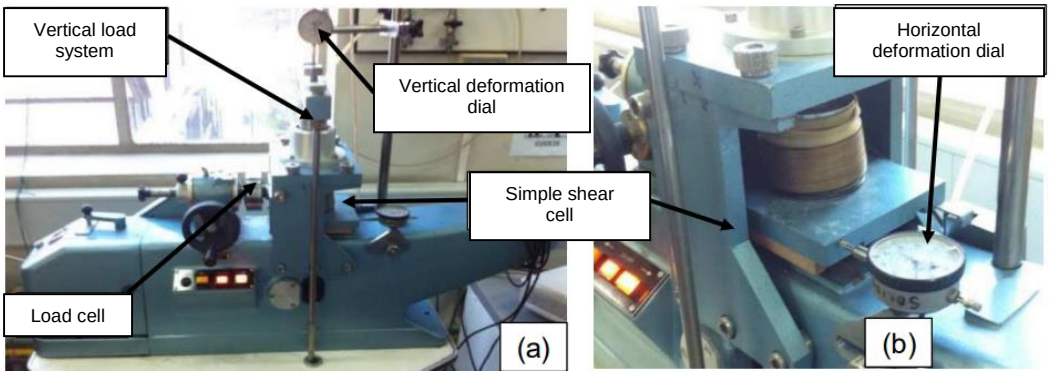

Figure 4-4: Simple shear equipment.

4.2.7 Scanning electron microscope (SEM)

The resolution of classical microscopy is limited by diffraction effects with respect to the wavelength of light (0.2 micrometers). This is why scanning electron microscopy provides a solution to observe small-scale particles, in a range between 3 and 20 nanometers. This technique produces images of the external morphology of a substance, similar to those seen with the human eye (Pardo Ojeda, 2020).

To obtain a scanning electron microscopy image, a very fine beam of electrons is focused on the surface of the solid sample. With analogous instruments, the electron beam sweeps across the sample in a raster scan using scanning coils. The resulting raster scan pattern is similar to that used in a television's cathode ray tube (CTR), in which the electron beam scans the surface in a straight line in the x-direction; then it returns to the starting position and moves down in the y-direction. This process is repeated until the desired area of the surface has been successfully scanned (Pardo Ojeda, 2020).

4.3 Testing Metodology

4.3.1 Mixing of materials

The tests are carried out with a mixture of Ottawa sand and laponite, the latter being a function of the mass of sand. For this study, the sand will be mixed with 1, 3, 5, 10, 15 and 20% laponite.

The mixture is made with a certain amount of Ottawa sand, which is divided into two. The first half of the material is deposited in a PVC container 16.7 cm high and 7.1 cm in diameter. Then, the corresponding amount of laponite is added. Finally, the other half of Ottawa sand is added, and the PVC container is hermetically closed. Then, the container is manually shaken for 20 minutes to homogenize the mixture. In this way, all the samples necessary for the tests described below are prepared.

4.3.2 Granulometry

The granulometric analysis is carried out as indicated in the ASTM D422 standard. The purpose of this test is not to determine the granulometric distribution of the Ottawa sand, which is already very well characterized, but is focused on determining the variation of the granulometric curve of the sand when adding laponite and observing the characteristics of the material that passes sieve #200. The test is carried out dry, as a result of the expansive characteristics of laponite.

To carry out the test, the use of the following sieves was defined:

Table 4-2: Diameter and sieve used.

Sieve Nº	Diameter [mm]
10	2.000
30	0.600
40	0.425
50	0.300
60	0.250
100	0.150
200	0.075

The methodology used to obtain the granulometric curve is the following:

1. A 50-100g sample of Ottawa sand with laponite is taken and poured into the sieve set.
2. The sieve set is shaken.

3. The sieves are taken individually and shaken over a container, the material that passes is deposited on the next sieve.
4. What is retained in each sieve is weighed on a balance.
5. The expressions that allow working with the data obtained are the following:

$$R_i = \frac{P_{ri}}{P_t} \cdot 100 \qquad 4\text{-}1$$

$$P_i = 100 - \sum_{j=i}^{i} R_j \qquad 4\text{-}2$$

$$C_u = \frac{D_{60}}{D_{10}} \qquad 4\text{-}3$$

$$C_c = \frac{D^2{}_{30}}{D_{10} \cdot D_{60}} \qquad 4\text{-}4$$

Where in Equation 4-1 Pri is the weight retained by the sieve i [gr], Pt is the total weight [gr] and Ri is the percentage of soil retained in the opening sieve D. In Equation *4-2* the sum corresponds to the percentages of soil retained in each of the larger opening sieves through which the soil has passed, up to the opening sieve Di. In Equation *4-3* and *4-4* D_{60} is the characteristic diameter through which 60% of the sample passes, this is repeated for the rest of the diameters, Cu is the uniformity coefficient [-] and Cc is the curvature coefficient [-].

4.3.3 Atterberg´s limits

The methodology used for the Atterberg Limits test is detailed, which is carried out as indicated in the ASTM D4318 standard.

1. Part of the material that was sieved under the #40 sieve (0.425mm) is selected.
2. It is moistened until it reaches a consistency that allows the test to be carried out up to 25-35 strokes.
3. The material is placed in the Casagrande cup, and the test is carried out.
4. The number of blows is counted and a sample of the material in the ladle is taken, weighed and oven dried.
5. The procedure is repeated for different moistures.
6. The samples are oven dried for 24 hours and the dry weight is recorded.

4.3.4 Relative density

The methodology used for the maximum density and minimum density tests carried out according to the ASTM D4254 standard is detailed.

1. The dimensions of the mold are measured.
2. A portion of the material is selected.
3. The material is placed in a funnel and slowly dropped into the mold with circular movements and at a height of no more than 1 cm from the base.
4. The mold is filled and leveled with a spatula, then weighed.
5. For maximum density, fill one tenth of the mold and hit it with the hammer evenly 100 times.
6. The previous step is repeated for the 10 layers of soil.
7. Once the mold is filled, it is leveled and weighed.
8. This procedure is repeated 3 times.

To work with the data obtained, the following expressions are used:

$$DR = \frac{e_{max} - e}{e_{max} - e_{min}} \quad \textit{4-5}$$

$$\rho_d = \frac{M_s}{V} \quad \textit{4-6}$$

$$e_{max} = \frac{\rho_w \cdot G_s}{\rho_{dmin}} - 1 \quad \textit{4-7}$$

Where in Equation 4-5 DR is the relative density [%], e_{max} is the maximum void ratio [-], e is the void ratio [-] and e_{min} is the minimum void ratio [-]. In Equation 4-6 ρ_d is the dry density [gr/cm^3], M_s is the mass of solids [gr] and V is the volume of the container [cm^3]. In Equation 4-7where ρ_w is the density of water and G_s is the specific gravity of solids [-].

4.3.5 Free swelling

The methodology used for the free swelling test is detailed.

1. A sample of Ottawa sand with laponite is placed in a consolidation load cell to the desired density by dry pluviation.
2. Filter paper and porous stones are placed together with the sample.
3. The load cell cover is placed.
4. The dial is placed on the load cell cover and the initial value is recorded.

5. Slowly saturate the cylinder and start the time when the dial needle begins to move.
6. Measurements of the dial are made at 0.25, 0.5, 1, 2, 4, 8, 15, 30, 60, 120, 240, 480, 1440, 2880, 4320, 5760, 7200 and 10080 min from the start of the test.

4.3.6 Oedometric consolidation

The methodology followed to carry out the oedometric consolidation test is detailed, this is carried out in accordance with the ASTM D2435 standard.

1. A sample of Ottawa sand with laponite is taken and compacted at the base of the consolidation cell to the desired density by dry pluviation.
2. The porous stones and filter paper are placed in the one-dimensional consolidation chamber along with the test tube.
3. The dial is set on the piston to register the change in volume.
4. The cylinder is allowed to swell for 7 days and the volume change is recorded..
5. The loading steps are carried out every 24 hours..
6. The specimen is loaded to 0.1-0.5-2-8-16 kgf/cm^2 and the deformation is recorded with each load increment.
7. The specimen is unloaded at 8-4-2-0.5-0.1 kgf/cm^2 and the deformation is recorded with each decrease in load.
8. The moisture of the sample is determined.

To work with the data obtained, the following expressions are used:

$$\gamma_d = \frac{\gamma}{1+w} \qquad \textit{4-8}$$

$$V_s = \frac{\gamma_d \cdot V_o}{G_s \cdot \gamma_w} \qquad \textit{4-9}$$

$$H_s = \frac{V_s}{A} \qquad \textit{4-10}$$

$$e_i = \frac{H_i - H_s}{H_s} \qquad \textit{4-11}$$

$$\Delta H = d - d_o - d_a \qquad \textit{4-12}$$

$$H_i = H_o - \Delta H \qquad \textit{4-13}$$

$$\epsilon = \frac{\Delta H}{H_o} \qquad 4\text{-}14$$

$$m_v = \frac{1\epsilon_i - \epsilon_0}{\sigma`_i - \sigma´_0} \qquad 4\text{-}15$$

$$C_c(\acute{o}C_r) = \frac{e_i - e_0}{log\left(\frac{\sigma´_i}{\sigma´_0}\right)} \qquad 4\text{-}16$$

Where in Equation 4-8, γ is the wet unit weight of the sample [g/cm^3], w is the moisture content of the sample [%] and γ_d is the dry unit weight of the sample [g/cm^3]. In Equation 4-9 Vs is the volume of solids [cm^3], V_0 is the volume of the specimen [cm^3], Gs is the specific gravity of the solids [-] and γ_w is the specific weight of water [g/cm^3]. In Equation 4-10 H_s is the height of solids and A is the cross-sectional area of the sample. In Equation 4-11 e_i is the void ratio in stage i [-] and H_i is the height of the sample in stage i [cm]. In Equation 4-12 ΔH is the height variation of the sample [cm], d_o is the deformation of the sample [cm] and gives correction for deformation of the apparatus [cm]. In Equation 4-13 H_o is the initial height of the soil [cm] and in Equation 4-14 ϵ [-]. In Equation 4-15 m_v is the compressibility modulus of the sample, ϵ_i is the unit strain in stage i [-] and $\sigma´_i$ is the effective vertical stress in stage i [kgf/cm^2]. In Equation 4-16 C_c is the compressibility index of the normally consolidated or preconsolidated soil.

4.3.7 Simple shear

The methodology followed to carry out the simple shear test is detailed, it is carried out in accordance with the ASTM D6528 standard.

1. A membrane is placed on the cut base, which is held in place by 3 o`rings.
2. Loading rings are placed on the outside of the membrane and a disposable latex membrane is placed around the rings.
3. Vacuum is applied to make the inner membrane fit the rings.
4. A sample of Ottawa sand with laponite is taken and compacted at the base of the single cut to the desired density by dry pluviation.
5. The “shear piston” is placed and the disposable membrane is removed.
6. The inner membrane is fixed to the piston by 2 o`rings.
7. The base is mounted on the simple shear cell.
8. The upper head of the cell is fixed and the specimen is consolidated for 1 hr.

9. The specimen is tested at a cutting speed of 0.12mm/min, allowing a maximum deformation of 20%.
10. Horizontal and vertical deformation is recorded every minute.
11. The moisture of the sample is determined.

To work with the data obtained, the following expressions are used:

$$h_{corr} = h_o - \delta_{vcons} \quad \textit{4-17}$$

$$A_{corr} = \frac{A_o}{1 - \frac{\delta_v}{h_{corr}}} \quad \textit{4-18}$$

$$\tau = \frac{F_h}{A_{corr}} \quad \textit{4-19}$$

$$\gamma = arctg\left(\frac{\delta_h}{h_{corr} - \delta_v}\right) \quad \textit{4-20}$$

Where in Equation *4-17* h_{corr} is the corrected height in meters, h_o is the initial height [m] and δ_{vcons} is the vertical deformation due to consolidation [m]. In Equation *4-18* A_o is the initial cross-sectional area [m^2] and A_{corr} is the corrected area [m^2]. In Equation *4-19* τ is the shear stress [kN/m^2] and Fh is the horizontal force [kN]. In Equation *4-20* γ is the angular strain [º].

5 Results

5.1 Minimum and maximum void ratio

Figure 5-1 presents the results of maximum and minimum void ratio of Ottawa sand with laponite obtained using the Japanese standard method (Mijic et al., 2021), that consist in a steel mold where the soil is deposited by a funnel for minimum density and it's deposited in layers and stroked with a wooden hammer for maximum density (Pardo Ojeda, 2020).

Both the minimum and maximum void ratios present a similar behavior, they increase with the addition of up to 1% fines, after that both start to decrease until approximately 15% of fine content, since 15% fines de maximum and minimum void ratio increases again.

The increment in the void ratio between 0 and 1% of fines content can be produced by the laponite particles located between the contacts of sand particles. As the fines content increases over 1%, the volume of empty space between sand grains, known as void volume, decreases due to the presence of laponite particles in the intergranular spaces. Consequently, the solid portion of the mixture increases. This trend continues until the fines content reaches a threshold of 15%. Once this threshold is surpassed, the void volume starts to increase again as the fines portion continues to increase, with the fine portion controlling the granular arrangement.

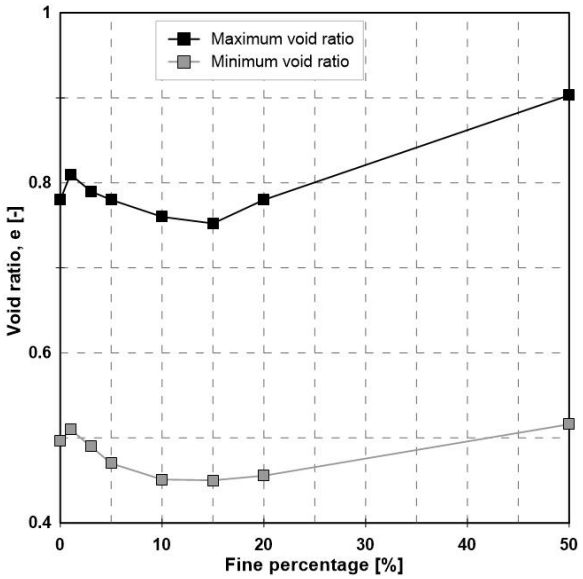

Figure 5-1: Maximum and minimum void ratio of Ottawa sand with laponite

5.2 Granulometry and particle interaction of the mixes

Figure 5-2 a) presents a summary of the grain size distribution of Ottawa sand with varying laponite content. Figure 5-2 b) shows that for low laponite percentages, the characteristic diameters D10, D30, and D60 have increased due to the increase of fines. For 1% of fines the three characteristic diameters increase, meaning that there is an apparent increase in the average particle size, observation which might be attributable to the adhesion of dry laponite particles to the surface of the sand particles. Even at 10% fines content, D60 and D30 are higher than the values of clean sand, meaning that there is also an apparent increase in bigger particles, which could be caused by the increment in size of smaller particles due to laponite sticking to the sand particles. Figure 5-2 c) presents the coefficients of curvature and uniformity of the granular mixes with the content of fines, observing that Cu and Cc increases with the fine percentage. As the Cu values are below 6 it is considered that all the samples up to 15% of laponite are poorly graded sand, for 20% of laponite the soil is poorly graded sand with clay. As the fine content increases the soil sample has a better graduation, so the increase in Cc and Cu can be seen as an effect of the heterogenization of the mixture.

a)

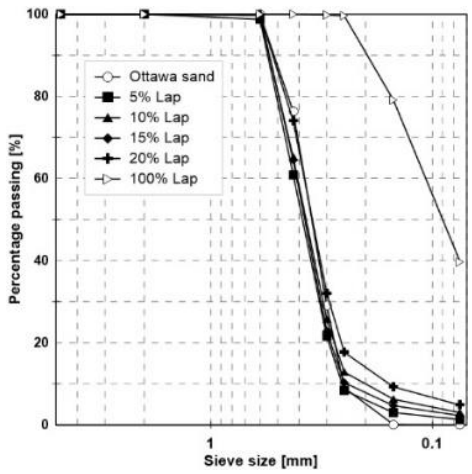

b)

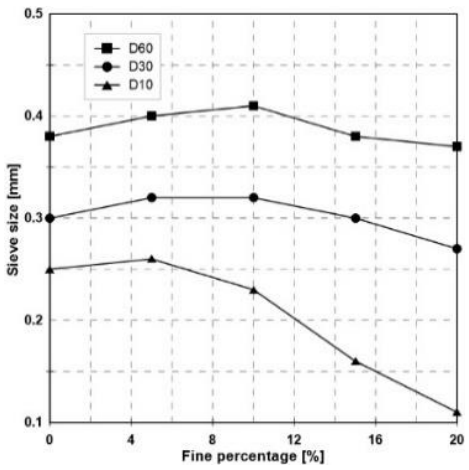

c)

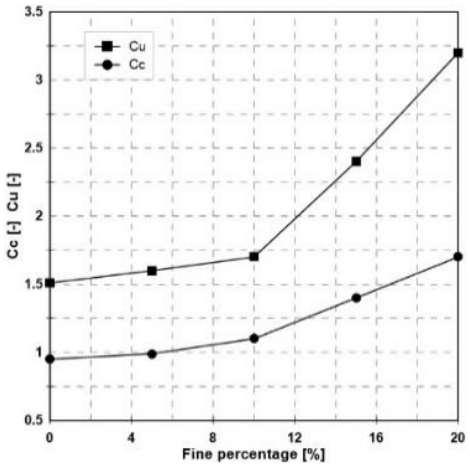

Figure 5-2: a) Granulometric curves for Ottawa sand with 5, 10, 15 y 20% of laponite, b) Characteristic diameters and c) Curvature and uniformity coefficient.

The granulometries were also compared with the ideal granulometry they should exhibit assuming there is no interaction between sand and Laponite whatsoever, to address the effects of the interaction of the laponite particles with sand.

Figure 5-3 a) present the theoretical granulometric curves made with a combination of Figure 4-1 a) and Figure 4-2 a) and represent the behavior of the granulometric curve of a mix with no interaction between sand and Laponite. Figure 5-3 b) present the experimental granulometric curves obtained by the regular granulometry test. Figure 5-3 c) shows the difference between the curves presented in Figure 5-3 a) and in Figure 5-3 b), for all Laponite concentrations both present consistent differences of up to 13% in some sieves. This implies that the dry behavior of the mixture of sand and laponite is the result of a significant interaction between them.

a)

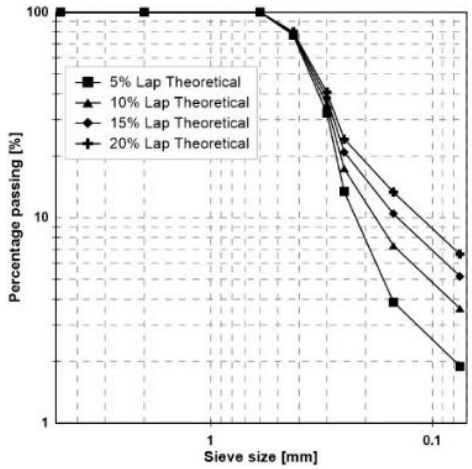

b)

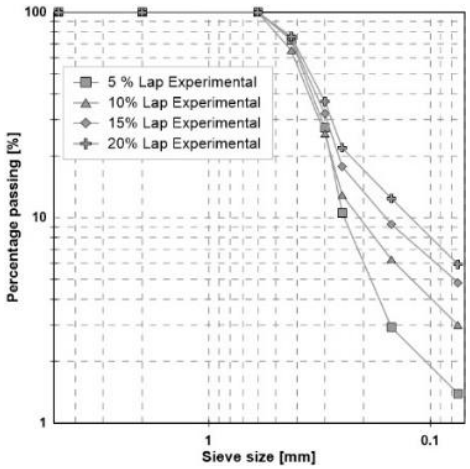

c)

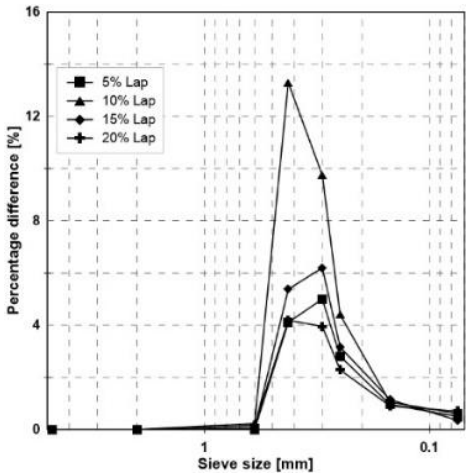

Figure 5-3: a) Theoretical granulometries, b) Experimental granulometries and c) Difference per sieve.

The results and observations from the granulometries and analytical exercises suggest that -partially- laponite particles adhere to the surface of sand particles, “apparently increasing” the sand particle diameter due to the attachment and coating of laponite throughout the surface of the sand particles. As a result, the percentage of fines is lower than expected. It is also interesting to note that the increment in the retained mass between sieves it’s not related to the amount of laponite in the mix.

Figure 5-4 a), b) and c) presents images obtained by the scanning electron microscope of Ottawa sand with laponite and a close-up of their interaction at the particles surface. Ottawa sand particles with 5, 10 and 20% of laponite are observed evidencing the adhesion of large laponite particles to the sand. These pictures are further evidence of the interaction that exists between laponite and sand particles.

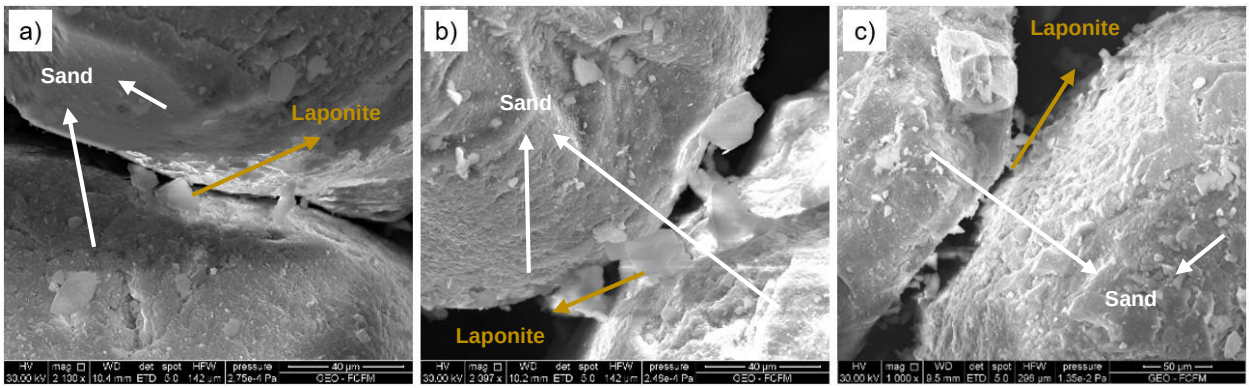

Figure 5-4: SEM image of Ottawa sand with a) 5%, b) 10% and c) 20% laponite (Dry).

These observations (Figure 5-4 a), b) and c)) support the idea that Laponite adhering to the sand particles “apparently” increases the average particle size, inducing differences that can be as much as 13% in the particles retained per sieve as depicted in Figure 5-3 c).

Figure 5-5 shows a test to identify the interaction between sand particles with and without Laponite, the tests consist in taking a sand particle close to other particles and see its interaction. Figure 5-5 a) shows the test without Laponite and there is no visible interaction between the sand particles. Figure 5-5 b) shows the same tests but the sand particles are mixed with Laponite and at the moment the sand particle with laponite touch a smaller particle this adheres to the bigger one and can be lifted.

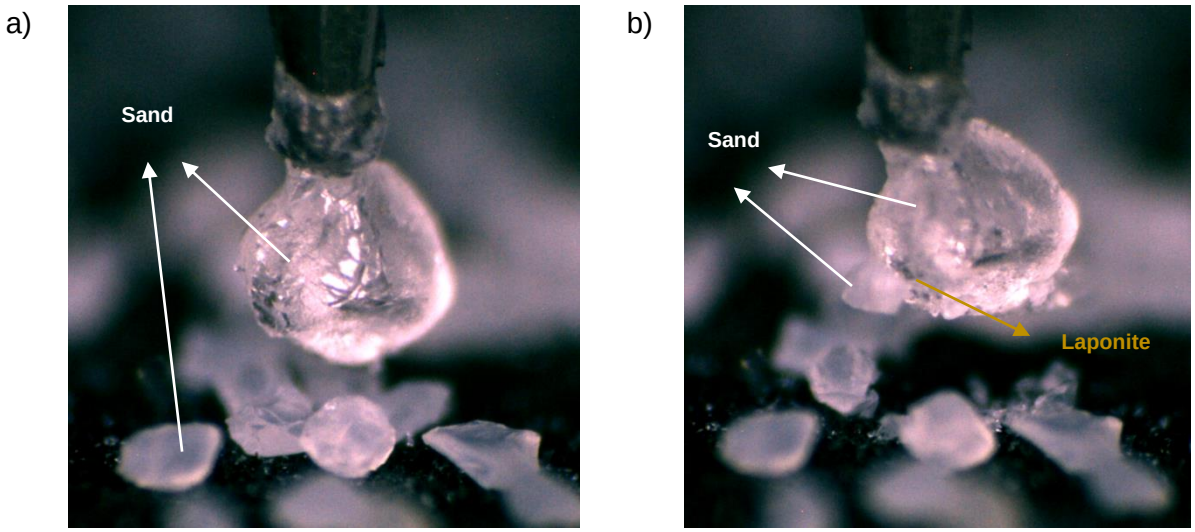

Figure 5-5: Sand with Laponite lifting a smaller sand particle due to attractive forces.

5.3 Mechanical properties of dry mix of sand with laponite

5.3.1 Simple Shear

Figure 5-6 present the shear strength versus angular strain of mixtures of Ottawa sand and Laponite. Figure 5-6 a) shows the behavior in simple shear of clean Ottawa sand, for the same vertical confinement the dense samples have greater shear strength. Figure 5-6 b) shows the shear strength versus angular strain of the mixture of Ottawa sand with 1% Laponite, this mixture presents the same behavior of the clean Ottawa sand but in this case the difference in the shear strength between the loose and dense samples is less than that of the clean Ottawa sand. Figure 5-6 c) shows the results of the mixture with 3% Laponite, in this case for a confinement of 1

kgf/cm^2 the loose and dense samples present almost the same shear strength, the other curves are like the mixture of 1%. Figure 5-6 d) shows the results of the mixture of 5% Laponite and the behavior observed is similar to that of the mixture of 3% laponite, the curve of 1kgf/cm^2 have similar shear strength. Figure 5-6 e) present the shear strength of pure Laponite where the behavior is roughly the same, meaning that the shear strength increases with the vertical confinement.

a)

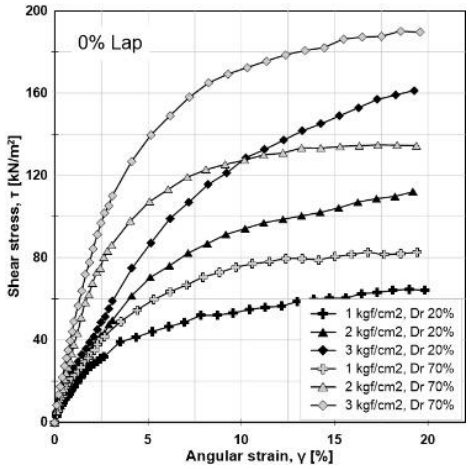

b)

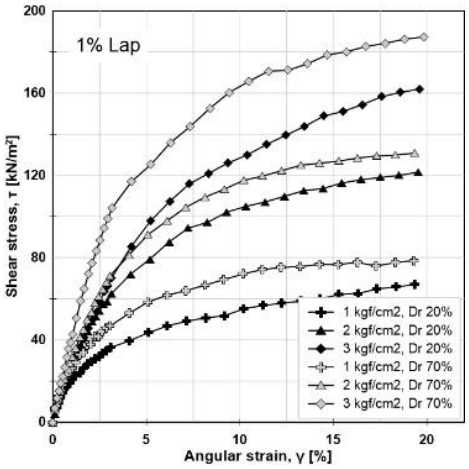

c)

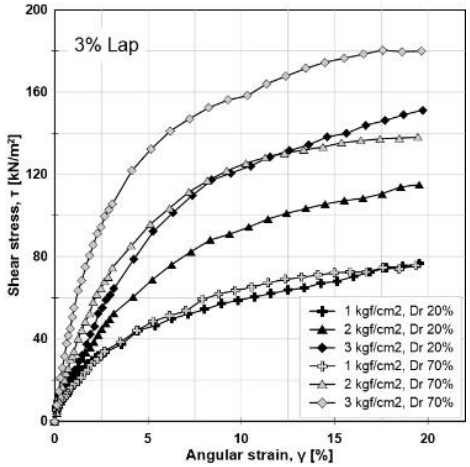

d)

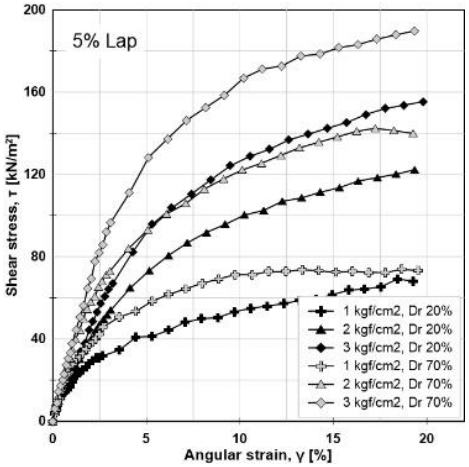

e)

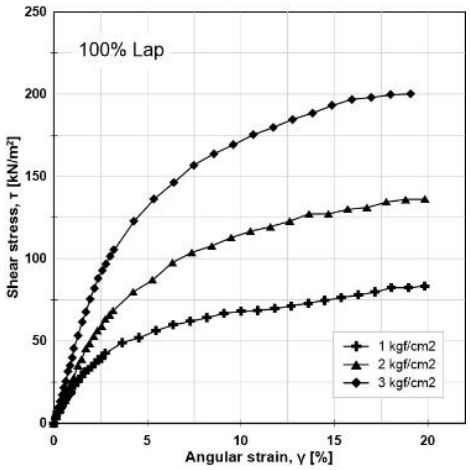

Figure 5-6: Shear stress vs angular strain for Ottawa sand with a) 0%, b) 1%, c) 3% d) 5% at Dr 20% and Dr 70% and e) pure laponite.

In general, the shear strength increases with vertical confinement for both densities, and the shear strength for the same level of vertical confinement is higher for the denser arrangement, as expected.

Based on the results of the simple shear tests, the critical state line (CSL) was constructed for all samples at 30% of the angular strain. In Figure 5-7, the strength parameters obtained from the critical state line (CSL) for Ottawa sand with different percentages of laponite (0%, 1%, 3%, and 5%) are presented. Figure 5-7a) presents the critical state friction angle that decrease with the percentage of Laponite in the mix for both densities and Figure 5-7 b) presents the cohesion of the mixes that increase with the percentage of Laponite.

a)

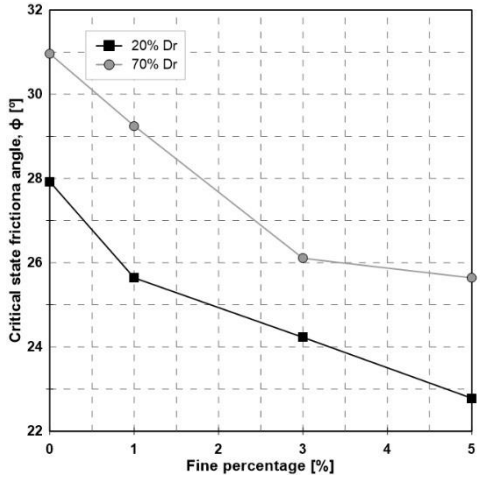

b)

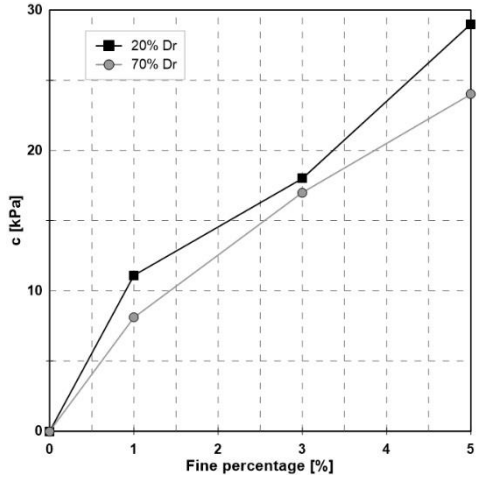

Figure 5-7: Critical state friction angle and b) cohesion for laponite mixes at 30% of angular strain.

As the critical state friction angle reflects the frictional nature of the contacts between the particles, its decrease means that laponite is effectively affecting the contacts between sand particles. It's possible that Laponite begins to allocate in the cavities of the sand particles smoothing their surfaces and therefore reducing the friction angle.

The increase in the cohesion with the Laponite percentage of the mix is to be expected, as the amount of Laponite increase the cohesion of the mix tends to approach to the value of that of pure Laponite.

Another aspect of interest is the effects of Laponite in the shear modulus of the mixes. Several studies have addressed the dependence of the shear modulus with confinement (Drnevich et al., 1978; Hardin et al., 1972, 1963). This relation between the shear modulus and the confinement can be addressed considering the calculation of the normalized shear modulus G/Pa at 1% strain with the normalized confinement σ/Pa.

In Figure 5-8 a) and b) the normalized shear modulus G at 1% strain is graphed versus the normalized vertical stress, in loose and dense states respectively, and a power regression is generated to identify a correlation between them. Figure 5-8 c) shows the Normalized Shear Modulus vs the fine content obtained in simple shear, the shear modulus increases with the vertical confinement, and tend to decrease with the fine content. However, there is a peak in the Shear Modulus at 1% fines for the loose specimens indicating an increase in the shear resistance of the soil compared to the clean sand, this increment with 1% laponite is not observed in the dense specimens due to a difference in the soil structure and fine distribution.

a)

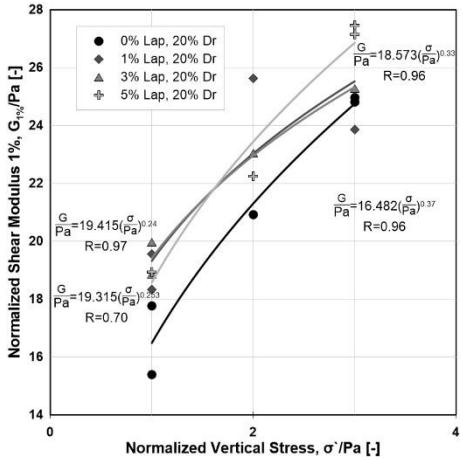

b)

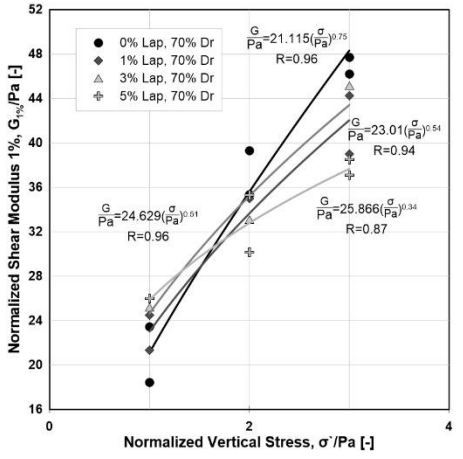

c)

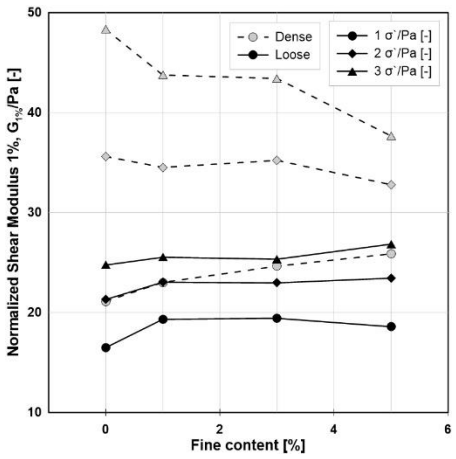

Figure 5-8: a) b) Normalized maximum shear modulus versus normalized vertical stress and c) normalized shear modulus versus fine content from regression.

With the data presented in Figure 5-8 a) and b) the parameters obtained from the power regression are plotted in Figure 5-9 finding a linear correlation between them. The parameter Cz obtained can be related to the grain characteristics or nature of grains, fabric or microstructure of geomaterial and the nz parameter can be related to the contact between particles and strain amplitude (Sawangsuriya, 2012).

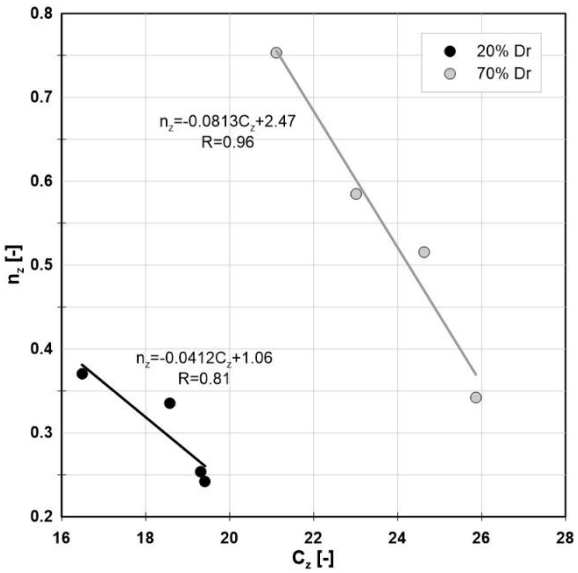

Figure 5-9: Cz versus nz from regression.

5.3.2 Fabric interpretations from saturated specimens of sand and laponite

Figure 5-10 a) shows the free swelling results of Ottawa sand-laponite mixes with 1, 3, 5, 10, 15 and 20% of fines and a logarithmic regression of the data presented for the loosest state. The volumetric strain increases with the percentage of Laponite of the mix and has an approximately linear behavior in the maximum volumetric strain reached. It is important to note that with 1% of

Laponite content there is swelling. Figure 5-10 b) present the free swelling results of Ottawa sand-laponite mixes with 1, 3, 5, 10, 15 and 20% of fines and a logarithmic regression of the data presented for the densest state. The volumetric strain increases with the percentage of Laponite of the mix and has an approximately linear behavior in the maximum volumetric strain reached. In this case with 1% laponite there is no recordable value of swelling.

When compared the loose and dense state for the same amount of Laponite the dense samples tend to have a greater maximum volumetric strain, except for 1% Laponite where the dense sample doesn't swell, and the loose sample presents measurable swelling. Two factors intervene at low laponite content that explains the irregularities in the swelling process. The first is the presence of fines in the contact zone between particles, and the second is the inhomogeneous distribution of the particles in the intergranular spaces. It is important to consider that according to theoretical calculations, the intergranular spaces are saturated with laponite at approximately 2% mass versus sand mass, considering a Laponite deposition of 10kN/m3.

For the loosest states, Laponite particles stay in the contact between sand particles and push them apart when its hydrated. For dense samples that show little or no swelling, the laponite particles found in the contacts move towards the intergranular spaces due to the application of energy to compact the samples, it also happens that the larger laponite particles are crushed in the contact area, so they are divided, falling into the spaces that remain available. To this it can be added that, as the soil is more compact, the friction of it with the edges of the chamber that contains the specimen increases, producing a force in the opposite direction to the swelling.

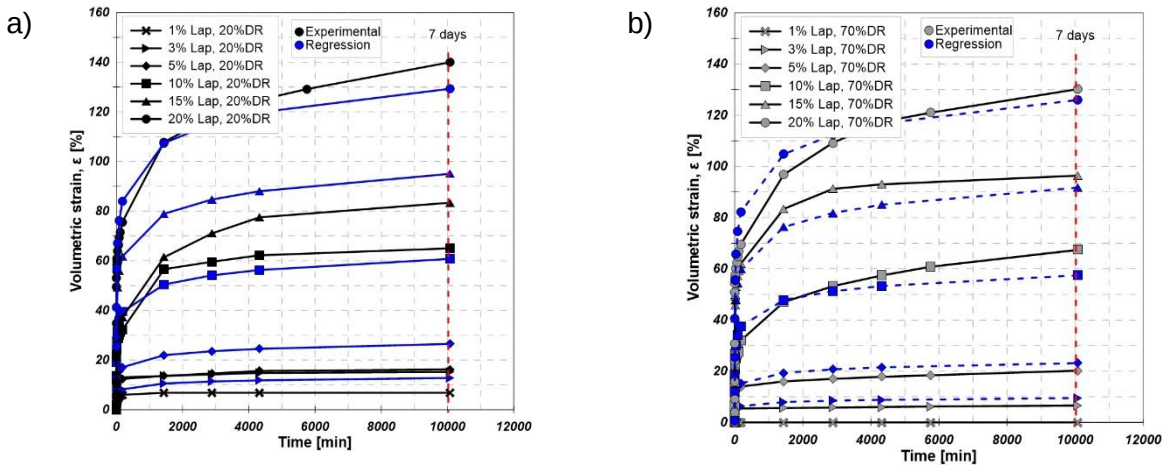

Figure 5-10: Experimental and theoretical free swelling curves a) Loose samples and b) Dense samples.

From the results obtained, it is possible to propose an equation that predicts the behavior of the Ottawa sand and laponite mixtures. For this, a logarithmic regression is performed with the free swelling data obtained for concentrations from 1 to 20% of laponite for the two densities studied.

With the data, an equation is proposed that predicts the behavior of a certain mixture of sand and laponite, dependent on time, the amount of laponite, and density. The equation is as follows:

$$\varepsilon = A * ln(t) + B \quad (21)$$

Where the parameters A and B are dependent on the density and fine content of the mixture. As can be seen in Figure 5-10 a) and b), the theoretical curves fit the experimental ones. As the fines content increases, the function behaves better in terms of maximum swelling prediction and correlation with the experimental curves.

Figure 5-11 presents images of Ottawa sand samples with laponite concentrations of 20%, these samples were left in free-swelling for 7 days and then oven-dried for 24 hrs. In Figure 5-11 a) with a 400x magnification a laponite “bridge” between three sand particles is observed and depicts the separation between sand particles provoked by the hydration of laponite. In Figure 5-11 b) with a 3000x magnification a structure of laponite layers is observed, this layered structure is characteristic of Laponite.

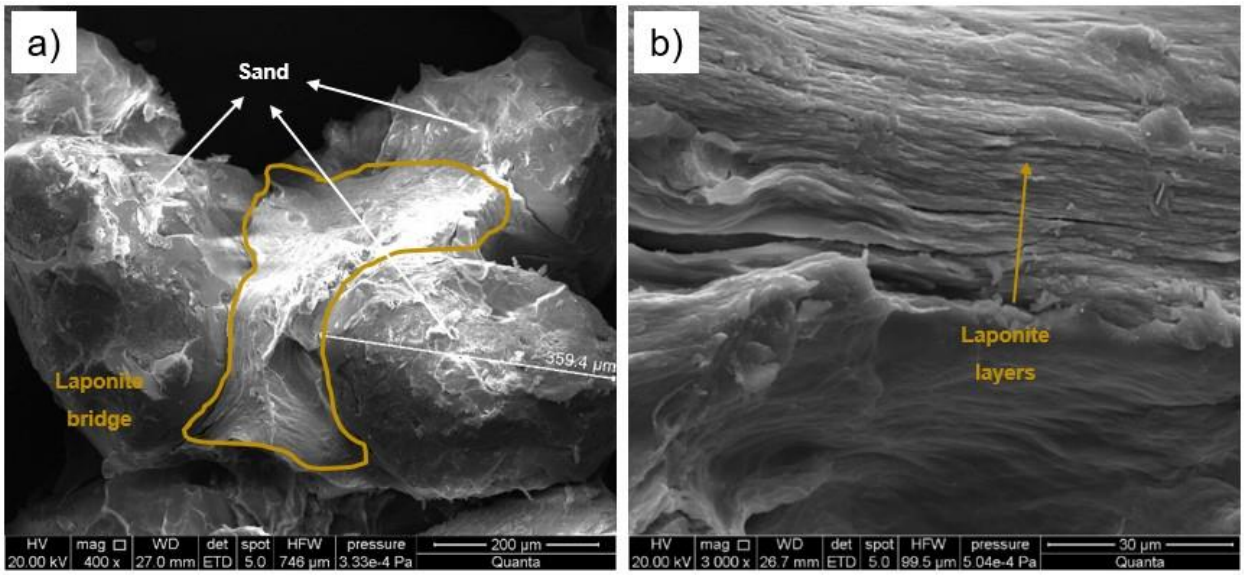

Figure 5-11: SEM image of Ottawa sand with 20% laponite in free swelling (Wet).

5.3.3 Swelling pressure

Figure 5-12 shows the maximum pressure reached by different mixtures of sand and laponite. Pure Laponite presents the maximum pressure between the samples, and it reached its peak at approximately 2 days of started the tests, the mixes reached its maximum at approximately 1 day of started the test.

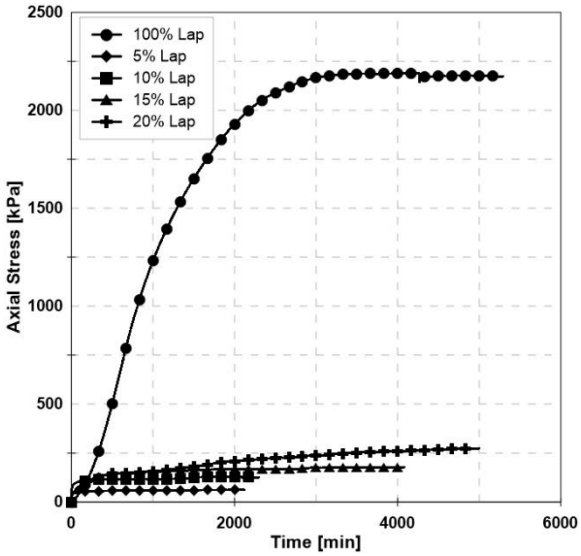

Figure 5-12: Swelling pressure of sand and laponite samples.

The results show that the maximum axial stress and the time it takes to reach that value highly depends on the amount of laponite of the mixture. With less laponite the permeability of the mixture increases, making it easier to hydrate all laponite particles, meanwhile with more laponite it takes more time to reach the peak due to the decrease in the permeability. The behavior of the peak stress is according to the expected, with more laponite the maximum stress value increases and the value obtained for the sand-laponite mixture is a portion of that of the pure laponite.

5.3.4 Consolidation

Figure 5-13 presents a diagram of the consolidation process for the samples of 5 to 20% laponite with Ottawa sand. The process depicted in Figure 5-13 begins with a free swelling phase, after seven days the sample is loaded in intervals of 24hrs, when the maximum load is reached the sample is unloaded in the same time intervals.

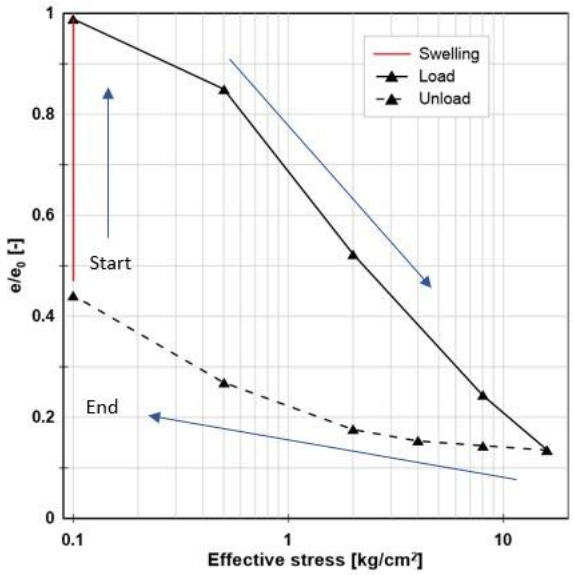

Figure 5-13: Diagram of consolidation process.

Figure 5-14 a) shows the consolidation parameters of the Ottawa sand with 5, 10, 15 and 20% laponite. It is observed that as laponite is added, the re-compression index increases by 850%, 1200% and 1180%, compared to sand alone, for 20% relative density and by 580%, 1000% and 1245% for 70% relative density. For the compression index, it is observed that by adding laponite, it increases by 700%, 1400% and 1550% compared to sand alone for 20% of the relative density and by 600%, 1240% and 1830% for 70% relative density.

Figure 5-14 b) present the ratio between the recompression and compression coefficients, for the loose samples there is a change in the slope of the curve at 15% fines content, meaning that the difference between the compression and recompression coefficient is beginning to stabilize. For the dense samples the slope change occurs at 10% fine content. The stabilization observed for both curves points out the limit fine content of these properties, i.e. the fine content in which the dominant particle of the mix change from sand to Laponite.

The tests suggest that the increase in fine content results in a greater difference between the initial and final void ratio, indicating that the compressional behavior of the mixes is influenced by the presence of laponite. Therefore, is expected that the curves tend to follow the properties of pure laponite as the percentage of fines increases.

a)

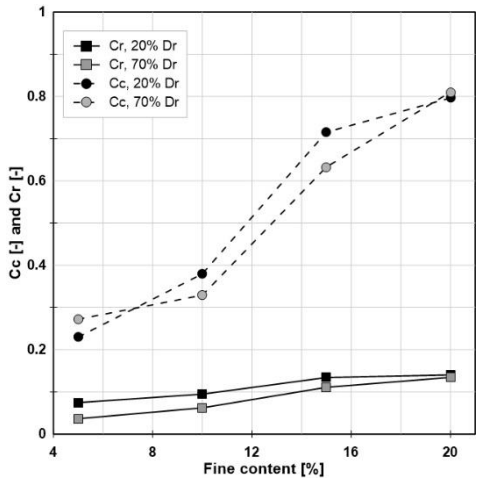

b)

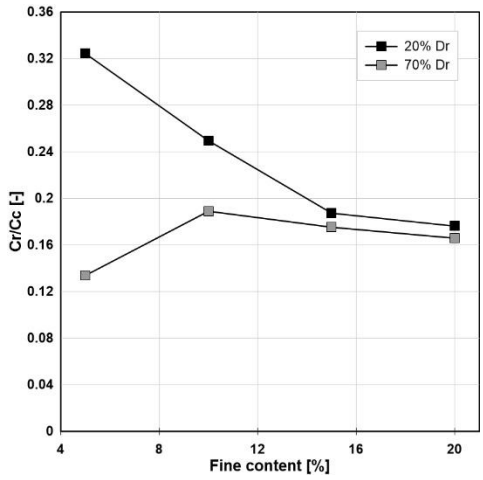

Figure 5-14: a) Compression and recompression coefficient versus fine content and b) ratio between recompression and compression coefficient versus fine content.

Figure 5-15 a) present the compression curve for the skeleton void ratio versus the effective stress of the loose samples and Figure 5-15 b) present the compression curve for the skeleton void ratio versus the effective stress of the dense samples. For both graphs the compression curves are almost parallel between 0.4 and 2 kgf/cm^2 however after that the curves for 5 and 10% Laponite tends to stabilize indicating that the coarse grains are aggregating. For 15% and 20% fines, the skeleton void ratio continues to decrease, indicating that the coarse grains are still compressing and are separated by the laponite. This can be explained by the greater amount of fines present in the mixes, which segregate the coarse grains.

Figure 5-15 c) present the granular compression index of the mixes, this shows a seemingly linear behavior without the expected change in slope between 10 and 20% fine content. However, there seems to be a change in this behavior under 10% FC, that can be explained by the fact that the limit fine content is located below the 10% fines and is close to 5% FC.

a)

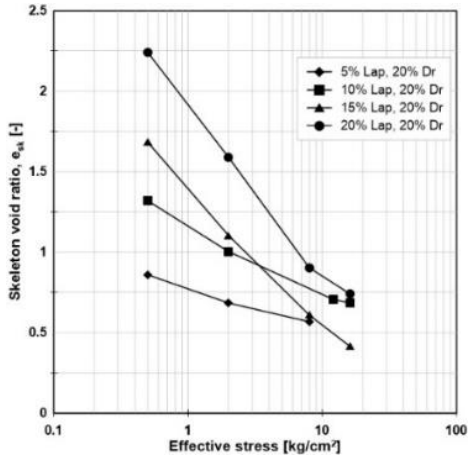

b)

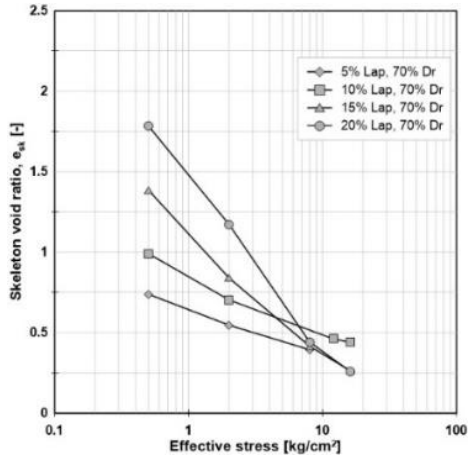

c)

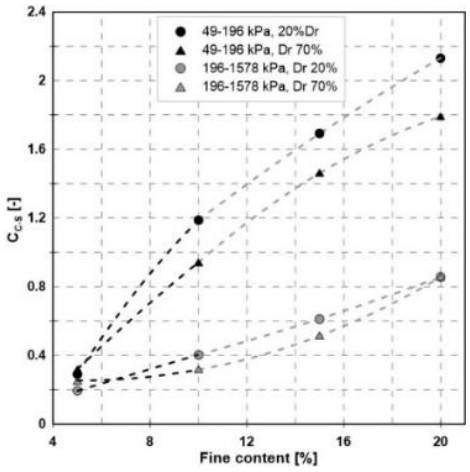

Figure 5-15: Skeleton void ratio vs effective stress, compression curve for a) Dr 20% and b) Dr 70%, c) granular compression index vs fine content.

6 Discusssion

6.1 Granular arrangement

Figure 6-1 is an interpretation of the behavior of the granular arrangement of the mixes based on the data obtained from the tests of this study. This interpretation has some nuances that make it different from the arrangement of other types of particles. First, the fine particles adhere to the coarse grains even in very low concentrations, at the same time the fine portion tend to settle in the interparticle spaces, causing a decrease in the maximum and minimum void ratio, however, as the number of fines increases, the intergranular spaces are filled, so the coarse particles are displaced by the fine ones. Depending on the form of deposition or the characteristics of the particles involved, what can happen is that the fines are not only distributed towards the intergranular spaces, but also remain in the contact zone, which causes some changes in the behavior of mixtures with small amounts of fines.

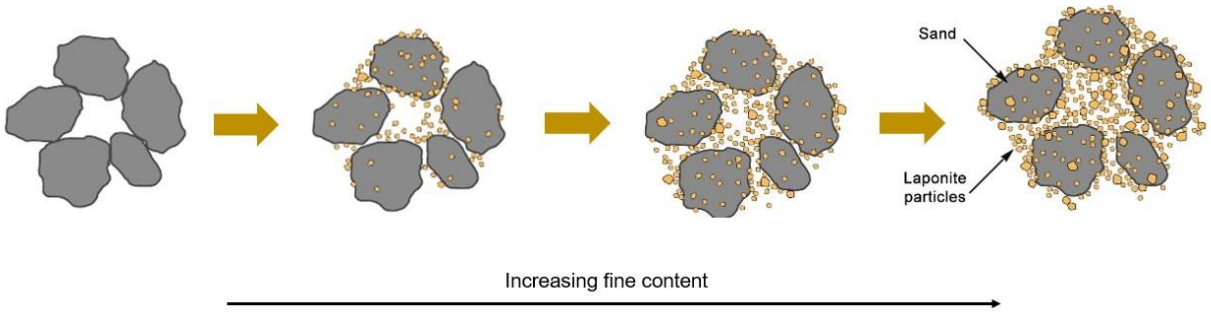

Figure 6-1: Progression of the fine particle distribution on a coarse matrix.

This repeated and peculiar result, not observed with sands with natural fines, was already described in (Ochoa-Cornejo et al., 2019) and it can be attributed to the unique characteristics of laponite, particularly its small size and tendency to aggregate of the nanoparticles. This property allows laponite particles to easily penetrate the asperities of sand grains, causing the separation of the particles in low dosages.

6.2 Particle interactions in the mixes

Figure 5-3 shows the two assumptions with which we worked in regard of interaction between sand and Laponite, the left image represents the assumption that there is no interaction between the fine and coarse grains. The right image represents the adherence of the fines to the coarse particles.

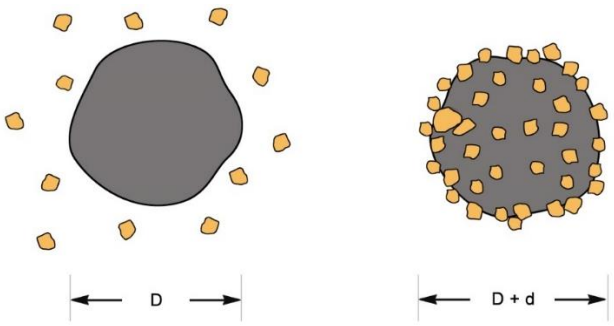

Figure 6-2: Behavior of laponite particles with Ottawa sand.

The behavior shown in Figure 6-2 explains the increment in the retained mass per sieve observed in the experimental curves of Figure 5-3 c), the apparent diameter of the sand particles increases, meaning that particles that previously could pass certain sieve are no longer able to due to the adhered laponite..

6.3 Shear strength of sand-clay mixes

As the Shear Modulus is associated with the force transmission chains between particles (Wichtmann & Triantafyllidis, 2009), in a non-uniformly composed granular packing, strong and weak force chains are formed through the interparticle contacts. A contact is defined as “strong” if it transmits a normal force N_C greater than the average value N_{AVC} of all contacts, if $N_C < N_{AVC}$ applies, the contact is “weak” (Wichtmann & Triantafyllidis, 2009).

The increment observed at 1% fine content (Figure 5-8 c)) indicates that laponite is ubicated in the contact zone of the sand particles and is adding stiffness to the contact generating a stronger force transmission chain. The behavior observed in the dense samples for confinement of 2 and 3 can be explained by the application of energy to compact the samples, this allows the laponite particles found in the contacts to move towards the intergranular spaces making the contact between sand similar to its original state or adding to the weak force transmission chains, decreasing the normal force between sand particles and in turn decreasing the shear modulus.

Above 1% fine content the shear modulus decreases because laponite starts to occupy all spaces between the sand particles decreasing the normal force between them and acting as a lubricant between the contact decreasing its stiffness.

6.4 Swelling of sand-clay mixes

Figure 6-3 presents the differences between the tests carried out in this study and the results of Komine & Ogata (1999), who worked with sand-bentonite mixtures, Cui et al. (2012) who worked with bentonite mixed with quartz sand, Schanz & Elsawy, (2015) who worked with bentonite mixed with limestone and Jain et al. (2022), who worked with bentonite and sand obtained from Dahmi Kalan village, Jaipur Rajasthan. Even though these differ in magnitude, the general behavior of the curves is similar, so the conclusions obtained from the study are applicable. The higher the density, the greater the ratio of laponite to void volume, so it is expected that it will have less free space to swell, allowing the entire granular matrix to deform. Similarly, the higher the percentage of laponite in the mix, the greater the relationship with the volume of voids, so it would tend to behave in the same way.

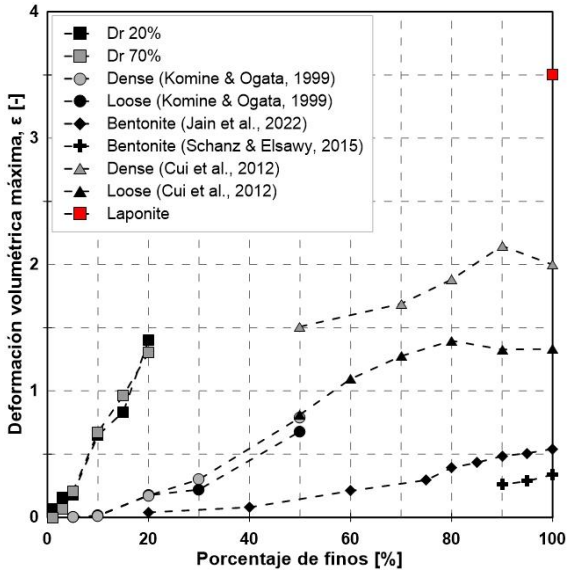

Figure 6-3: Comparison between the free swelling data of this study and the ones of Komine y Ogata (1999), Cui et al. (2012), Schanz & Elsawy, (2015) and Jain et al. (2022).

It is important to note that the maximum swelling for the bentonite samples from the various studies for 80% of the fines content is similar, for some cases, to the maximum swelling of laponite for 20% of fines, this shows the great capacity of swelling that laponite has compared to bentonite.

6.5 Compression of sand-clay mixes

Figure 6-4 compares the results of the granular compression index obtained with those of M. Monkul et al., (2005), Shi et al., (2017) and (Vijaya Kumar, 1996). It can be noted that the granular compression coefficient is higher for the case of laponite than for kaolinite, this can be explained by the highest plasticity index of laponite, it can be assumed that the values exhibited in this study

correspond to the second or final part of the curve, therefore the data would be missing for lower percentages of fines to determine the limit fines content for those stresses and densities.

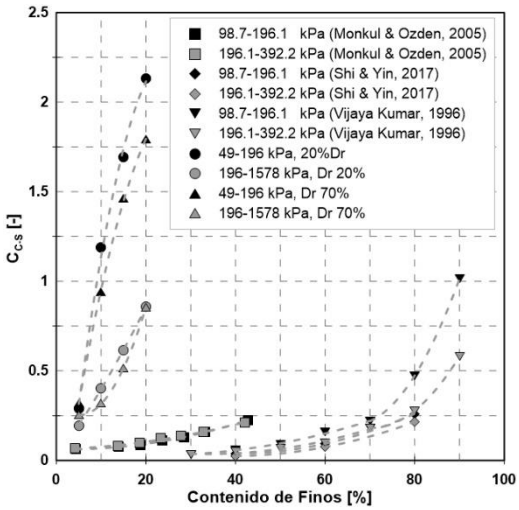

Figure 6-4: Comparison of granular compression index vs fine content.

7 Conclusions and Recomendations

7.1 Conclusions

Nanomaterials present a great opportunity to improve current technologies and can provide a huge benefit to civil engineering. This discipline is slowly but steadily approaching these materials.

In the case of laponite its high plasticity makes it a good replacement for other clays used in engineering, such as bentonite, the behavior of laponite is controlled by diverse factors, concentration, temperature, concentration of salts, etc. That makes its application a problem of many variables that must be investigated deeply to fully understand its potential, even though, most authors coincide in the chemical properties of laponite, making it ideal for investigation due to its homogeneity, what's more challenging it's the interaction it has with other materials.

The addition of laponite produces an increase in some properties of sand, cement, and soils. This increment in liquefaction resistance, compressive strength, or viscosity depends on the amount of laponite added to the material but all tests presented a peak in the improvement i.e., more laponite do not necessary implies an increment in the materials characteristic. This peak is related to the disposition of laponite between the particles of the materials, this also implies that there is an optimum of laponite in which the improvement is maximum.

Lastly, the use of laponite seems to be cost efficient due to the small quantities required to produce changes in the behavior of some materials in addition to the homogeneity of laponite which makes it reliable and low risk.

The experimental results from granulometries, simple shear, free swelling and consolidation tests conducted on loose and dense specimens of Ottawa sand and Ottawa sand containing laponite in concentrations of 1 to 20% by dry mass of sand. The objectives of the work were to determine the effects of the dry structure generated in the sand laponite mixtures and how this is reflected in wet conditions.

The tests show that the maximum and minimum void ratio present a variation in accordance with what was presented in other works such as those by Vallejo & Mawby (2000), that is, they approach a minimum point with the increase in the content of fines, which is within the 15-20% fines content, from this point onwards the laponite is expected to control the void ratio. With these observations and the SEM images a slightly different model of granular arrangement is proposed for sand-laponite mixtures.

The granulometries carried out in this study account for the adhesion capacity of the laponite to the sand particles. There is a 5% increase in the weight retained in the #40 sieve (0.425 mm) product of the laponite adhered to the particles. This also implies that the distribution of the laponite is not direct towards the intergranular spaces, at least in low fines content.

According to the shear strength tests carried out in this study, it is concluded that the peak shear strength in sands is insensitive to the addition of small amounts of fines, in the same way as the peak angle of internal friction, this is consistent with what was studied by Vallejo & Mawby (2000) in direct shear tests.

In the study, it was found that although the critical state line obtained may not accurately represent the actual behavior of the soil due to test conditions, the friction angle tends to decrease with the increase in fine content. The observed differences between the dense and loose specimens align with the expected behavior observed in simple shear tests.

It was found that for loose samples the addition of 1% laponite increases the shear modulus, indicating that laponite locates in the contact zone of the sand particles strengthening the force transmission chains. For 3% and 5% of laponite content the shear modulus decreases as the laponite located in the intergranular space forms a weak force transmission chain.

For low fines contents, from 1 to 5% laponite, the swelling test is extremely sensitive to the manufacturing conditions of the specimen, which alters the results, this is especially noticeable in the decrease in the maximum swelling of the densest specimens in compared to the loose ones. The distribution and redistribution of the laponite after applying the compaction energy necessary to achieve the desired densities plays a fundamental role in the behavior of the mixtures in free swelling, the energy applied for the densest cases allows the redistribution of the laponite located in the interparticle contacts towards the intergranular spaces as a result of their breakage or separation, causing the mixtures to behave differently than expected in cases of low concentration (1-5%).

For consolidation studies, the addition of laponite caused an increase in the compression and recompression coefficients. These values would be expected to approach those of pure laponite as the percentage of fines added to the mix increases.

The observations obtained from the wet studies help to understand the behavior of the particles of laponite in the intergranular spaces of the dry mixtures and reinforce the concept that it’s inevitable that these particles are deposited in the contact between coarse particles producing a

change in its behavior. However, is relevant to point that the concept of limit fine content that is extensively used is only valid for expansive soils under certain conditions, as showed the LFC changes according to the studied property and the presence of water in the mixture so it cannot be used freely without specifying the conditions in which the soils was tested.

7.2 Future research scope

It is recommended to carry out the battery tests again, but with higher percentages of Laponite, paying special attention to the tests of free swelling, consolidation, granulometries and simple shear.

It is recommended to carry out a dry one-dimensional compression study to relate the behavior of the dry and wet mix. It would be recommendable to reach values of up to 30% laponite to observe the critical point where the change in soil behavior occurs. In addition, it is recommended to carry out consolidations for concentrations between 1 and 10% of laponite in order to accurately find the concentration of fines for which the behavior of the mixture changes.

To better evaluate the shear resistance, it is recommended to add tests of direct shear and vane shear. For direct shear, it is recommended to carry out a campaign of both drained and undrained tests, dry and wet, with laponite percentages from 1 to 100%.

It is important to re-evaluate the methodologies corresponding to each test and look for improvements that allow less interference with the swelling capacity of the laponite and establish the reaction times of the mixture correctly and precisely. For example, for consolidation, establish adequate swelling, loading and unloading times based on test trials. In the same way, establish suitable containers for free swelling, which allow sliding without friction on the edges of the sample.

Finally, the equation found for free swelling with Ottawa sand should be verified for higher concentrations of laponite and verify if it is valid for other types of sand.

8 Bibliography

Al-Mukhtar, M., Qi, Y., Alcover, J.-F., Conard, J., & Bergaya, F. (2000). *Hydromechanical effects: (II) on the water-Na-smectite system*. http://pubs.geoscienceworld.org/claymin/article-pdf/35/3/537/3308245/537.pdf?casa_token=FQeNUz6oCBUAAAAA:1mvOgMxVEbu4m6Gw60J6s4ZtDts5_hprgFdQXi6lLZerrmohT2U3RkAfSbmgvnQHdVcH

Alshibli, K. A., Asce, M., Alsaleh, M. I., & Asce, A. M. (2004). Characterizing Surface Roughness and Shape of Sands Using Digital Microscopy. *JOURNAL OF COMPUTING IN CIVIL ENGINEERING*. https://doi.org/10.1061/(ASCE)0887-3801(2004)18:1(36)

Amonette, J. E. (2002). *Chapter 5 Methods for Determination of Mineralogy and Environmental Availability* (J. B. Dixon & D. G. Schulze, Eds.).

Amri, S., Akchiche, M., Bennabi, A., & Hamzaoui, R. (2019). Geotechnical and mineralogical properties of treated clayey soil with dune sand. *Journal of African Earth Sciences*, *152*, 140–150. https://doi.org/10.1016/j.jafrearsci.2019.01.010

Azam, S. (2007). Study on the swelling behaviour of blended clay-sand soils. *Geotechnical and Geological Engineering*, *25*(3), 369–381. https://doi.org/10.1007/s10706-006-9116-1

Bao, X., Jin, Z., Cui, H., Chen, X., & Xie, X. (2019). Soil liquefaction mitigation in geotechnical engineering: An overview of recently developed methods. In *Soil Dynamics and Earthquake Engineering* (Vol. 120, pp. 273–291). Elsevier Ltd. https://doi.org/10.1016/j.soildyn.2019.01.020

Barber, J. R., & Ciavarella, M. (2000). Contact mechanics. In *International Journal of Solids and Structures* (Vol. 37). https://www.sciencedirect.com/journal/international-journal-of-solids-and-structures/vol/37/issue/1 Charitidis, C. A., Georgiou, P., Koklioti, M. A., Trompeta, A. F., & Markakis, V. (2014). Manufacturing nanomaterials: From research to industry. In *Manufacturing Review* (Vol. 1). EDP Sciences. https://doi.org/10.1016/S0020-7683(99)00075-X

Conejera, A. (2016). *Efecto de la Fábrica y la Estructura en la Resistencia no Drenada de Relave Integral*.

Cui, S. L., Zhang, H. Y., & Zhang, M. (2012). Swelling characteristics of compacted GMZ bentonite-sand mixtures as a buffer/backfill material in China. *Engineering Geology*, *141–142*, 65–73. https://doi.org/10.1016/j.enggeo.2012.05.004

Dafalla, M. A. (2017). The Compressibility and Swell of Mixtures for Sand-Clay Liners. *Advances in Materials Science and Engineering*, *2017*. https://doi.org/10.1155/2017/3181794

Daniyal, M., Azam, A., & Akhtar, S. (2018). *Application of Nanomaterials in Civil Engineering* (pp. 169–189). https://doi.org/10.1007/978-981-10-6214-8_6

Das, I., & Ansari, S. A. (2009). Nanomaterials in science and technology. *Journal of Scientific & Industrial Research*, *68*, 657–667.

Dash, H. K., & Sitharam, T. G. (2011). Undrained monotonic response of sand-silt mixtures: Effect of nonplastic fines. *Geomechanics and Geoengineering*, *6*(1), 47–58. https://doi.org/10.1080/17486021003706796

De, A., Ferreira Guimarães, M., Sampaio, V., & Ciminelli, T. (2007). Surface Modification of Synthetic Clay Aimed at Biomolecule Adsorption: Synthesis and Characterization. In *Materials Research* (Vol. 10, Issue 1).

Dolez, P. (Ed.). (2015). *Nanoengineering*.

Drnevich, V. P., Hardin, B. O., & Shippy, D. J. (1978). Modulus and Damping of Soils by the Resonant-Column Method. In *Dynamic Geotechnical Tesitng* (pp. 91–125).

El Howayek, A. (2011). *Characterization, rheology and microstructure of laponite suspensions* [Purdue University]. https://docs.lib.purdue.edu/dissertations/AAI1501215/

El Mohtar, C. S., Bobet, A., Santagata, M. C., Drnevich, V. P., & Johnston, C. T. (2013). *Liquefaction Mitigation Using Bentonite Suspensions*. https://doi.org/10.1061/(ASCE)GT.1943-5606.0000865

Elkatatny, S. (2019). Development of a homogenous cement slurry using synthetic modified phyllosilicate while cementing HPHT wells. *Sustainability (Switzerland)*, *11*(7). https://doi.org/10.3390/su11071923

Elkatatny, S. (2021). Improved carbonation resistance and durability of Saudi Class G oil well cement sheath in CO2 rich environments using laponite. *Journal of Petroleum Science and Engineering*, *196*. https://doi.org/10.1016/j.petrol.2020.107812

Fan, J., Rowe, R. K., & Brachman, R. W. I. (2022). Compressibility and permeability of sand–silt tailings mixtures. *Canadian Geotechnical Journal*, *59*(8), 1348–1357. https://doi.org/10.1139/cgj-2021-0356

Gallagher, P. M., Asce, A. M., Pamuk, A., & Abdoun, T. (2007). *College of Engineering Drexel E-Repository and Archive (iDEA) Stabilization of Liquefiable Soils Using Colloidal Silica Grout*. https://doi.org/10.1061/(ASCE)0899-1561(2007)19:1(33)

Gallagher, P. M., & Mitchell, J. K. (2002). *Influence of colloidal silica grout on liquefaction potential and cyclic undrained behavior of loose sand*. https://doi.org/10.1016/S0267-7261(02)00126-4

Getchell, A., Ochoa-Cornejo, F., & Santagata, M. (2022). Behavior of Dry-Mixed and Permeated Laponite-Treated Sand: From Small Strains to Critical State. *Geotechnical and Geological Engineering*, *40*(11), 5307–5331. https://doi.org/10.1007/s10706-022-02216-4

Ghafarian, D., Imam, S. M. R., & Zarei, M. (2020). Modeling the behavior of sand-fines mixtures using a critical state model. *Soil Dynamics and Earthquake Engineering*, *139*. https://doi.org/10.1016/j.soildyn.2020.106271

Ghasabkolaei, N., Janalizadeh Choobbasti, A., Roshan, N., & Ghasemi, S. E. (2017). Geotechnical properties of the soils modified with nanomaterials: A comprehensive review. In *Archives of Civil and Mechanical Engineering* (Vol. 17, Issue 3, pp. 639–650). Elsevier B.V. https://doi.org/10.1016/j.acme.2017.01.010

Gratchev, I. B., Sassa, K., Osipov, V. I., & Sokolov, V. N. (2006). The liquefaction of clayey soils under cyclic loading. *Engineering Geology*, *86*(1), 70–84. https://doi.org/10.1016/j.enggeo.2006.04.006

Hardin, B. O., & Richart Jr, F. E. (1963). Elastic Wave Velocities in Granular Soils. *Journal of the Soil Mechanics and Foundations Division*, *89*(1).

Herrera, N. N., Letoffe, J. M., Putaux, J. L., David, L., & Bourgeat-Lami, E. (2004). Aqueous dispersions of silane-functionalized laponite clay platelets. A first step toward the elaboration of water-based polymer/clay nanocomposites. *Langmuir*, *20*(5), 1564–1571. https://doi.org/10.1021/la0349267

Huang, X., Lv, K., Sun, J., Lu, Z., Bai, Y., Shen, H., & Wang, J. (2019). Enhancement of thermal stability of drilling fluid using laponite nanoparticles under extreme temperature conditions. *Materials Letters*, *248*, 146–149. https://doi.org/10.1016/j.matlet.2019.04.005

Huang, Y., & Wang, L. (2016). Laboratory investigation of liquefaction mitigation in silty sand using nanoparticles. *Engineering Geology*, *204*, 23–32. https://doi.org/10.1016/j.enggeo.2016.01.015

Huang, Y., Wen, Z., Wang, L., & Zhu, C. (2019). Centrifuge testing of liquefaction mitigation effectiveness on sand foundations treated with nanoparticles. *Engineering Geology*, *249*, 249–256. https://doi.org/10.1016/j.enggeo.2019.01.005

Inshakova, E., & Inshakov, O. (2017). World market for nanomaterials: Structure and trends. *MATEC Web of Conferences*, *129*. https://doi.org/10.1051/matecconf/201712902013

Ishihara, K. (1993). *Liquefaction and flow failure during earthquakes* (Vol. 43, Issue 3).

Iskander, M., Bathurst, R. J., & Omidvar, M. (2015). Past, present, and future of transparent soils. *Geotechnical Testing Journal*, *38*(5), 557–573. https://doi.org/10.1520/GTJ20150079

Israelachvili, J. N. (2011). Van der Waals Forces between Particles and Surfaces. In *Intermolecular and Surface Forces* (pp. 253–289). Elsevier. https://doi.org/10.1016/b978-0-12-375182-9.10013-2

Jain, A. K., Jha, A. K., & Akhtar, P. M. (2022). Assessing the Swelling and Permeability Behavior of Novel Marble Dust–Bentonite with Sand–Bentonite Mixes for Use as a Landfill Liner Material. *Indian Geotechnical Journal*, *52*(3), 675–690. https://doi.org/10.1007/s40098-022-00602-6

Jiang, X., & Rutherford, C. (n.d.). *Soil Improvement by Re-Orienting Magnetic Particles Using a Magnetic Field*.

Kaothon, P., Lee, S. H., Choi, Y. T., & Yune, C. Y. (2022). The Effect of Fines Content on Compressional Behavior When Using Sand–Kaolinite Mixtures as Embankment Materials. *Applied Sciences (Switzerland)*, *12*(12). https://doi.org/10.3390/app12126050

Kolay, P. K., & Ramesh, K. C. (2016). Reduction of Expansive Index, Swelling and Compression Behavior of Kaolinite and Bentonite Clay with Sand and Class C Fly Ash. *Geotechnical and Geological Engineering*, *34*(1), 87–101. https://doi.org/10.1007/s10706-015-9930-4

Komine, H., & Ogata, N. (1996). *Prediction for swelling characteristics of compacted bentonite*. 11–22.

Komine, H., & Ogata, N. (1999). Experimental study on swelling characteristics of sand-bentonite mixture for nuclear waste disposal. *Soils and Foundations Japanese Geotechnical Society*, *39*(2), 83–97.

Kuo, C.-Y., Frost, J. D., Lai, J. S., & Wang, L. B. (1996). Three-Dimensional Image Analysis of Aggregate Particles from Orthogonal Projections. *Transportation Research Record: Journal of the Transportation Research Board*, 98–103.

Lee W., A., Lee, T., Sharma, S., & Boyce, G. (n.d.). *Slope stability and stabilization methods* (Second Edition).

Liu, X., & Yang, J. (2018). Influence of size disparity on small-strain shear modulus of sand-fines mixtures. *Soil Dynamics and Earthquake Engineering*, *115*, 217–224. https://doi.org/10.1016/j.soildyn.2018.08.011

Majeed, Z. H., & Raihan Taha, M. (2013). A Review of Stabilization of Soils by using Nanomaterials. *Australian Journal of Basic and Applied Sciences*, *7*(2), 576–581.

Martins, F. B., Bressani, L. A., Coop, M. R., & Bica, A. V. D. (2001). Some aspects of the compressibility behaviour of a clayey sand. *Canadian Geotechnical Journal*, *38*(6), 1177–1186. https://doi.org/10.1139/cgj-38-6-1177

Meier, A. J., & Shackelford, C. D. (2017). Membrane behavior of compacted sand-bentonite mixture. *Canadian Geotechnical Journal*, *54*(9), 1284–1299. https://doi.org/10.1139/cgj-2016-0708

Mekkiyah, H., & K Huat, B. B. (2015). Behavior of Clay Soil Mixed with Fine Sand During Consolidation Settlement Criteria of Reinforced Soil System View project Soil improvement View project. *Applied Research Journal*, *1*(8), 437–443.

Mele, L., Flora, A., Lirer, S., Anna D'onofrio, ;, & Bilotta, E. (n.d.). *Experimental Study of the Injectability and Effectiveness of Laponite Mixtures as Liquefaction Mitigation Technique*.

Mishra, A. K., Dhawan, S., & Rao, S. M. (2008). Analysis of swelling and shrinkage behavior of compacted clays. *Geotechnical and Geological Engineering*, *26*(3), 289–298. https://doi.org/10.1007/s10706-007-9165-0

Mohtar, E., Santagata, C. S., Drnevich, A., & Johnston, C. (n.d.). *Effect of plastic fines on the small strain stiffness of sand*.

Mollins, L. H., Stewart, D. I., & Cousens, T. W. (1996). Predicting the Properties of Bentonite-Sand Mixtures. In *Clay Minerals* (Vol. 31).

Monkul, M. M., & Ozden, G. (2007). Compressional behavior of clayey sand and transition fines content. *Engineering Geology*, *89*(3–4), 195–205. https://doi.org/10.1016/j.enggeo.2006.10.001

Monkul, M., Ozden, G., & Murat Monkul, M. (2005). *Effect of Intergranular Void Ratio on One-Dimensional Compression Behavior*. https://www.researchgate.net/publication/248707321

Ochoa-Cornejo, F. (2015a). *Cyclic Behavior of Sands With Superplastic Fines*. Ph.D. Dissertation, School of Civil Engineering, Purdue University, West Lafayette, IN 47906, USA.

Ochoa-Cornejo, F. (2015b). *Liquefaction mitigation with nanoparticles Liquefaction mitigation with nanotechnologies* [Purdue University]. https://doi.org/10.13140/RG.2.2.22946.27842

Ochoa-Cornejo, F. (2017). *Dynamic Behavior of Sand with NanoParticles*.

Ochoa-Cornejo, F., Bobet, A., el Howayek, A., Johnston, C. T., Santagata, M., & Sinfield, J. v. (2017). Discussion on: “Laboratory investigation of liquefaction mitigation in silty sand using nanoparticles” [Eng.Geol.204:23–32]. In *Engineering Geology* (Vol. 216, pp. 161–164). Elsevier B.V. https://doi.org/10.1016/j.enggeo.2016.11.015

Ochoa-Cornejo, F., Bobet, A., Johnston, C., Santagata, M., & Sinfield, J. V. (2019). Dynamic properties of a sand – nanoclay composite. *Geotechnique*, *0*(0), 1–16.

Ochoa-Cornejo, F., Bobet, A., Johnston, C., Santagata, M., & Sinfield, J. V. (2020). Dynamic properties of a sand–nanoclay composite. *Geotechnique*, *70*(3), 210–225. https://doi.org/10.1680/jgeot.18.P.017

Ochoa-Cornejo, F., Bobet, A., Johnston, C. T., Santagata, M., & Sinfield, J. V. (2016). Cyclic behavior and pore pressure generation in sands with laponite, a super-plastic nanoparticle. *Soil Dynamics and Earthquake Engineering*, *88*, 265–279. https://doi.org/10.1016/j.soildyn.2016.06.008

Olar, R. (2011). *NANOMATERIALS AND NANOTECHNOLOGIES FOR CIVIL ENGINEERING*.

Pàlkovà, H., Madejovà, J., Zimowska, M., & Serwicka, E. M. (2010). Laponite-derived Porous Clay Heterostructures: II. FTIR Study of the Structure Evolution. *Microporous and Mesoporous Materials*, 237–2.

Pardo Ojeda, K. I. (2020). *Física/Química/Geotecnia de Laponita: Potenciales aplicaciones*. Universidad de Chile.

Pardo Tobar, G. S., & Orense, R. P. (2017). Experimental study on the self-healing effect of laponite on the liquefaction resistance of sand. In *GJ Alexander & CY Chin*.

Phanikumar, B. R., Dembla, S., & Yatindra, A. (2021). Swelling Behaviour of an Expansive Clay Blended With Fine Sand and Fly Ash. *Geotechnical and Geological Engineering*, *39*(1), 583–591. https://doi.org/10.1007/s10706-020-01480-6

Popov, V. (n.d.). *Contact Mechanics and Friction*. Springer.

Popov, V. L., Heß, M., & Willert, E. (n.d.). *Handbook of Contact Mechanics*.

Qi, Y., A1-Mukhtar, M., Alcover, J.-F., & Bergaya, F. (1996). Coupling analysis of macroscopic and microscopic behaviour in highly consolidated Na-laponite clays 1. In *Applied Clay Science* (Vol. 11).

Rahman, M. M., & Sitharam, T. G. (2020). Cyclic liquefaction screening of sand with non-plastic fines: Critical state approach. *Geoscience Frontiers*, *11*(2), 429–438. https://doi.org/10.1016/j.gsf.2018.09.009

Reddi, L. N., & Bonala, M. V. S. (1997). *Critical shear stress and its relationship with cohesion for sand-kaolinite mixtures*.

Rodriguez, C. B. (2019). *Respuesta cílica de arenas de relaves con nanopartículas*.

Salgado, B. R., Bandini, P., Member, S., & Karim, A. (2000). Shear Strength and stiffness of Silty Sand. *Journal of Geotechnical and Geoenviromental Engineering*.

Santamarina, J. C. (2003). *Soil Behavior at the Microscale: Particle Forces*. 25–56. https://doi.org/10.1061/40659(2003)2

Santamarina, J. C., Klein, K., & Fam, M. (2001). *Soils and waves*. John Wiley & Sons.

Sawangsuriya, A. (2012). Wave Propagation Methods for Determining Stiffness of Geomaterials. In *Wave Processes in Classical and New Solids*. InTech. https://doi.org/10.5772/48562

Scalisi, F., & Sposito, C. (2017). Performance of Earth Bricks Supplemented by Nanoparticles and their Application in Architecture. *Applied Mechanics and Materials*, *864*, 8–13. https://doi.org/10.4028/www.scientific.net/amm.864.8

Schanz, T., & Elsawy, M. B. D. (2015). Swelling characteristics and shear strength of highly expansive clay–lime mixtures: A comparative study. *Arabian Journal of Geosciences*, *8*(10), 7919–7927. https://doi.org/10.1007/s12517-014-1703-5

Sellin, P., & Leupin, O. X. (2014). The use of clay as an engineered barrier in radioactive-waste management - A review. *Clays and Clay Minerals*, *61*(6), 477–498. https://doi.org/10.1346/CCMN.2013.0610601

Shafran, K., Jeans, C., Kemp, S. J., & Murphy, K. (2020). Dr Barbara S. Neumann: clay scientist and industrial pioneer; creator of Laponite®. *Clay Minerals*, *55*(3), 256–260. https://doi.org/10.1180/clm.2020.35

Shen, M. (2014). *Rheological Properties of Laponite And Chemically Modified Laponite Suspensions*. https://docs.lib.purdue.edu/open_access_theses/253/

Shi, X. S., & Yin, J. (2017). Experimental and theoretical investigation on the compression behavior of sand-marine clay mixtures within homogenization framework. *Computers and Geotechnics*, *90*, 14–26. https://doi.org/10.1016/j.compgeo.2017.05.015

Shi, X. S., & Yin, J. (2018). Consolidation Behavior for Saturated Sand–Marine Clay Mixtures Considering the Intergranular Structure Evolution. *Journal of Engineering Mechanics*, *144*(2). https://doi.org/10.1061/(asce)em.1943-7889.0001391

Siddique, S. N., Deng, J., & Mohamedelhassan, E. (2023). Improving the Strength Properties of Sand Using Laponite, a Promising Nanoparticle. *International Journal of Civil Engineering*, *21*(4), 679–693. https://doi.org/10.1007/s40999-022-00791-4

Tanaka, H., Meunier, J., & Bonn, D. (2004). Nonergodic states of charged colloidal suspensions: Repulsive and attractive glasses and gels. *Physical Review E - Statistical, Nonlinear, and Soft Matter Physics*, *69*(3 1). https://doi.org/10.1103/PhysRevE.69.031404

Vadlamudi, S., & Mishra, A. K. (2018). Consolidation Characteristics of Sand–Bentonite Mixtures and the Influence of Sand Particle Size. *Journal of Hazardous, Toxic, and Radioactive Waste*, *22*(4). https://doi.org/10.1061/(asce)hz.2153-5515.0000409

Vallejo, L. E., & Mawby, R. (2000). Porosity influence on the shear strength of granular material-clay mixtures. In *Engineering Geology* (Vol. 58). https://doi.org/10.1016/S0013-7952(00)00051-X

Verdugo, R., & González, J. (2015). Liquefaction-induced ground damages during the 2010 Chile earthquake. *Soil Dynamics and Earthquake Engineering*, *79*, 280–295. https://doi.org/10.1016/j.soildyn.2015.04.016

Vijaya Kumar, G. (1996). *Some Aspects of the Mechanical Behaviour of Mixtures of Kaolin and Coarse Sand*.

Wallace, J. F., & Rutherford, C. J. (2015). Geotechnical properties of LAPONITE RD®. *Geotechnical Testing Journal*, *38*(5), 574–587. https://doi.org/10.1520/GTJ20140211

Walton, W. H. (1948). Ferets Statistical Diameter as a Measure of Particle Size. *Nature*, 329–330.

Wang, D. W., Zhu, C., Tang, C. S., Li, S. J., Cheng, Q., Pan, X. H., & Shi, B. (2021). Effect of sand grain size and boundary condition on the swelling behavior of bentonite–sand mixtures. *Acta Geotechnica*, *16*(9), 2759–2773. https://doi.org/10.1007/s11440-021-01194-w

Wichtmann, T., & Triantafyllidis, T. (2009). *Influence of the Grain-Size Distribution Curve of Quartz Sand on the Small Strain Shear Modulus G max*. https://doi.org/10.1061/(ASCE)GT.1943-5606.0000096

Xenaki, V. C., & Athanasopoulos, G. A. (2003). Liquefaction resistance of sand-silt mixtures: An experimental investigation of the effect of fines. *Soil Dynamics and Earthquake Engineering*, *23*(3), 1–12. https://doi.org/10.1016/S0267-7261(02)00210-5

Xiong, Z. Q., Li, X. D., Fu, F., & Li, Y. N. (2019). Performance evaluation of laponite as a mud-making material for drilling fluids. *Petroleum Science*, *16*(4), 890–900. https://doi.org/10.1007/s12182-018-0298-y

Yamamuro, J. A., & Lade, P. V. (1998). Experiments and modelling of silty sands susceptible to static liquefaction. In *MECHANICS OF COHESIVE-FRICTIONAL MATERIALS Mech. Cohes.-Frict. Mater* (Vol. 4).

Yang, H., Baudet, B. A., & Yao, T. (2016). Characterization of the surface roughness of sand particles using an advanced fractal approach. *Proceedings of the Royal Society A: Mathematical, Physical and Engineering Sciences*, *472*(2194). https://doi.org/10.1098/rspa.2016.0524

Yang, J., Wei, L. M., & Dai, B. B. (2015). State variables for silty sands: Global void ratio or skeleton void ratio? *Soils and Foundations*, *55*(1), 99–111. https://doi.org/10.1016/j.sandf.2014.12.008

Yang, S., Choi, J. C., Vanneste, M., & Kvalstad, T. (2018). Effects of gas hydrates dissociation on clays and submarine slope stability. *Bulletin of Engineering Geology and the Environment*, *77*(3), 941–952. https://doi.org/10.1007/s10064-017-1088-2

Yang, S., Lacasse, S., & Sandven, R. (2005). Determination of the Transitional Fines Content of Mixtures of Sand and Non-plastic Fines. *Geotechnical Testing Journal*, *29*(2), 102–107. https://doi.org/10.1520/GTJ14010

Yi, L. da, Lv, H. bin, Ye, T., & Zhang, Y. P. (2018). Quantification of the Transparency of the Transparent Soil in Geotechnical Modeling. *Advances in Civil Engineering*, *2018*. https://doi.org/10.1155/2018/2915924

Yin, K., Fauchille, A.-L., Filippo, E. Di, Kotronis, P., & Sciarra, G. (2021). A Review of Sand-Clay Mixture and Soil-Structure Interface Direct Shear Test A Review of Sand-Clay Mixture and Soil-Structure Interface Direct Shear. *Test. Geotechnics*, *1*, 260–306. https://doi.org/10.3390/geotechnics1020014

Zhang, Y., Hu, M., Ye, T., Chen, Y., & Zhou, Y. (2020). An experimental study on the rheological properties of laponite RD as a transparent soil. *Geotechnical Testing Journal*, *43*(3). https://doi.org/10.1520/GTJ20180348

Annex A

Morphology and particle distribution through SEM

a)

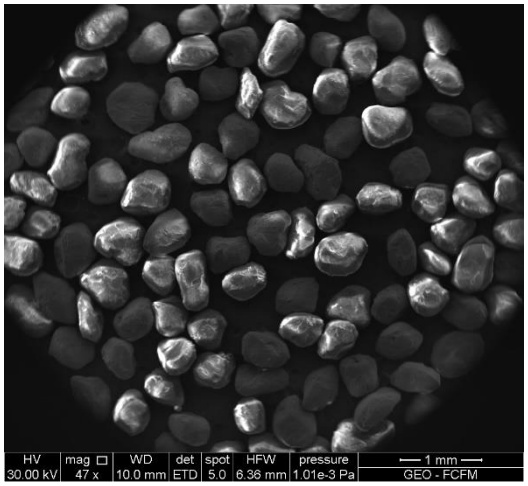

b)

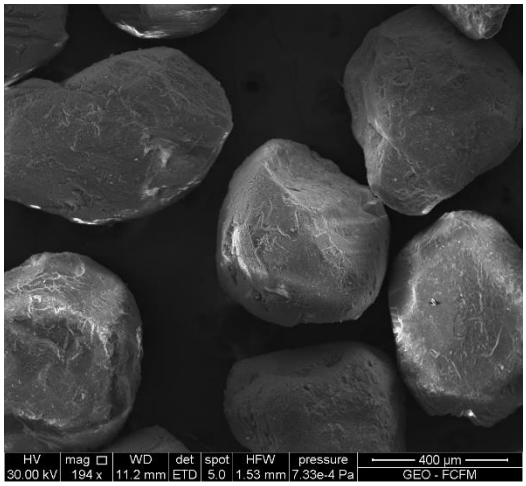

c)

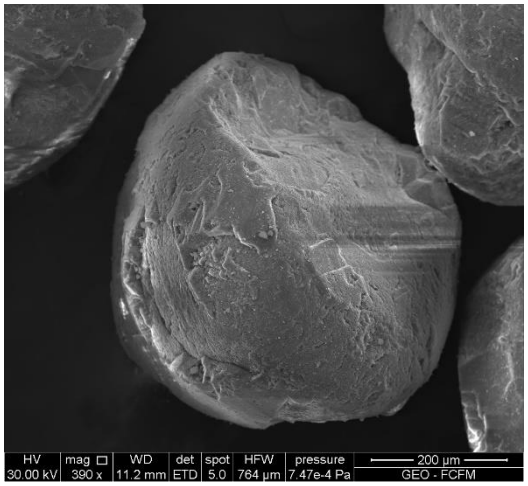

d)

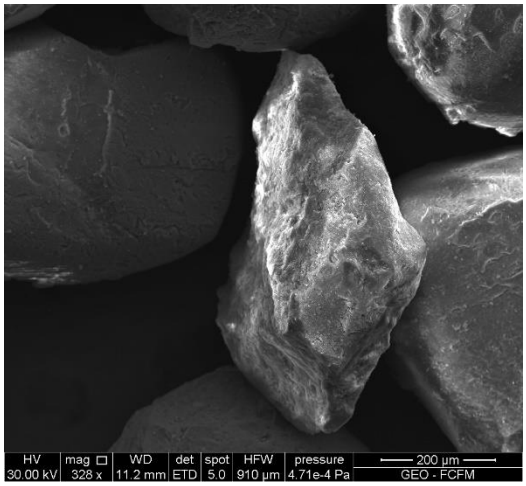

Figure 0-1: 5% laponite, sieve #40.

a)

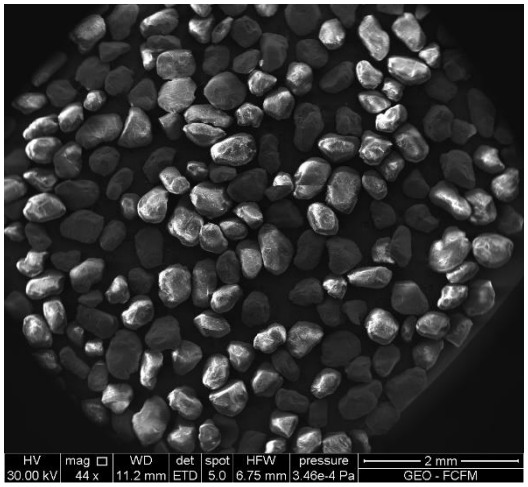

b)

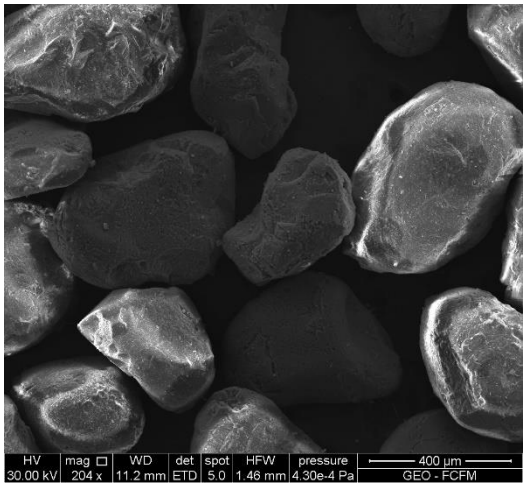

c)

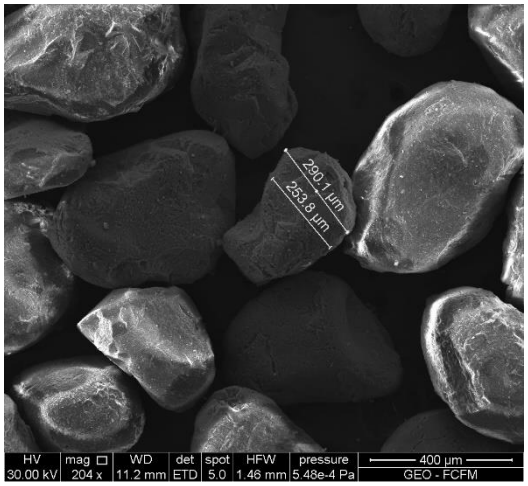

d)

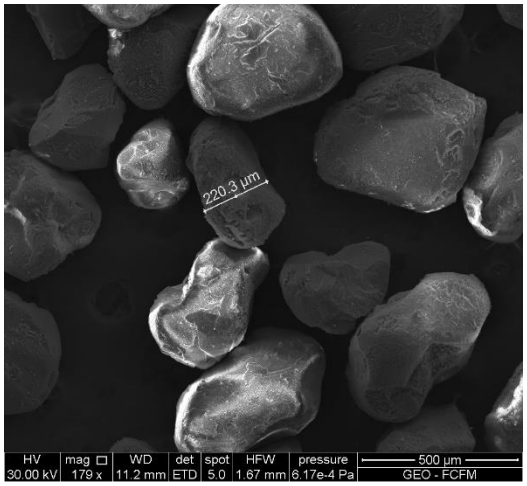

Figure 0-2: 5% laponite, sieve #60.

a)

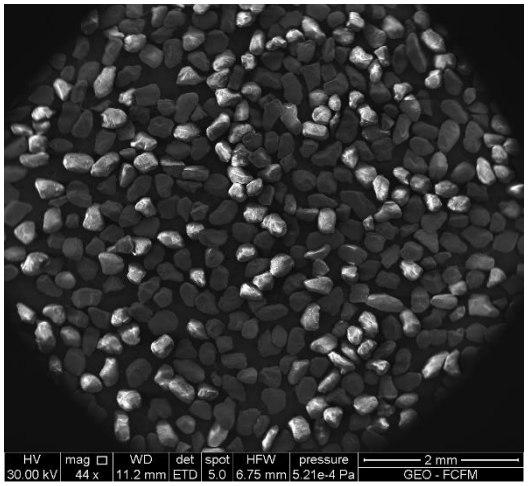

b)

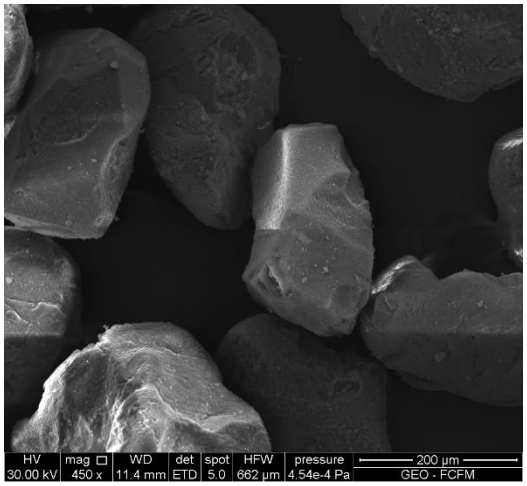

Figure 0-3: 5% laponite, sieve #100.

a) b)

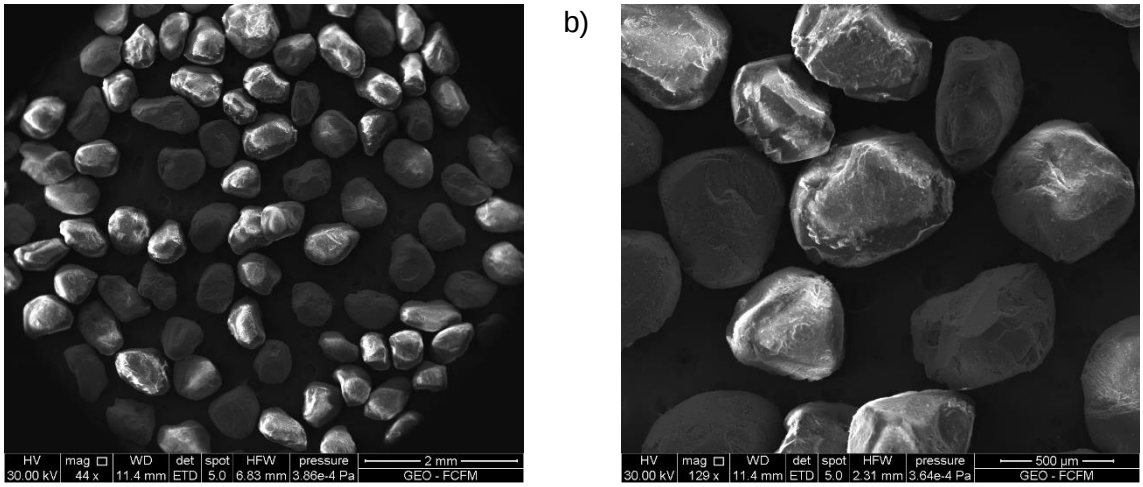

Figure 0-4: 10% laponite, sieve #40.

a) b)

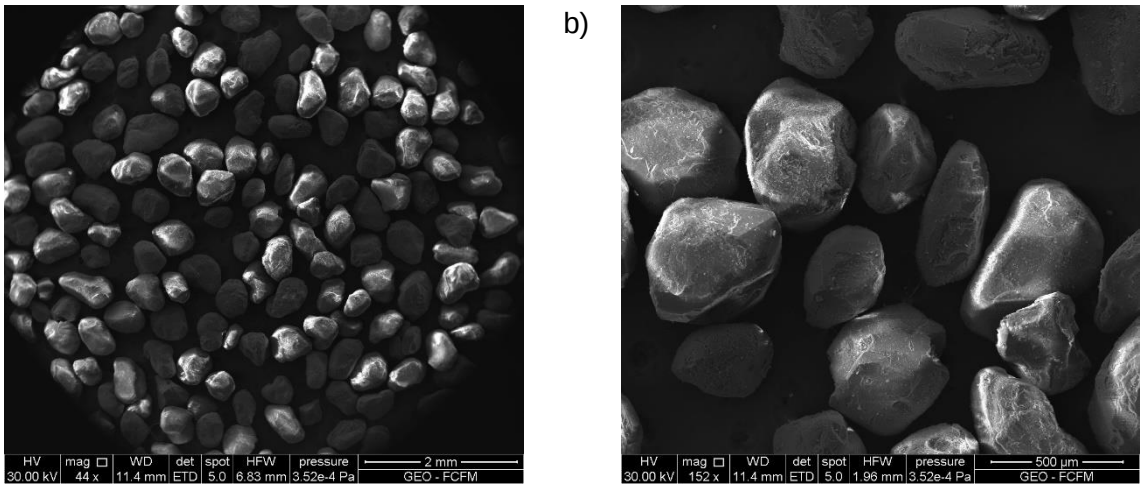

Figure 0-5: 10% laponite, sieve #60.

a)

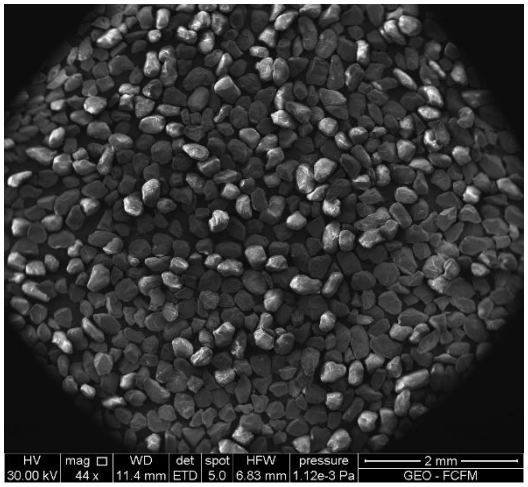

b)

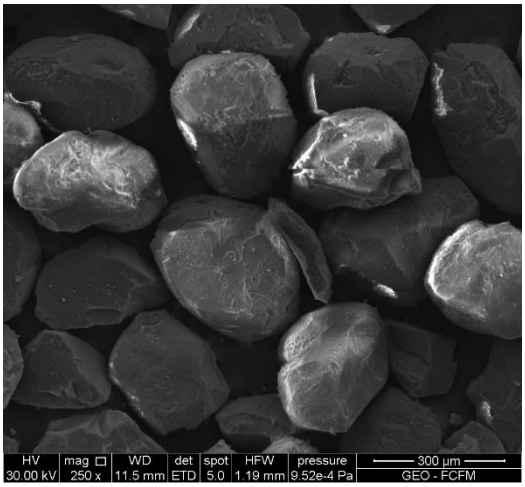

c)

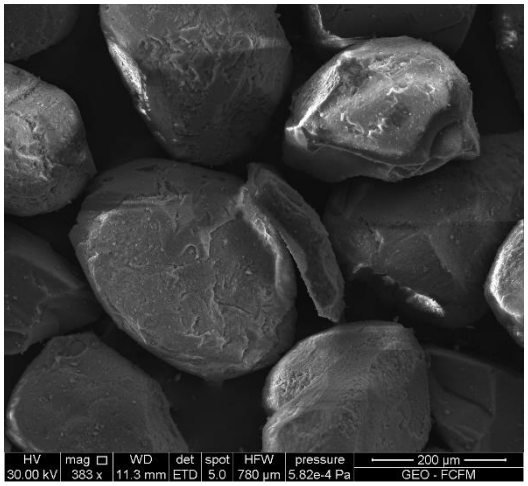

d)

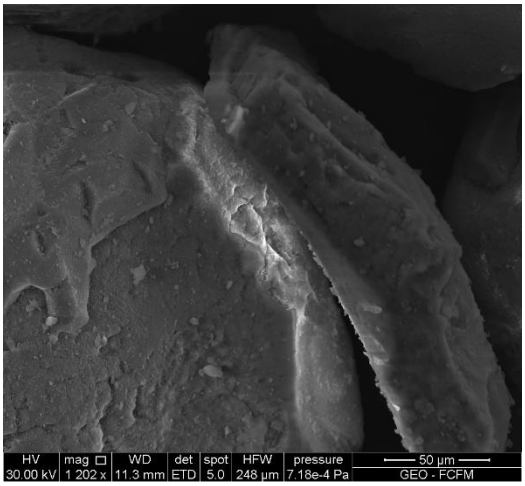

Figure 0-6: 10% laponite, sieve #100.

a) b)

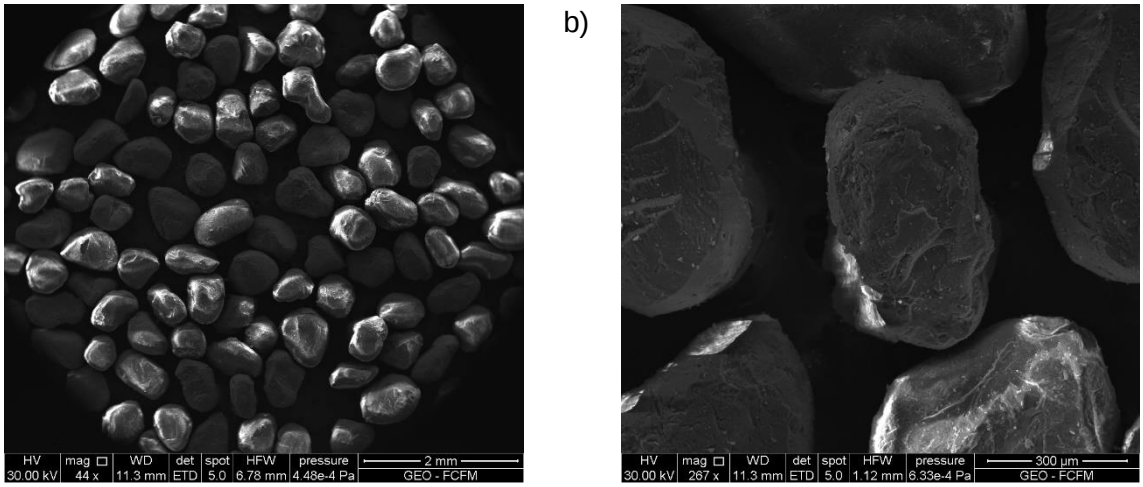

Figure 0-7: 15% laponite, sieve #40.

a) b)

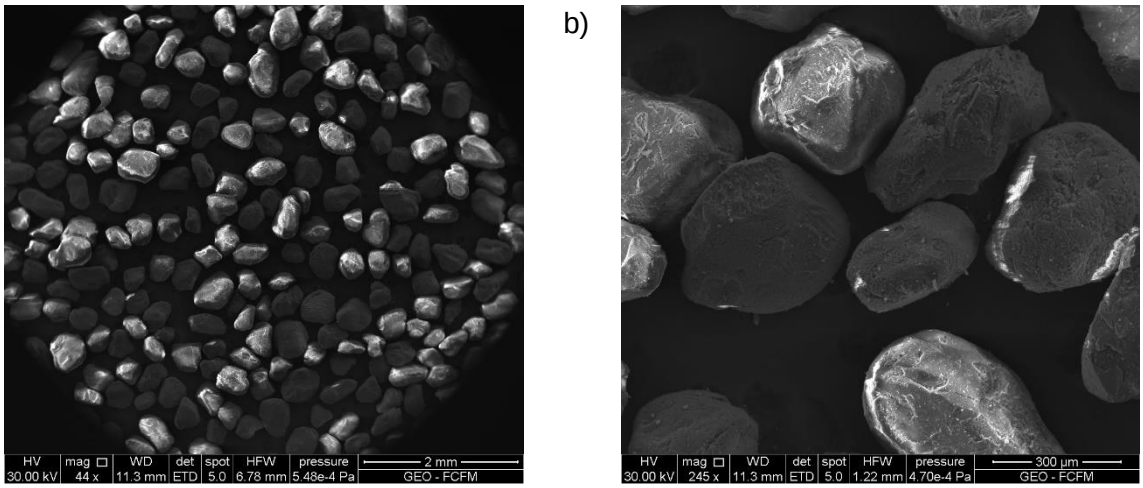

Figure 0-8: 15% laponite, sieve #60.

a) b)

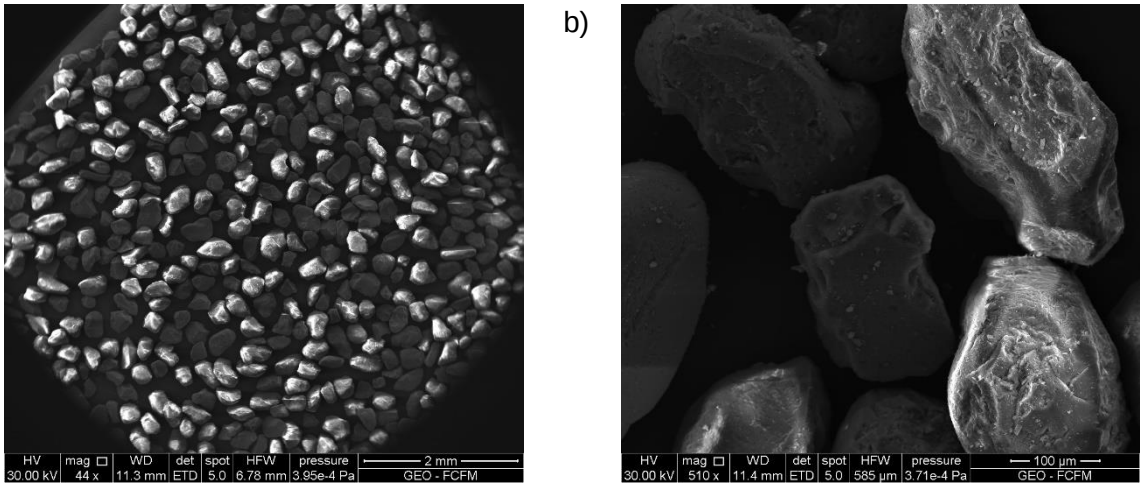

Figure 0-9: laponite, sieve #100.

Annex B

Atterberg`s limits

Table 0-1: Atterberg`s limits for Ottawa sand with laponite.

Laponite	LL [%]	LP [%]	IP [%]
3%	28.65	-	-
5%	54.37	24.3	30.07
10%	89.44	20.16	69.29
15%	134.87	26.98	107.89
20%	277.32	54.55	222.78

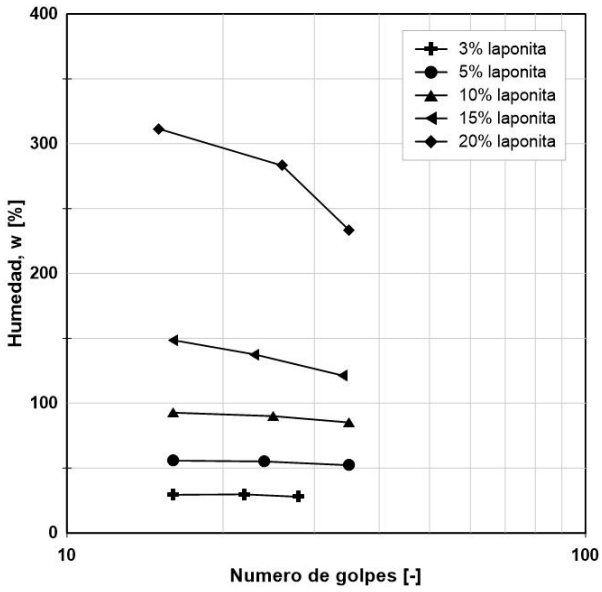

Figure 0-1: LL for Ottawa sand with laponite.